"Methanol Production via Solar Reforming of Methane"

„Methanolherstellung durch solare Reformierung von Methan"

Von der Fakultät für Maschinenwesen der Rheinisch-Westfälischen Technischen Hochschule Aachen zur Erlangung des akademischen Grades eines Doktors der Ingenieurwissenschaften genehmigte Dissertation

vorgelegt von

Henrik von Storch

Berichter: Univ.-Prof. Dr.-Ing. Bernhard Hoffschmidt

Univ.-Prof. Dr.-Ing. André Bardow

Tag der mündlichen Prüfung: 27.06.2016

Preface

The present work was accomplished at the Institute of Solar Research at the German Aerospace Center (DLR e.V.) in Jülich.

I would like to thank Prof. Dr.-Ing. Bernhard Hoffschmidt for his kind supervision of this work. His constructive comments have helped me to see the big picture and greatly improve this dissertation. I would also like to thank Prof. Dr.-Ing. André Bardow, who has acted as second examiner, for his fruitful ideas and support that he has kindly provided from a very early stage on. Furthermore, I would like to thank Prof. Dr.-Ing. Dipl.-Wirt.-Ing. Günther Schuh for acting as the president of the examination board. I am very grateful for the pleasant and friendly atmosphere these three have created during my examination.

Next, I owe very special thanks to Dr. Martin Roeb and Dr. Hannes Stadler for their everyday support with small and big problems throughout my work. Martin has greatly helped me in defining an overall strategy and by being a great group leader. Hannes has supported me to the same extend by advising me on scientific procedures and making me try to get rid of each and every flaw. Together, they have complemented each other perfectly in preparing me for a scientific career.

Furthermore, I am very grateful to Prof. Dr.-Ing Robert Pitz-Paal and Prof. Dr. rer. nat. Christian Sattler who have both, in their role as heads of institute and department, given me very helpful advice repeatedly. Both also contribute constantly to generating a wonderful working environment.

Despite all this great support from supervisors and other senior scientists, I cannot imagine making it through writing a dissertation without the my fellow colleagues, with whom I have laughed so many times, who are great sparring partners for brain storming, who always lend an ear to listen to each other's problems and many of whom have become good friends. Among these, very special thanks go to Robert Flesch, Arne Tiddens, Matthias Lange, Jan Felinks, Friedemann Call, Simon Dieckmann, Matthias Offergeld, Silvan Siegrist and Sebastian Richter.

Certainly I want to thank my family for the support they have given to me, that has allowed me to develop in a carefree environment. Special thanks go to my mother Angelika.

Last but certainly not least I would like to thank my wife Katja for her continuous and loving support. With just the right degree of "push and pull" she has helped me to make it through this work.

Contents

Kurzfassung

In der vorliegenden Arbeit wird ein solarer Reformierungsprozess zur Methanolherstellung untersucht. Der Prozess stellt eine Möglichkeit dar, die mit diesem Herstellungsprozess verbundenen Treibhausgasemissionen zeitnah bedeutend zu reduzieren. Hiermit wäre ein wesentlicher Schritt in der Entwicklung einer nachhaltigeren Chemieindustrie geleistet. Darüber hinaus lässt sich Methanol auch als Brennstoff einsetzen. So kann Methanol einen Beitrag zu einer klimaschonenderen Energieversorgung leisten, wenn er durch solare Reformierung produziert wird.

Zunächst wurde in der Arbeit ein Gesamtprozess auf Basis der indirekt beheizten solaren Reformierung entwickelt. Hierbei war ein Ziel die anfallenden Abwärmeströme zu nutzen. Infolgedessen wird ein großer Teil der Abwärme in einem Wasser-Dampf-Kreislauf zur Stromproduktion genutzt, da es hierfür keine sinnvolle Verwendung im Prozess gibt. Darüber hinaus wird der Off-Gas-Strom der Methanolsynthese teilweise zur Stromproduktion eingesetzt.

Der entwickelte Prozess nutzt Sonnenenergie und Erdgas und produziert hieraus Methanol und elektrischen Strom. Das Verhältnis der verschiedenen Ströme zueinander ist hierbei durch Parametervariation veränderbar. Eine Optimierung mit herkömmlichen Bewertungskriterien wie Energie- oder Exergiebilanzen ist daher nicht möglich. Folglich wurde ein Bewertungskriterium entwickelt, dass auf dem Ziel basiert den Verbrauch der Fossilen Rohstoffe und die damit verbundenen Treibhausgasemissionen zu reduzieren.

Auf Basis dieses Bewertungskriteriums wurde der Prozess mithilfe von Parametervariationen optimiert. Die Ergebnisse zeigen, dass der Prozess das Potential hat Sonnenenergie effektiver zu nutzen, als dies bei der reinen Stromproduktion der Fall ist. Eine anschließende Wirtschaftlichkeitsbetrachtung zeigte, dass der Prozess zur konventionellen Sonnenenergienutzung theoretisch konkurrenzfähig ist. In der Praxis müssten hierfür jedoch entsprechende Fördermechanismen, wie sie für die Stromproduktion existieren, für die Herstellung von Chemierohstoffen eingeführt werden.

Abstract

In the present work, a solar reforming process for production of methanol was investigated. With this process, it is possible to reduce the greenhouse-gas emissions associated with the production of methanol significantly in the near-term future. This would be a significant step in the development of a more sustainable chemical industry. Furthermore, methanol can be applied as a fuel. Thus, methanol can contribute to a more climate friendly energy supply, if it is produced via solar reforming.

First of all, the overall reforming process was developed based on the concept of indirectly heated solar reforming. One central aspect of this was to make use of the waste-heat streams. As a consequence a large fraction of the off heat is converted into electricity in a water steam cycle, because no other demand exists for this heat. Furthermore, the off-gas stream of the methanol synthesis is partly used for additional electricity production.

The developed process uses solar energy and natural gas to produce methanol and electricity. The ratio between the different streams can be changed by parameter variation. An optimization of the process with conventional criteria such as energy- or exergy-balances is therefore not possible. Thus, a new evaluation criterion was developed. This criterion is based on the target to reduce fossil fuels reduction and the associated greenhouse-gas emissions.

Based on this evaluation criterion, the process was optimized by parameter variation. The results show that the process has the potential to make more efficient use of solar energy than is the case for sole production of electricity. A subsequent economic investigation showed that the developed process can in theory be competitive with conventional solar energy utilization. However, in practice support mechanism, as they exist for solar electricity production, would have to be implemented for solar production of chemical feedstocks.

List of Figures

Nomenclature

Latin Characters

A	Area	m²
a	Volume specific surface area for heat transfer	m^{-1}
ARR	Air return ratio	-
b	Thickness of wall/struts in absorber structure	m
C	Cost	$
C_{Annuity}	Annuity of investment cost	
C_{BM}	Bare module cost	$
C_{GR}	Grass roots cost	$
C_{P}	Purchase price	$
C_{TM}	Total module cost	$
C_{Cav}	Ratio of aperture to absorber area in cavity receiver	-
C_{Conc}	Concentration factor in CSP	
d	Diameter	m
d_{h}	Hydraulic diameter	m
$E_{\mathrm{Renewable}}$	Renewable energy input	MWh
E_{Solar}	Solar energy input	MWh
$\Delta E_{\mathrm{Fuel/NG}}$	Reduction in fuel/NG consumption	MWh
F	Molar flow rate	kmol/s
F_{GR}	Factor for calculation of grass roots costs	-
F_{TM}	Factor for calculation of total module cost	-
f_{Corr}	Correction factor for heliostat field efficiency when flux density deviates from 700 kW/m²	-
f_{Split}	Fraction of off-gas from methanol synthesis used for temperature lift in reforming	-
h_{i}	Mole-specific enthalpy of stream i	kJ/kmol
h	Efficiency of SOLME according to evaluation scheme	-

h_{W}	Wall heat transfer coefficient	
$\Delta H^{0}_{\mathrm{R,298K}}$	Heat of reaction at standard conditions (1 atm and 298 K)	kJ/mol
I	Flux Density	kW/m²
$\Delta LCOE_{\mathrm{Process}}$	Difference in LCOE between SOLME process and reference system	$/MWh
$\Delta LCOE_{\mathrm{System}}$	Difference in LCOE between SOLME system and reference system	$/MWh
$LCOE$	Levelized cost of electricity	$/MWh
$LCOM$	Levelized cost of methanol	$/t
M	Parameter for description of syngas composition	-
m	Mass output of methanol	t
n_{Tubes}	Number of tubes in AHR in relation to mole flow	s/mole
Nu	Nusselt Number	
p	pressure	bar
Pr	Prandtl Number	
$\dot{Q}_{\mathrm{ARR}}$	Heat losses due to incomplete air return in receiver	
$\dot{Q}_{\mathrm{Conv}}$	Convective heat losses of receiver	kW
$\dot{Q}_{\mathrm{Cond}}$	Conductive heat losses of receiver	kW
$\dot{Q}_{IC}$	Intercept radiation onto receiver aperture	kW
$\dot{Q}_{\mathrm{Process,nominal}}$	Nominal heat consumption by SOLME process	kW
Q_{Storage}	Energy stored in storage	MWh
$Q_{\mathrm{Storage,Max}}$	Maximum capacity of heat storage	MWh
$\dot{Q}_{Use}$	Thermal output of the receiver (useful energy)	kW
$Q_{\mathrm{Use,An}}$	Annual sum of thermal output of the receiver	MWh
$\dot{Q}_{\alpha}$	Absorbed radiation	kW
$\dot{Q}_{\varepsilon}$	Re-emitted radiation	kW
r_i	Rate of reaction i	kmol/kg$_{\mathrm{Cat}}$K
$r_{\mathrm{i,eff}}$	Effective rate of reaction	
r	radius	m

Re	Reynolds Number	
s	width of absorber channel	m
SM	Solar multiple	
S/NG	Steam to natural gas ratio in inlet stream for reforming reaction	-
t	Time in year for receiver / storage simulation	-
Δt	Time interval in receiver / storage simulation	h
T	Temperature	°C
$\Delta T_{\mathrm{Upper}}$	Temperature difference at hot end of AHR	
X_i	Conversion of species i	-
Δx	Cell size in receiver model	
z	control variable for AHR length	m
z_i	mole fraction of component i	mol/mol

Greek Symbols

α	Absorptivity	-
ε	Emissivity	-
η_{r_i}	Effectiveness factor for reaction i	
η_{HF}	Heliostat field efficiency	
η_{Receiver}	Receiver Efficiency	
λ	Thermal conductivity	
$\lambda_{\mathrm{eff,Abs}}$	Effective thermal conductivity of absorber	W/m²K
σ	Stefan-Boltzmann constant 5.67e-8 W/m²K⁴	
$\rho_{\mathrm{cat,bed}}$	Density of catalyst bed	kg/m³
ψ	porosity	

Subscripts

Abs	In/of the absorber

air	Of the air flow
An	Accumulated annual value
an	Annulus of AHR
Ap	In/of the aperture
c	cross sectional in AHR
CH_4	Methane
CO_2	Carbon dioxide
DNI	Direct normal irradiance
DP	Design Point
El	Electricity
Generic	Of generic process
H_2	Hydrogen
H_2O	Water
HA	Hot Air (from solar receiver)
in	Inner
MeOH	Methanol
n	Last cell in model
N_2	Nitrogen
NG	Of natural gas
o	Outer
Off-Gas	Total off gas from methanol synthesis part
Off-Gas, TL	Fraction of off-gas from methanol synthesis part for reforming temperature lift
PB,ref	Power block in reference solar power plant
RA	Return Air (to the solar receiver)
Ref	Outlet condition of reforming reactors
Reference	Of the reference system (for evaluation)
Ref MeOH	Reference methanol plant
Solarized	Of the solarized system
SPT	Reference solar power tower

SOLME, Process-Only	Of SOLME process only
SOLME, System	Of SOLME System
Total	Total gas flow
tube	Reactor tube in AHR
W	Wall in the absorber channels

Superscripts

0	Inlet conditions of reactor

Abbreviations and Acronyms

AHR	Air heated reformer
CCGT	Combined cycle gas turbine power plant
CEPCI	Chemical engineering cost index
DNI	Direct normal irradiance
GHG	Greenhouse gas
HP	High pressure stage in WSC
HTF	Heat transfer fluid
IPCC	Intergovernmental panel on climate change
LHV	Lower heating value
LP1	Low pressure stage 1 in WSC
LP2	Low pressure stage 2 in WSC
MP	Medium pressure stage in WSC
MS	Methanol Synthesis
OVR	Open volumetric receiver
SecRef	Secondary reformer in SOLME process
SOLME	Solar methanol production process
SR	Steam reforming reaction
SR + WGS	Combined reaction of steam reforming and water gas shift

TES	Thermal energy storage
TL	Temperature lift of reforming temperature, carried out in SecRef
WGS	Water gas shift reaction
WSC	Water steam cycle

1. Introduction

In the past decades, it has become clear that global warming will be one of the predominant challenges of the 21st century. Furthermore, today it is broadly accepted that global warming is mainly caused by anthropogenic emissions of greenhouse gases (GHG), of which carbon dioxide (CO_2) is the most important one. As the working group one (WG I) of the intergovernmental panel on climate change (IPCC) reported in 2013, the concentration of CO_2 in the atmosphere reached a value of 391 ppm in 2011, exceeding all values determined for the past 800,000 years [1]. Energy supply of humanity is the major source of GHG emissions, therefore it is the main driver of the anthropogenic climate change [2]. The working group two (WG II) of the IPCC addressed the positive and negative effects that are to be expected from climate change in its report [3]. In the report it is stated that most effects vary significantly with location, at times causing a positive effect in one region and a negative effect in another. However, the overall effect is expected to be clearly negative on many aspects of live such as human health, settlement and society, industry and coastal systems. For instance, deaths, diseases and injuries due to heatwaves and other natural events are expected to increase globally. It is furthermore stated that especially developing countries will suffer from floodings in the future, since adaption will be more challenging for them than for industrialized countries. From these findings it becomes obvious that there is a strong urge to prevent or reduce the extent of climate change. In order to do so, it is necessary to significantly reduce the GHG emissions.

Opposing the need to reduce emissions, a rise in the global energy demand, for a large part caused by strongly increasing demand in Asia, particularly in China, can currently be observed [4]. Even among those accepting that actions have to be taken to reduce GHG emissions, it is commonly accepted that the standard of living should not suffer from these actions and that the increase of the standard of living in developing countries should not be impeded. As currently more than 90 % of the world's energy demand is supplied by fossil fuels and nuclear energy [4], a broad field of implementation possibilities for renewable energies still exists. The most efficient possibilities to reduce GHG emissions should be identified and implemented with particular urge.

Currently a large effort is expended on the implementation on renewable energies in some countries. For instance, in Germany 11 % of the primary energy supply was derived from renewable resources in 2011. For comparison: The share was below 2 % until 1997. Internationally, the single largest role within the renewable energies is currently occupied by biomass. A large part of the renewable energies are implemented into the electricity generation system, in Germany, they account for 30 % of the total electricity production in 2015, with wind, biomass, photovoltaics and hydropower as the major resources [5]. Considering that biomass is the only renewable feedstock that can relatively easily be used as chemical feedstock by conversion into base chemicals such as naphta or methanol, its utilization as energy carrier is questionable when establishing a global economy purely based on renewable feedstocks. Furthermore, very little success can be observed in implementing renewable energies in the direct provision of process heat in industrial processes: 11.2 % of the global end-energy consumption in 2012 can be attributed to industrial use of natural gas and oil [4], making up approx. 42,379 PJ annually. Assumingly the majority of this energy is used for provision of heat. Biomass and solar thermal applications appear to be the most appropriate candidates to provide this energy from renewable resources. They both use the intermediate step of heat generation in most applications. Therefore, they can be operated demand oriented, in contrast to wind, photovoltaics and hydropower that produce electricity directly. As mentioned previously, biomass should preferably be used as a material feedstock in production of commodities. Furthermore its availability is limited, whereas solar energy's availability is abundant [6]. Therefore, in this work the possibility of implementation of solar energy into industrial processes for provision of heat is investigated through the example of solar reforming.

1.1. Utilization of synthesis-gas from solar reforming

Conventionally, reforming of natural gas is carried out with combustion of additional natural gas for heat provision. The process can be considered state of the art and is widely practiced. Rostrup-Nielsen et al. [7] give an overview of the different applications for the reforming product synthesis gas (or syngas), a mixture of hydrogen, carbon monoxide and carbon dioxide. They state that it is a key intermediate product in chemical industry.

Furthermore, according to Rostrup-Nielsen et al., in 2000 the main applications were production of ammonia, methanol and pure hydrogen. As shown by Bartholomew and Farrauto [8], ammonia synthesis is merely an additional step after production of purified hydrogen. Therefore, there are only two main applications for conventionally generated syngas: Production of purified hydrogen and production of methanol.

Different concepts for energetic utilization of syngas exist. However, these are not meaningful for conventional reforming of natural gas: According to the principle of energy conservation, there cannot be a benefit from energetic utilization of synthesis gas compared to the energetic utilization of the total natural gas that was previously used for production of the syngas. In contrast to that, when utilizing solar energy to fuel the heat of reaction to the reforming reactor, the process can be considered a storage concept for solar energy. Therefore, energetic utilization of the syngas produced with solar energy is an option for decoupling the energy utilization temporally and spatially from the solar energy supply. In principal two concepts for the energetic utilization of solar syngas have been proposed: The combustion in a gas turbine and utilization in a solar chemical heat pipe [9].

In the SOLASYS project, a consortium around DLR has produced syngas via solar reforming of liquefied petroleum gas (LPG). The syngas was then combusted in a modified gas turbine to generate electricity. The turbine was fed with a mixture of LPG and syngas with up to 40 % of syngas without significant efficiency losses [10]. Both McNaughton [11] as well as Sheu and Mitsos [12] have conducted simulations of a solar reforming and gas turbine process and evaluated its efficiency potential. Both came to the conclusion that high solar-to-electric efficiencies are feasible, making this process a viable alternative to conventional CSP power plants or other concepts for solar-gas hybrid power plant concepts. Finally, in the project SolBioPolysy [13], landfill gas was reformed with solar energy and combusted in an internal combustion engine. However, to the best of the authors knowledge, no results concerning the engine operation are available.

The solar chemical heat pipe is a concept that literally uses the syngas as thermochemical heat storage. The reactants and products are kept in a closed loop. The endothermic reforming reaction is reversed at another time and/or location by the exothermic

methanation reaction to recover high temperature heat. The concept was originally proposed to utilize nuclear energy in the ADAM-EVA project by KFA Jülich [14]. There, the concept was successfully tested at a 10 MW scale in the early 1980s [15]. The original idea of the heat pipe, pursued in the ADAM-EVA concept was the distribution of nuclear energy from high temperature gas-cooled reactors over large distances to individual users, remote from the nuclear reactor. Between 1989 and 1991, a group from the Weizmann Institute of Science (WIS) operated a solar chemical heat pipe with an irradiated tubular solar receiver-reactor successfully at different configurations. However, in their experimental set-up, the methanation reactor mainly served the purpose of closing the loop and proofing the concept of the heat pipe, rather than giving results on energetic efficiency [16]. To the best of the author's knowledge there are no current activities pursuing this concept.

Both, the combustion of the syngas in a gas turbine as well as the solar chemical heat pipe have the inherent disadvantage of utilizing the syngas as storage media. In a report on the topic of syngas storage, Apt et al. [17] discuss its difficulties and the potential in intermediate storage in integrated gasification combined cycle power plants. They state the difficulties that the syngas has low volumetric energy density and that the contained hydrogen makes most metals brittle. They come to the conclusion that syngas storage is feasible for some hours in integrated gasification power plants. However, the feasible time scales do not provide an advantage compared to conventional thermal energy storage, when considering solar generated syngas. Furthermore, the low energy density makes transport over large distances unfeasible. For instance, for the transport of 100 MW energy chemically stored in syngas a minimum 3 MW per 100 km of compressor work are necessary (round trip).

Regarding the production of hydrogen or methanol from solar synthesis gas, there cannot be a definite choice as to which is more advantageous. However, the production of methanol features some aspects that make it an attractive option: Methanol is a broadly applied substance in chemical industry and, as discussed by Bertau et al. [18], has the potential to be applied as an energy carrier in the future. Its production by means of solar reforming can significantly reduce the associated natural gas consumption, hence reducing the greenhouse-gas emissions. When methanol is used as an energy carrier and produced

via solar reforming, it is a partly solar fuel. As such, it features some advantages compared to other possible solar fuels. Those advantages are listed in the following. The arguments are based on observations by Olah et al. [19].

- Methanol synthesis is well understood and has been practiced industrially for several decades
- It has a high volumetric energy density (17.9 MJ/l), therefore it is economically
    - transportable over large distances
    - storable in large amounts over long time intervals
- It offers a broad range of possible applications as chemical feedstock, transportation fuel or chemical energy storage medium:
    - Combustion in internal combustion engines
    - Combustion in gas turbines
    - Highly efficient utilization in direct methanol fuel cells is being developed.

It should be added that in China methanol is already widely used both in the chemical industry as well as blend-in for gasoline and that a strong increase in methanol production can be observed there [20]. This increasing implementation of the so-called methanol economy in China will most probably be adapted by other countries and cause a major increase in global methanol demand, too. With the production of partly solar methanol, as proposed in this work, CO_2 emissions attributed to the methanol economy can be significantly reduced.

1.2. The present study

Even though intensive investigation of solar reforming with different concepts has been carried out in the past, the subsequent conversion into methanol or another liquid fuel has not been taken into account. In most research projects the potential efficiency of different types of solar reforming concepts was experimentally assessed. However, the conditions in the reforming reactor were chosen rather arbitrarily or dictated by design limitations. An optimization of the process parameters in context with the subsequent utilization process and determination of overall process efficiency has not been carried out.

It is the central intention of this study to investigate the possibility of efficient utilization of concentrated solar power in a reforming process for production of methanol. In order to allow for a broad and representative assessment of the technologies potential, a numerical investigation is carried out.

In chapter 2 the necessary theoretical background on reforming of methane, methanol synthesis and utilization of concentrated solar power is given. Furthermore, the state of the art of solar reforming is presented. Based on this information, in the subsequent chapter 3, a new process for methanol production via solar reforming of natural gas is developed. In 4 a criterion is developed to allow for a meaningful evaluation of processes that use renewable energy for production of products besides electricity. The application of the developed criterion to the investigated process is also presented. The model of the investigated process is presented in chapter 5. In chapter 6, the procedure for process simulation as well as the results are presented. The economic performance of the process is investigated in chapter 7. In order to do so, a methodology is developed and the results are presented. Finally conclusions regarding the overall potential of the investigated process are drawn in chapter 8.

2. Technology Status

Reforming of natural gas is an industrially practiced and well understood process. Therefore, a large amount of knowledge and experience exists that can be widely applied to solar reforming as well. Most importantly, this concerns the availability of commercial catalysts and the already discussed variety of well-developed syngas applications. Due to the difference between the heat sources for conventional reforming and solar reforming, namely combustion of natural gas and concentrated solar radiation, several differences and challenges occur in process design. In more than 25 years of investigation of solar reforming, several concepts for solar reforming where developed and investigated. No specific solar reforming technology is developed in this work, but the potential of the technology in general is assessed. In order to allow for a meaningful investigation, it is necessary to distinguish between the general heating concepts that are discussed in section 2.3. In order to ensure comprehensiveness of the discussion of the different solar reforming concepts, the theoretical background is provided in the following two sections. In section 2.1 and 2.2 the thermochemistry and thermodynamics of the reforming reaction and the fundamentals of the utilization of concentrated solar power are briefly presented.

2.1. Thermochemistry and thermodynamics

In the following two sub-sections, the thermochemistry and thermodynamics of the reforming reactions and the methanol synthesis are briefly discussed. In the discussion the necessary theoretical information is given in order to allow for comprehensibility of this work. An extensive discussion of this topic, is provided in different text books and review articles (e.g. [7, 8, 14, 21]).

2.1.1. Reforming reactions

From a thermodynamic point of view, the reforming of methane can be described by two independent chemical equilibrium reactions, the steam reforming reaction (SR) and the water-gas-shift (WGS). The reactions are presented in Eqs. (2.1) and (2.2) respectively.

$$CH_4 + H_2O \rightleftharpoons 3H_2 + CO \qquad \Delta H^0_{R,298K} = 206 \frac{kJ}{mol} \qquad (2.1)$$

$$CO + H_2O \rightleftharpoons H_2 + CO_2 \qquad \Delta H^0_{R,298K} = -41 \frac{kJ}{mol} \qquad (2.2)$$

For complete description of the reaction system and consideration of kinetics, two further reactions have to be taken into account. These are the reforming of methane with carbon dioxide, the so-called dry reforming reaction (DR), presented in Eq.(2.3), and the combined SR and WGS reaction (SR+WGS), presented in Eq.(2.4).

$$CH_4 + CO_2 \rightleftharpoons 2H_2 + 2CO \qquad \Delta H^0_{R,298K} = 247 \frac{kJ}{mol} \qquad (2.3)$$

$$CH_4 + 2H_2O \rightleftharpoons 4H_2 + CO_2 \qquad \Delta H^0_{R,298K} = 165 \frac{kJ}{mol} \qquad (2.4)$$

As can be seen from the heat of reaction of the different reactions, the process is highly endothermic. Hence, an increase of the heating value of the products compared to the reactants is achieved. Furthermore, the endothermic character indicates that the process is favored by high temperatures. It can also be seen that according to stoichiometry the reactions lead to an increase of moles, therefore the reactions are favored by low pressures. Despite these characteristics, in practice the reactions are carried out at elevated pressures in order to allow for high mass flows and due to pressure requirements of subsequent processes. In industrial applications reforming is operated with outlet temperatures of up to 1000 °C and pressures between 20 – 40 bar [7, 9, 22, 23].

The reforming reactions are catalyzed by transition metals of the VII group of the periodic system. In practice, Ni-based catalysts supported on mixed oxides are commonly used due to low cost and high catalytic activity. Noble metals like ruthenium and rhodium are also suitable but rarely used due to high cost. In order to prevent catalyst poisoning, the reactants have to be free of sulfur contaminants. Therefore, pretreatment of the hydrocarbon material is nearly always necessary. This is commonly done via hydro-desulfurization, which can be considered state of the art [7, 8, 14, 22].

Carbon formation can occur through three different routes: methane cracking (cf. eq. (2.5)), Boudouard reaction (cf. eq. (2.6)) and reduction of carbon monoxide (cf. eq. (2.7)) [7]. Bartholomew and Farrauto [8] state that the use of noble metal, such as rhodium or

ruthenium, can alleviate the risk of carbon formation. For an industrial application this is not a feasible possibility, because noble metals are scarce and expensive. Conditions within the reactor have to be controlled carefully when commercial catalysts are used.

$$\mathrm{CH_4} \rightleftharpoons \mathrm{C} + 2\mathrm{H_2} \qquad \Delta H^0_{\mathrm{R,298K}} = -75\,\frac{\mathrm{kJ}}{\mathrm{mol}} \qquad (2.5)$$

$$2\mathrm{CO} \rightleftharpoons \mathrm{C} + \mathrm{CO_2} \qquad \Delta H^0_{\mathrm{R,298K}} = 172\,\frac{\mathrm{kJ}}{\mathrm{mol}} \qquad (2.6)$$

$$\mathrm{CO} + \mathrm{H_2} \rightleftharpoons \mathrm{C} + \mathrm{H_2O} \qquad \Delta H^0_{\mathrm{R,298K}} = -131\,\frac{\mathrm{kJ}}{\mathrm{mol}} \qquad (2.7)$$

As can be seen from Eqs. (2.5), (2.6) and (2.7), not all three reactions have the same thermodynamic characteristics. While methane cracking and carbon monoxide reduction are exothermic, the Boudouard reaction is endothermic. Therefore, neither very low nor very high temperatures can provide a reaction regime that securely prevents carbon formation. It can be seen that for hydrogen-free feed gas, an increased risk of carbon formation at the entrance exists due to methane cracking. The Boudouard reaction can occur when high carbon monoxide and low carbon dioxide concentration are present in the reactor at high temperatures. The reduction of carbon monoxide is unlikely to occur in steam reforming, when excess steam is added. Furthermore, excess steam will lead to formation of carbon dioxide and prevent occurrence of carbon formation through the Boudouard reaction at appropriate temperatures. However, Boudouard reaction equilibrium will set the maximum temperature and methane cracking will limit the minimum temperature that will allow carbon-free operation. Rostrup-Nielsen [14] states that in steam reforming processes for methanol or hydrogen production with reasonably high steam to natural gas ratio, carbon formation is unlikely to occur. Therefore, in this work, carbon formation in the reactor will not be dealt with and an appropriate ratio of steam to natural gas is set in the simulations. However, for the actual design of reforming reactors this issue has to be dealt with carefully in order to prevent catalyst deactivation. Bartholomew and Farrauto [8] give a detailed approach on how to evaluate carbon formation in a reforming reactor.

2.1.2. Methanol synthesis reactions

The methanol synthesis reactions that are given in Eqs. (2.8) and (2.9) are both exothermic and cause a reduction in amount of substance.

$$\mathrm{CO} + 2\mathrm{H_2} \rightleftharpoons \mathrm{CH_3OH} \qquad \Delta H^0_{\mathrm{R,298K}} = -90.7\ \frac{\mathrm{kJ}}{\mathrm{mol}} \tag{2.8}$$

$$\mathrm{CO_2} + 3\mathrm{H_2} \rightleftharpoons \mathrm{CH_3OH} + \mathrm{H_2O} \qquad \Delta H^0_{\mathrm{R,298K}} = -49.5\ \frac{\mathrm{kJ}}{\mathrm{mol}} \tag{2.9}$$

They are therefore promoted by low temperatures and high pressures. However, as can be seen from the kinetics published by van den Bussche and Froment [24], the reaction rates are promoted by high temperatures. Olah et al. [19] give values for typical pressure and temperatures in the methanol reactor when state of the art copper-zinc based catalysts are used. They give values of 200 °C and 300 °C for temperature and 50 – 100 bar for pressure. However, according to Bartholomew and Farrauto [8] the conversion of hydrogen into methanol per pass is limited to 8 – 15 % at those conditions. They state that a separation of water and methanol from the reactor product and recycle of the unreacted components to the reactor is state of the art. They report typical recycle ratios of 3-7 for commercial methanol plants.

In order to obtain a syngas suitable for methanol synthesis, a favorable ratio of H_2, CO_2 and CO has to be achieved. Different forms of these ratios have been proposed, all refer to mole fractions z of the species. A ratio of 1.05 for H_2 / (2 CO + 3 CO_2) is proposed by Bartholomew and Farrauto [8] while Huber et al. [25] proposes a ratio of 2.05 for the ratio M that is defined according to Eq. (7.5). It quantifies the ratio of the difference between the molar hydrogen and carbon dioxide fraction to the sum of molar carbon dioxide and carbon monoxide fraction.

$$M = \frac{z_{\mathrm{H_2}} - z_{\mathrm{CO_2}}}{z_{\mathrm{CO_2}} + z_{\mathrm{CO}}} \tag{2.10}$$

2.2. Concentrated solar power for reforming processes

A variety of technologies for concentration and utilization of solar energy exists. The technologies for concentration of the radiation can generally be distinguished between line-

focusing and point focusing. Due to the finite dimensions of the picture of the sun on earth, the concentration of the radiation is geometrically limited. On earth, these limits are a concentration ratio of 213 for linefocusing systems and 45,613 for point-focusing systems [26]. The concentration factor C_{Conc} is defined in Eq.(2.11): The flux onto the aperture I_{Ap} in relation to the direct normal radiation at the surface of the earth DNI (direct normal irradiance). In practice, line-focusing systems achieve concentration ratios around 100, power towers 500 to 1000 and dish-systems can achieve several thousand.

$$C_{\mathrm{Conc}} = \frac{I_{\mathrm{Ap}}}{DNI} \tag{2.11}$$

A detailed description of the solar power tower technology and its components goes beyond the scope of this work and can be reviewed in available textbooks and literature (e.g. Pitz-Paal et al. [27], Stieglitz and Heinzel [26]). However, the general principle has to be kept in mind: As shown in Figure 2-1, a large number of heliostats is used to redirect the solar radiation to the central receiver that is located at the top of a tower. They compensate for the apparent movement of the sun by *tracking*, i.e. adjustment of their orientation, so that the reflection of the sun is always redirected in the direction of the receiver. In the solar receiver the concentrated radiation - usually between a few hundred to a thousand kW/m² in the aperture area of the receiver - is absorbed by a solid material, and thereby converted into heat. The heat is transferred to a heat transfer fluid (HTF) which is used to transport the heat to the process that is supposed to be heated which is most commonly a water steam cycle (WSC) or, as in the case of this work, the reforming reactor. Some aspects regarding the efficiency of the solar receiver are discussed in more detail in the following.

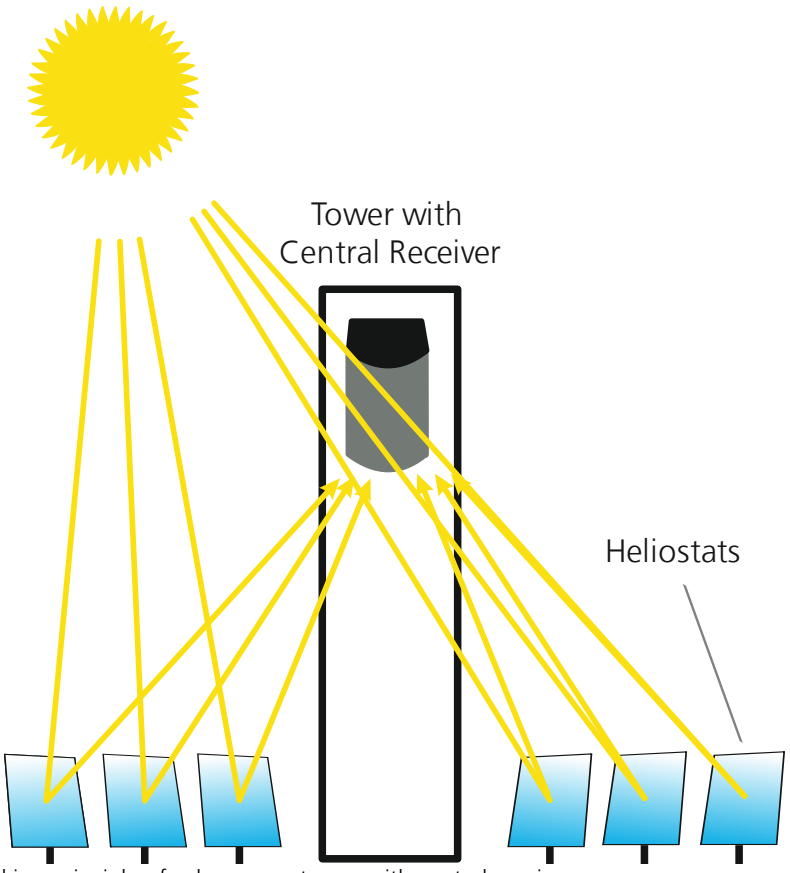

Figure 2-1: Working principle of solar power tower with central receiver

In Eq. (2.12) a generic energy balance of a solar receiver is given it includes all terms that principally occur independently of the type of receiver. The useful heat flow $\dot{Q}_{\mathrm{use}}$ is the difference between the absorbed radiation $\dot{Q}_{\alpha}$ and the re-emitted heat flux $\dot{Q}_{\varepsilon}$ and the heat losses by convection and conduction, $\dot{Q}_{\mathrm{Conv}}$ and $\dot{Q}_{\mathrm{Cond}}$ respectively. An ideal receiver will have neither conductive nor convective losses, hence its energy balance will simplify to Eq. (2.13); these assumptions may also be valid for some real receivers. In Eq. (2.13), the first term represents the absorbed radiation, i.e., the product of the effective absorptivity of the aperture α_{Ap}, the area of the aperture A_{Ap} and the incident flux density onto the aperture I_{AP}. The second term of the equation represents the losses through re-radiation, i.e., the product of emissivity $\varepsilon_{\mathrm{AP}}$, the aperture area, the Stefan-Boltzmann constant σ and the absorber surface temperature to the power of 4. An ideal receiver will behave as a black body absorber. Therefore, the value for the absorptivity α_{Ap} as well as the value for the emissivity $\varepsilon_{\mathrm{AP}}$ will equal 1 [28].

$$\dot{Q}_{\mathrm{use}} = \dot{Q}_{\alpha} - \dot{Q}_{\varepsilon} - \dot{Q}_{\mathrm{Conv}} - \dot{Q}_{\mathrm{Cond}} \tag{2.12}$$

ideal receiver:
$$\dot{Q}_{\mathrm{use}} \approx \alpha_{\mathrm{Ap}} A_{\mathrm{Ap}} I_{\mathrm{Ap}} - \varepsilon_{\mathrm{Ap}} A_{\mathrm{Ap}} \sigma T_{\mathrm{Abs}}^4 \tag{2.13}$$

The energy efficiency of a solar receiver is commonly defined as the useful heat flow divided by the intercept radiation. For an ideal, non-volumetric receiver without convective or conductive losses, the efficiency can be described as shown on the right hand side of Eq. (2.14) [29].

$$\eta_{Receiver} = \frac{A_{Ap} I_{Ap} - A_{Ap} \sigma T_{Abs}^4}{A_{Ap} I_{Ap}} = 1 - \frac{\sigma T_{Abs}^4}{I_{Ap}} \tag{2.14}$$

Considering that the flux density onto the aperture is determined through direct normal irradiance (DNI) that hits the heliostat field area A_{HF} multiplied with the heliostat field efficiency η_{HF}, the receiver efficiency can be expressed as shown in Eq. (*2.15*).

$$\eta_{Receiver} = 1 - \frac{\sigma T_{Abs}^4}{DNI \cdot A_{HF} \cdot \eta_{HF}} \tag{2.15}$$

In Figure 2-2 the efficiency of an ideal receiver, in dependence of absorber surface temperature and concentration factor is shown. It can be seen that the efficiency for line focusing systems decreases significantly for temperatures above 700 K. Therefore, in order to achieve the temperatures required for solar reforming (>> 600 °C / 873 K) point-focusing technologies seem more suitable than line-focusing systems with lower concentration ratios. Furthermore, it can be expected that solar reforming will be carried out in plants with a capacity of at least several MW thermal power in order to benefit from lower specific plant cost for large scale. Dish concentrators will likely be limited to capacities below this [27]. Therefore, only solar power towers appear to be suitable for provision of solar energy to the reforming reaction.

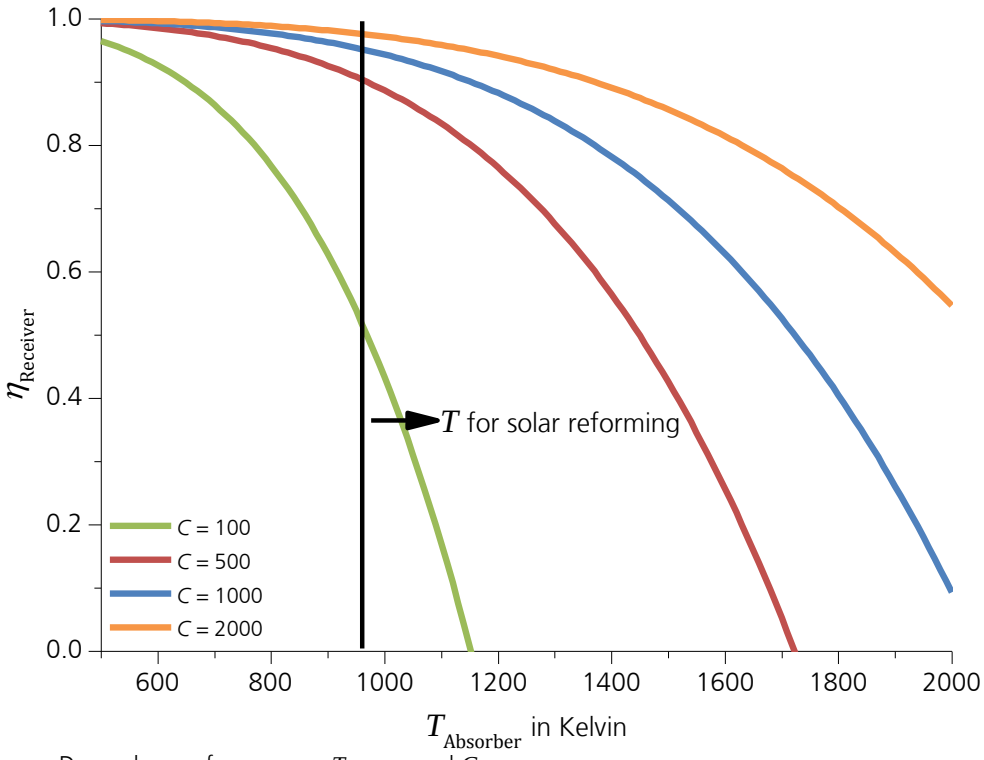

Figure 2-2: Dependency of η_{Receiver} on T_{Absorber} and C_{Conc}

For a solar receiver with a cavity-type geometry, the aperture area is smaller than the absorber area, whereas for a regular receiver the areas are identical. In an ideal cavity type receiver, the radiation into the aperture will be well distributed on the absorber area A_{Abs} inside the cavity, resulting in a lower flux onto the absorber than into the aperture. The ratio is approximated by the ratio of the areas (Eq.(2.16)).

$$C_{\text{Cav}} = \frac{A_{\text{Ap}}}{A_{\text{Abs}}} \approx \frac{I_{\text{Abs}}}{I_{\text{Ap}}} \tag{2.16}$$

The ratio of aperture to absorber area is called C_{Cav} in the following. The difference between a flat absorber and a cavity absorber is further illustrated in Figure 2-3:

Geometry and flux density of a flat- and a cavity type . In the figure, it is indicated, how the radiation is distributed over the absorber area. The distribution results in a reduction of flux density onto the absorber compared to a flat receiver.

Figure 2-3: Geometry and flux density of a flat- and a cavity type absorber

Furthermore, the cavity geometry will increase absorptivity and emissivity of the cavity, as (multiple) reflections occur on the absorber surface walls before the radiation leaves the cavity [29]. The effective absorptivity α_{Ap} of a receiver can be calculated as presented in Eq. (2.17). The calculation can be applied to the emissivity as well. It can be seen that for small values of C_{Cav} the effective absorptivity approaches the value 1. Therefore, the influence of the intrinsic absorptivity of the absorber α_{Abs} structure on the optical properties of the receiver is small for receivers with small values of C_{Cav}. This indicates that for cavity absorbers the effective optical properties are improved compared to flat absorbers.

$$\alpha_{Ap} = \frac{\dot{Q}_{\alpha}}{I_{\mathrm{Ap}} \cdot A_{\mathrm{Ap}}} = \frac{\alpha_{\mathrm{Abs}}}{C_{\mathrm{Cav}} + \alpha_{\mathrm{Abs}} \cdot (1 - C_{\mathrm{Cav}})} \tag{2.17}$$

In utilization of concentrated solar power, energy storage systems are commonly used in order to extend the time of operation for several hours beyond sunset or even allow for base-load operation nearly continuously [30]. For instance, solar reserve reports In order to allow for high capacity factors of the power block, the capacity of the solar part of the system is designed larger than the power block. The factor between the nominal capacity of the solar part and the nominal capacity of the power block is commonly referred to as solar multiple (SM). In this work, the solar multiple is defined as the nominal thermal capacity of the receiver in relation to the nominal capacity of the subsequent process.

2.3. Solar reforming concepts

In the past, a large number of concepts for introduction of solar energy into the reforming reactor have been proposed. Except for some more exotic concepts, all concepts can be categorized as one of the two following:

1. Indirectly heated reactor with use of a heat transfer fluid (HTF)
2. Directly irradiated receiver-reactor

In the following paragraphs, these two concepts are discussed regarding their general characteristics and an overview of the corresponding research activities is given. However, no detailed review of past research projects is provided. An extensive overview of past research projects is given by Agrafiotis et al. [9] and by Sheu et al. [31].

2.3.1. Indirectly heated reactor

Solar reforming with an indirectly heated reactor refers to a concept where a HTF is heated in any type of solar receiver that is capable of providing the required temperature. The HTF is then transported to a reforming reactor where it provides heat to the endothermic reaction. A sketch of this concept is depicted in Figure 2-4.

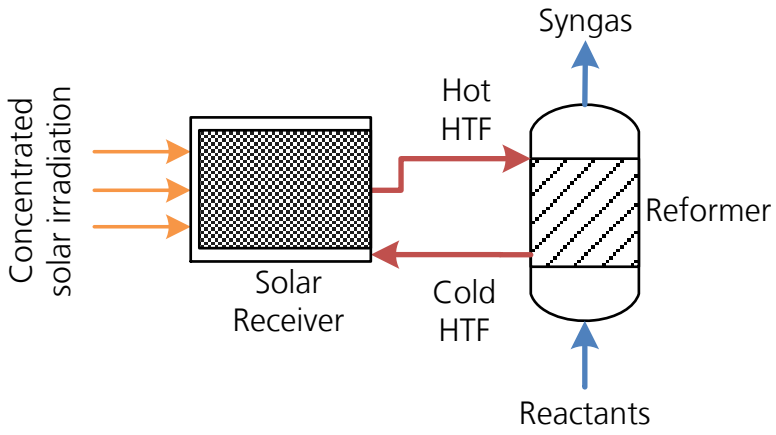

Figure 2-4: Concept of solar reforming with indirectly heated reactor

The main disadvantage of this system is the reduction of efficiency due to the temperature difference between absorber temperature and reforming temperature: The importance of high temperature for high conversion in reforming was stated. When achieving a given syngas outlet temperature the absorber temperature has to be higher than the syngas outlet temperature. As mentioned previously, thermal radiation of the receiver front due to its elevated temperature is a significant factor for the efficiency of CSP systems. Therefore, in this concept the radiative losses will be higher than in a directly irradiated concept. Another disadvantage that was already reported by Langnickel and Böhmer [32] in 1993 refers to the start-up of the system which will take several hours even after shutdown only for the night due to constraints in the heat-up rate of the reforming reactor. Therefore, continuous operation of the process, either by utilization of heat storage or by co-firing, does not seem to be an option but rather a necessity. So far it has not been assessed if optimization of the reformer design can reduce the start-up time.

The general benefits of this concept are easier technical realization, more degrees of freedom in process design and as a result thereof, easier process control. In general, a wide range of solar receiver types can be used for this process. However, in order to achieve high conversion of methane in the reformer, the choice is limited to receivers that can provide a heat transfer fluid with a temperature exceeding 650 °C, in order to allow for methane conversion greater 85 % at ambient pressure and reasonable steam to methane ratios [9]. The same applies to the choice of heat transfer fluid: Because there is no contact between the reacting gases and the HTF, principally the only limitation in the choice of HTF is the

necessary temperature level (if corrosion and material degradation are neglected). For example, it is unlikely that molten salts will play a significant role in solar reforming, as operating temperatures of only 565 °C are state of the art and only 650 °C are anticipated in the medium term [33]. However, gases like air, nitrogen, carbon dioxide, or steam can be applied in solar reforming. The possibility of utilizing air as HTF enables the utilization of open receiver concepts. Furthermore, due to the separation of the heat transfer loop and the reforming part, integration of heat storage or co-firing, e.g. for continuous operation at lower values of DNI, as well as for an increase of the reforming temperature, are possible in this concept. McNaughton [34] also states those advantages are the main reasons for CSIRO's current activities dealing with an air heated solar reformer. Furthermore, he states another significant advantage compared to directly irradiated concepts for solar reforming: At non-uniform irradiation of a conventional receiver, the efficiency may decrease, but the outlet temperature can be kept constant, resulting in constant reforming conditions. In a directly irradiated concept, this is not the case. This will lead to an overall reduction in methane conversion and may furthermore cause carbon formation due to hot spots in the receiver.

2.3.2. Directly irradiated receiver-reactor

The solar reforming process can be intensified to a single core unit that would be most appropriately be called a *receiver-reactor,* because the solar receiver also serves as reactor. Within this concept a further distinction between two concepts is necessary. Firstly, reactors with irradiated outer surface and secondly with directly irradiated catalyst. In the latter a window is necessary to prevent mixing of the gases with the surrounding while letting in the radiation.

A schematic of a receiver-reactor with irradiated outer wall is shown in Figure 2-5. In this concept, the outer reactor wall absorbs the irradiation and transports it into the reaction volume conductively. The heat transfer from the outer reactor wall into the reaction volume is the limiting factor in heat supply. Therefore, the radiative flux onto the reactor tubes is very limited: Levitan et al. [16] report experiments with a maximum flux onto the reactor wall of 100 kW/m². Uhlig et al. [35] report a flux onto the tubes of a tubular air receiver

(that has similar characteristics in this respect) of approximately 50 kW/m². In this concept, the outer wall temperature of the reactor limits the reaction temperature, as that is the hottest part of the process. This temperature difference states a similar problem as already discussed for the indirectly heated concept. However, for the directly irradiated receiver-reactor concept, it is even more dominant, as the temperature difference between outer and inner surface of the tubes is usually larger. Due to the low limits of radiative flux and high required temperatures, it seems most reasonable to realize this concept in a cavity receiver geometry. It was studied by WIS in 1989 [16]. Later, the concept was further developed and tested by CSIRO with the SCORE and DCORE receiver-reactors [11].

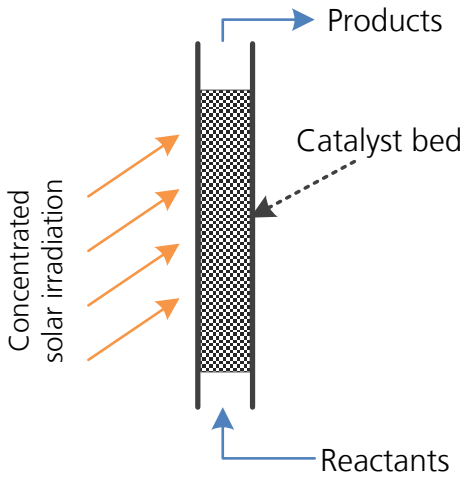

Figure 2-5: Concept of solar reforming with directly irradiated reactor

In the concept of the directly irradiated catalyst, a porous ceramic structure, coated with catalyst is used for absorption of the concentrated solar radiation and serves as reaction surface. The receiver-reactor is closed with a quartz window in order to prevent losses of the reactants, prevent intrusion of air and to enable operation above ambient pressure. A schematic of this concept is depicted in Figure 2-6 (left). In Figure 2-6 (right) an example of a porous ceramic absorber structure is shown.

The principal benefit of this concept is that the reaction takes place at the hottest site of the receiver. Furthermore, because the reforming reaction, which acts as a large energy sink, takes place in the absorber volume, high energy fluxes are possible, which leads to small apertures, resulting in lower re-radiation losses of the receiver [36]. Therefore, compared to the other concepts, the directly irradiated catalyst has the potential to achieve highest efficiencies. Beyond this, the system can respond rapidly to thermal transients and start-up time is short [36]. However, this is an ambivalent effect: On the one hand start-up and shut down times are reduced, on the other hand even small changes in DNI (e.g. cloud passage) can cause dramatic changes in reaction/absorber temperature and lead to coking in the catalyst or, damage the absorber. Furthermore, the previously stated difficulties with non-uniform radiation onto the absorber are especially severe for this concept when it is operated at high flux densities. Therefore, process control is a demanding challenge of this concept. As shown in the past research projects by Buck et al. [36] and Abele et al. [37], the difficult controllability can cause severe damage to the system.

Despite the challenges, this concept has been proved feasible. In the projects *SOLASYS* and *SOLREF*, a consortium of DLR and WIS, as well as other partners, constructed and tested receiver-reactors with catalytically active foam successfully [38, 39]. WIS successfully constructed and operated a receiver-reactor with their previously developed *porcupine* receiver [40].

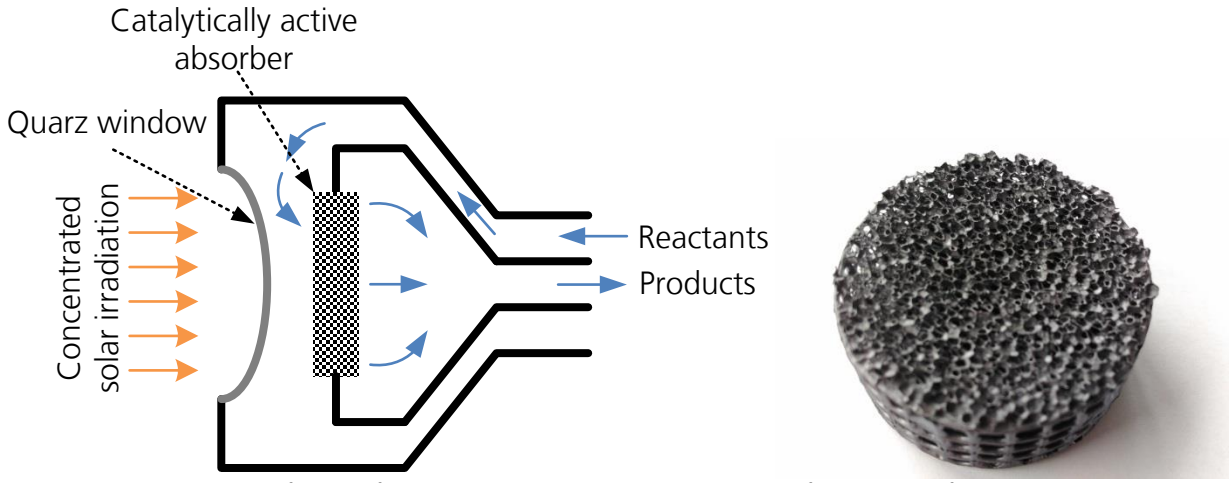

Figure 2-6: Concept of solar reforming with directly irradiated catalyst (left), example of porous ceramic absorber structure

A disadvantage of the directly irradiated catalyst is the limited pressure level. Even though the achievable temperatures would allow reforming pressures comparable to the ones realized in industrial practice (i.e. > 40 bar), the highest reported pressures for these types of receiver-reactors are 15 bar [9]. In addition to that, due to limitations in maximum diameter of the quartz window, the size of a receiver reactor is limited to below 1 m² aperture area. Therefore, for large scale utilization of this technology, a modular approach is necessary. This is expected to increase the costs significantly.

A major and principal disadvantage of both concepts of directly irradiated receiver-reactors is inherent to the concept itself: Due to the intensification of two process steps in one process unit (conversion of solar energy into heat and conversion of heat into chemical energy), the degree of freedom in design of the unit is significantly decreased. As early as 1991 the Russian researchers Vladimir I. Anikeev and Valery A. Kirillov state: "As a rule, the design of ideal receiver of solar radiation does not meet the requirements of ideal catalytic reactor" [41]. Therefore a receiver-reactor will always be a compromise between an ideal receiver and an ideal reactor. Furthermore, implementation of heat storage or co-firing for night time operation of the reactor is difficult in these concepts.

3. The SOLME Process

To the best of the authors knowledge, no process for production of methanol via solar reforming has been proposed in the past. Therefore, such a process is developed within this work. It will be called the SOLME (solar methanol) process and is the result of merging the solar reforming process part with conventional methanol synthesis. In order to allow for a specific design of the process, the solar reforming concept is selected in section 3.1. The SOLME process itself is developed in section 3.2. The different process parts are adjusted to yield an overall process which is energy – and material efficient. This aim is achieved by heat integration, hence minimizing waste energy streams.

3.1. Selection of investigated solar reforming technology

As discussed in the previous chapter, both indirectly heated solar reforming as well as directly irradiated solar reforming have advantages as well as disadvantages in comparison to the other concepts. The additional degrees of freedom in process design in the indirectly heated system, as well as the possibility to implement co-firing and heat storage for night-time operation makes the indirectly heated concept an interesting option for integration into a methanol synthesis plant. Furthermore, the imbalance in past research activities towards directly irradiated concepts underlines the necessity to investigate the indirectly heated concept further. Therefore, the indirectly heated concept is selected for investigation in this work.

For the indirectly heated concept, a heat transfer fluid for the heat transport between solar receiver and reforming reactor has to be selected. Due to the lack of commercially available non-gaseous heat transfer media suitable for the given temperature range, air is chosen as heat transfer medium for the process. This choice seems reasonable as air is abundantly available, not associated with any cost, and not harmful in any way. Only few solar receivers exist that use air as heat transfer fluid. One of those is the open volumetric receiver (OVR) as it is installed at the solar tower in Jülich [42]. The OVR is chosen as the receiver for these investigations, because it has the potential to provide air at suitable temperatures and its technical feasibility has been proven at the solar tower in Jülich.

However, not only the current state of the art of the OVR is taken into account, but parameter variations are conducted in order to assess possible improvements of process efficiency by modifications in receiver design. One crucial aspect that is investigated is the utilization of a cavity-type absorber in the receiver in order to enhance the receiver performance. As shown in a previous study, an open volumetric cavity receiver has the highest potential among the common air receivers for efficiently providing heat to a solar reforming reactor [43]. Another important parameter that is varied is the air return ratio of the receiver. For one part, it is varied because the actual value of the air return ratio is not known exactly. Furthermore, the improvement of the air return ratio is currently investigated in several research projects [44].

3.2. Process Description

The objective of the SOLME process is to produce methanol from natural gas via solar reforming. A simplified flowsheet of the process is presented in Figure 3-1. The flowsheet is developed in order to allow for a reasonable utilization of heat and mass flows of the different process parts. The process is divided into the three main process parts *Solar, Reforming*, and *Methanol Synthesis* (MS), as well as the secondary parts water-steam-cycle (*WSC*) and combined cycle gas turbine (*CCGT*). It can be seen that the required resources for the process are natural gas, solar energy and water, while electricity and methanol are the products. The mixture of natural gas and water is heated and reacts to syngas in the reforming part of the process. The required heat is mainly provided by the solar receiver, and to a smaller extent by combustion of off-gas from the methanol synthesis reactor. The syngas product is cooled in order to condensate excess water and compressed before entering the methanol synthesis part. In the methanol synthesis part, it reacts to methanol. Before distillation, the product is raw methanol with a water content of approximately 20% which needs further purification in a rectification column. Most of the heat required by the reboiler of the column can be provided by the off-heat from the methanol synthesis, if necessary, the rest is obtained by further cooling the hot air flow before returning it to the solar receiver. The heat supply for the column from hot air flow is not shown in the flow sheets in order to maintain clarity of the figures. A WSC is implemented into the process to

make use of off-heat from the reforming part. The MS also produces an off-gas stream with a significant heating value that can be combusted in a CCGT to produce electricity. Alternatively, a part of the off-gas stream can be combusted in a secondary reformer (SecRef) to allow for a lower receiver outlet temperature at constant reforming outlet temperature. This practice will positively influence the receiver efficiency, as the receiver outlet temperature can be decreased while the reforming temperature, which is decisive for the conversion, remains constant. As discussed in section 2.2 and shown in Figure 2-2, a decrease in absorber temperature will lead to a receiver efficiency increase. The extent of the efficiency increase depends on the concentration factor and the temperature. The improvement of solar receiver efficiency competes with the efficient conversion of the off gas into electricity. Determining the optimum fraction of off-gas to be used in the SecRef is a matter of optimization and dependent on other process parameters. The parameter that describes the fraction of off-gas that is used in the SecRef is called f_{Split}; it is defined as the ratio of the off-gas used for the temperature lift of the reforming reaction (TL) $F_{\mathrm{Off-Gas,TL}}$ to the total amount of off-gas $F_{\mathrm{Off-Gas}}$ (cf. eq. (3.1)).

$$f_{\mathrm{Split}} = \frac{F_{\mathrm{Off-Gas,TL}}}{F_{\mathrm{Off-Gas}}} \tag{3.1}$$

In the following, the process parts are described in detail. The CCGT part is not described because it is not modelled in detail. It is only taken into account for by assuming an efficiency for the conversion of heating value of the off-gas into electricity. The off-gas burner is also not described in detail, as it is merely a conversion of the heating value of the off-gas into heat, assuming a flue gas exit temperature of 100 °C. In both cases the lower heating value is considered.

3.2.1. Solar part

The solar part of the process, which is depicted in Figure 3-2, consists of the heliostat-field and the solar receiver, as well as the fan to transport the air through the system and optionally a thermal energy storage (TES). The heliostat field is designed to redirect the solar radiation onto the receiver to generate a concentrated flux of solar energy onto the receiver aperture. In the receiver, the radiation is converted into heat in order to increase the

temperature of the air that is used as HTF. The air is heated to temperatures between 600 °C and 1000 °C, the actual temperature is a matter of optimization. Subsequently, the air is cooled by providing heat to the reactants in the reforming part of the plant and to provide heat to the distillation column for purification of methanol. Finally, in order to make up for pressure drop in the process units, a blower is needed. Due to thermodynamic considerations, the blower is located at the coldest part of the air system, before the solar receiver. Hence, the pressure in the air circuit is below ambient pressure, i.e. the blower sucks the air through the system, rather than pushing it.

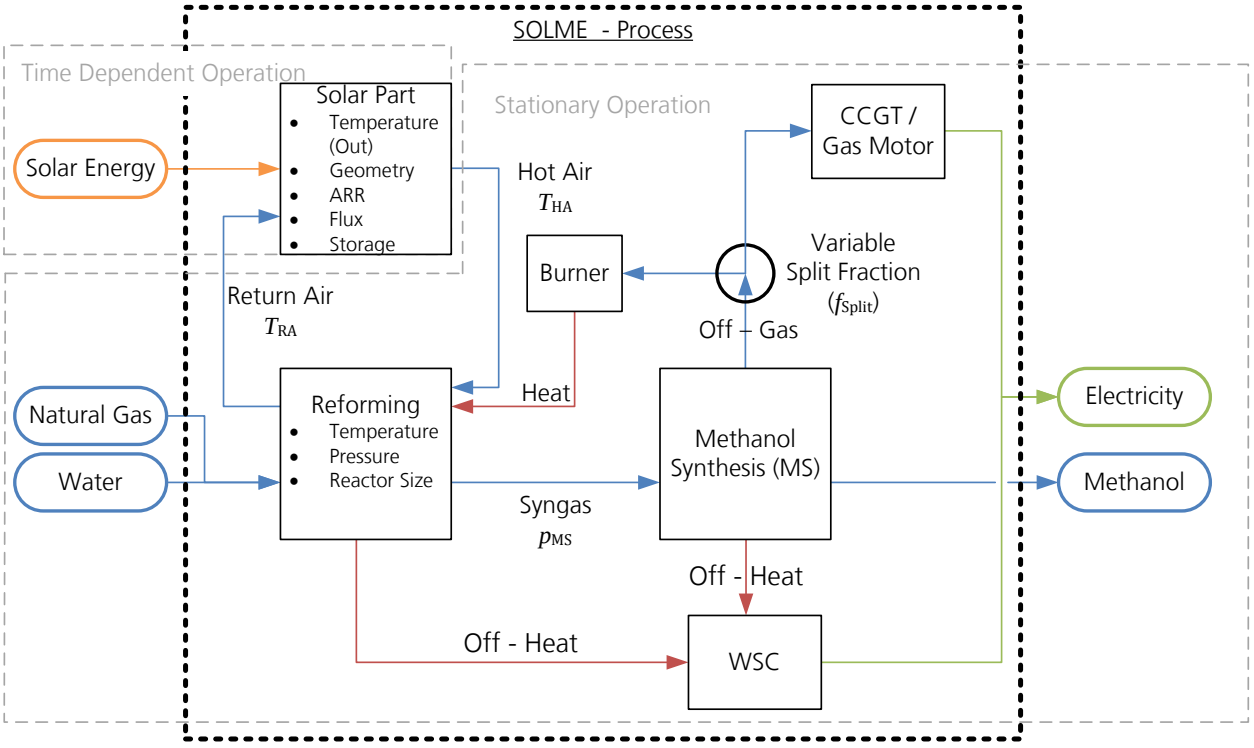

Figure 3-1: Overview of SOLME Process with central process parameters

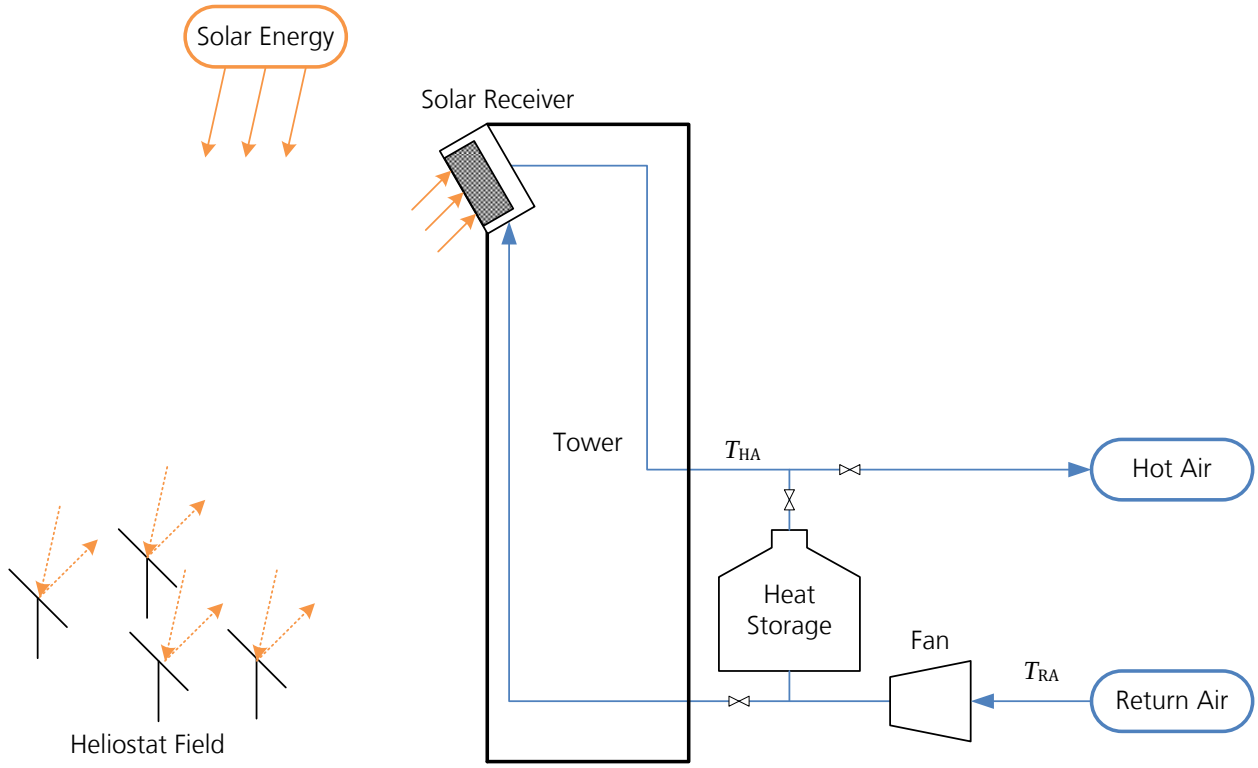

Figure 3-2: Solar part of the process

As mentioned in section 3.1, an open volumetric receiver is considered to provide solar heat to the process. However, not only the state of the art of this receiver type is taken into account, but also potential improvements are considered. For one part, this is taken account for by consideration of a receiver with a cavity-type absorber. Sketches of the principal geometry and air flows are shown in Figure 3-3 (right). The cavity geometry is expected to be beneficial for an absorber implemented into the reforming process, as it will reduce the re-radiation losses, which are particularly high for the high temperatures necessary for solar reforming (cf. section 2.2). The shape of the cavity and the value C_{Ap} are not predetermined and different shapes are possible. However, since this is not the central topic of this work, only one geometry is considered in this context: The absorber has the shape of a half cylinder, resulting in C_{Ap} = 0.637 (equal to 2/π).

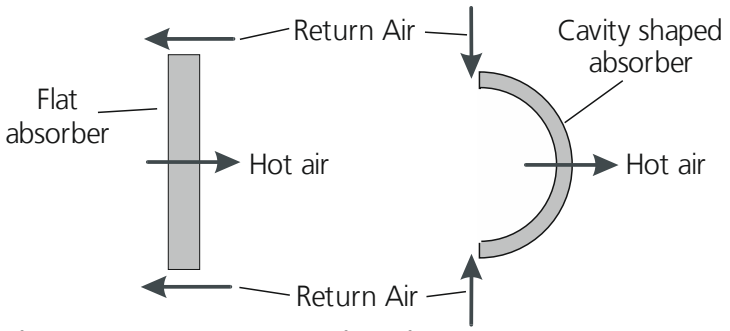

Figure 3-3: Sketch of open volumetric receiver with flat (left) - and with cavity (right) - absorber

An important feature of the open volumetric receiver to be discussed is the open air circuit with air return. In most receiver concepts, the HTF circuit is closed, hence the HTF is returned to the receiver after heating the process. Usually, this is the only possible configuration as most HTF's have significant costs and disposal after one circuit is not feasible, neither from an economic point-of-view, nor considering the associated logistics. Furthermore, usually the HTF still has a temperature well above ambient temperature when it leaves the process so that this heat can be recycled when the HTF is returned to the receiver after the process for re-heating. In contrast, the HTF circuit of an open volumetric receiver is open due to the nature of this concept. However, the air also leaves the process with a temperature above ambient temperature and its disposal will decrease the efficiency due to thermal losses. To reduce these losses, the return air is not ejected to the environment but ejected in vicinity of the absorber allowing for a partial recycling of the air. The location of the return air ejection can be varied and its optimal configuration is still a matter of research. The recycled air together with air from the environment are sucked through the absorber, where they are heated. A schematic of the air return concept is shown in Figure 3-4. The air return ratio (ARR) describes the fraction of the return air that is actually sucked into the absorber, hence recycled.

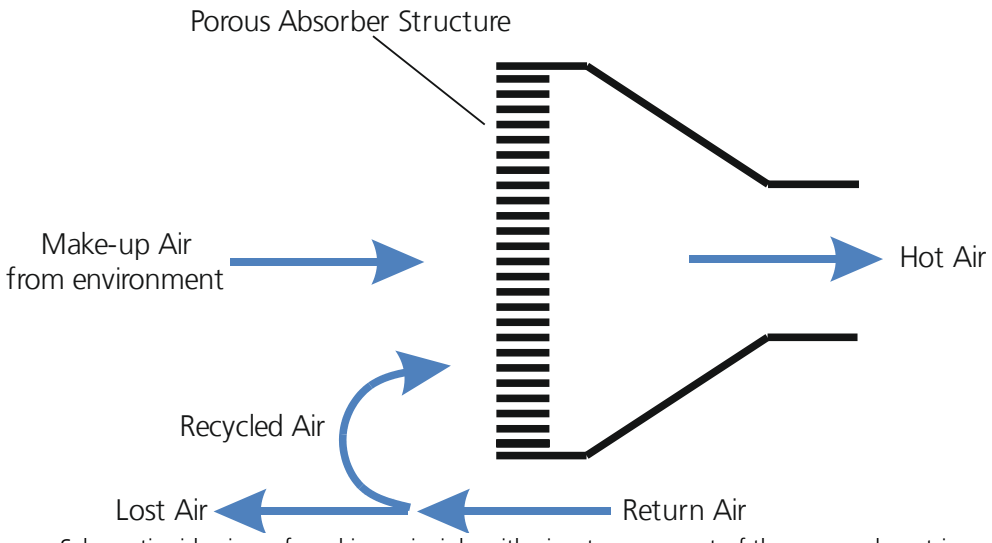

Figure 3-4: Schematic side view of working principle with air return concept of the open volumetric receiver

Due to limited availability of solar radiation, the receiver produces the hot air flow during less than 4000 h per year with approximately 2000 full load hours per year. Therefore, the load factor of the methanol plant will be less than 0.25 if no TES is implemented. In order to be able to produce the same amount of methanol with a significantly smaller methanol plant, a TES can be implemented. Considering the high temperatures at which the process is operated, a regenerator-type heat storage made from ceramic structures, as implemented in the solar tower in Jülich (cf. [45]), seems to be the most feasible technology to be implemented. In this storage concept, the hot air passes through the ceramic structures, which are heated up to the air temperature. To discharge the storage, the air flow is reversed and air is heated by flowing through the structures.

The design of the TES for any type of a solar plant is a matter of economic optimization, as no significant thermodynamic benefits can be expected from its implementation. Therefore, in the thermodynamic investigations in chapter 6, the TES will not be investigated, but an ideal storage, which distributes the heat provided by solar energy evenly over time, is considered. Hence, the hot air flow provided by the solar part is assumed to be constant and fluctuations in solar energy provision only influence operation of the solar receiver, but not the reforming - or methanol synthesis part of the process.

3.2.2. Reforming part

In the reforming part, the natural gas and water input is converted into syngas, under presence of a Nickel-based catalyst. The flowsheet of this process section is presented in Figure 3-5: The hot air from the solar part provides the heat required to perform the reaction in the air-heated reactor (AHR) which is in principle a heat exchanger with countercurrent flow and a catalyst located in the reaction volume on the cold side of the heat exchanger. After leaving the reactor, the HTF still contains sufficient heat to evaporate the water for the reaction. The temperature of the natural gas feed is increased during compression, so that the reactant mixture entering the reactor already has a temperature well above 300 °C. The actual temperature strongly depends on reforming pressure. The compression to the reforming pressure causes a significant expenditure of electrical energy, while the energy necessary for pumping the water is negligible. In the reforming reactor, the gas mixture reacts according to the Eqs. (2.1) and (2.2). Those two reactions are sufficient to describe the overall conversion, as the reactions (2.3) and (2.4) are linear combinations of Eqs. (2.1) and (2.2). If a fraction of the off-gas is combusted to provide heat to the reforming reaction, a secondary reformer (SecRef) operating at a temperature higher than the temperature of the hot air flow is implemented. The product of the AHR is referred to as the intermediate reforming product, while the product of the SecRef is referred to as the reforming product. After leaving the reforming reactors, the hot syngas is cooled by transferring its heat to the water steam cycle. The heat from the syngas cannot be used to pre-heat the reactants, because the temperature of the warm air would be significantly increased and hence the receiver efficiency would be reduced.

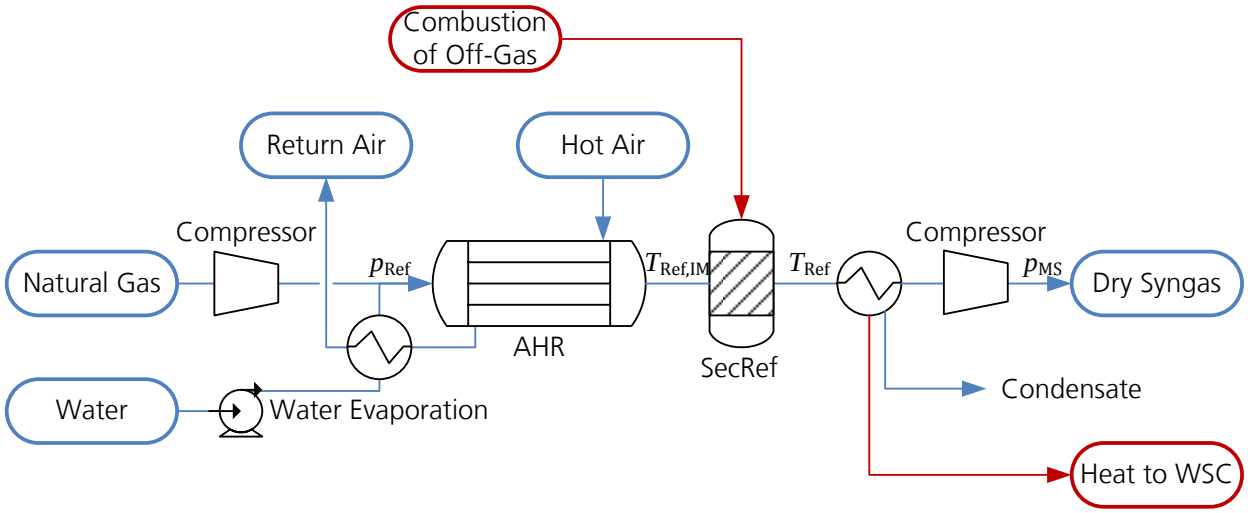

Figure 3-5: Reforming part of the SOLME process

The AHR is carried out as a bundle of jacketed tubes, where the inner tube is the reaction volume and filled with catalyst pellets, while the hot air flows through the annulus. This geometry was studied intensively by Wesenberg [46] to be applied as a gas-heated reformer. In contrast to the work presented by Wesenberg, where hot syngas serves as heating medium and only partial conversion (approx. 30 %) is aimed for, close to complete conversion is aimed for in the AHR. However, the jacketed-tube reactor only serves as an example for a gas-heated reformer in this work. It is chosen because of its simplicity and similarity to conventional reformers, but other applicable geometries exist. One promising candidate type for this application is the catalytic-plate microchannel reactor, as investigated by Pattison and Baldea [47]. These types of reactors are especially promising for small-scale reforming of methane. Therefore, they may be well applicable to solar reforming, too. However, as catalytic plate microchannel reactors are still a matter of research, the scope of this work will be limited to the jacketed tube type reactor.

3.2.3. Methanol synthesis part

As can be seen in the flowsheet of the methanol synthesis in Figure 3-6, the product from the methanol synthesis reactor is cooled and the liquid fraction (mainly methanol and water) is separated from the unreacted gaseous fractions in the product stream. The gaseous fraction is recycled to the reactor feed. The recycle stream and the inlet syngas stream are preheated with the reactor outlet stream. A small fraction of the recycle stream

is purged in order to prevent accumulation of inert species in the loop (methane and nitrogen). This purge gas stream is the previously mentioned off-gas. The liquid output of the separator is further purified by a flash-unit, where the pressure is reduced to 2 bar and most of the remaining content of hydrogen, carbon monoxide, carbon dioxide, methane and nitrogen are evaporated and returned to the reactor inlet. The liquid outlet of the flash unit is raw methanol with a mole fraction of water of around 0.2 and minor impurities. The raw methanol is then purified in a distillation column to 99%mol- % with a recover ratio of 99.9 mol-%.

The methanol synthesis reactor is a tubular boiling-water reactor with the reactions (2.8) and (2.9) occurring inside the tubes. Note that reaction (2.9) is a linear combination of the reactions (2.8) and (2.2). This type of reactor is chosen because of the advantages stated by Bartholomew and Farrauto [8]: High thermal efficiency, long catalyst life and low yield of byproducts. Outside the tubes pressurized water is evaporated in order to remove the heat of the exothermic reactions. The pressure level of the water is selected to provide an isothermal heat sink at the desired temperature (evaporation temperature at the given pressure) to the reactor. The steam could also be used in the WSC if another heat stream was available for heating the distillation column.

In Figure 3-6 the methanol synthesis part of the process with the fixed values for central process parameters in the process is shown. Most of the process parameters are chosen in accordance with the study presented by Luyben [48]. The pressure in the methanol synthesis is set to 100 bar, the pressure of the cooling water is set to 39.25 bar, resulting in a temperature of 252 °C of the saturated steam and a product temperature of 265 °C. The temperature in the separator is set to 38 °C and the pressure in the flash unit to 2 bar. The fraction of the purge stream in relation to the overall recycle stream is 0.023, which should not be confused with the previously introduced split fraction for the off gas f_{Split}.

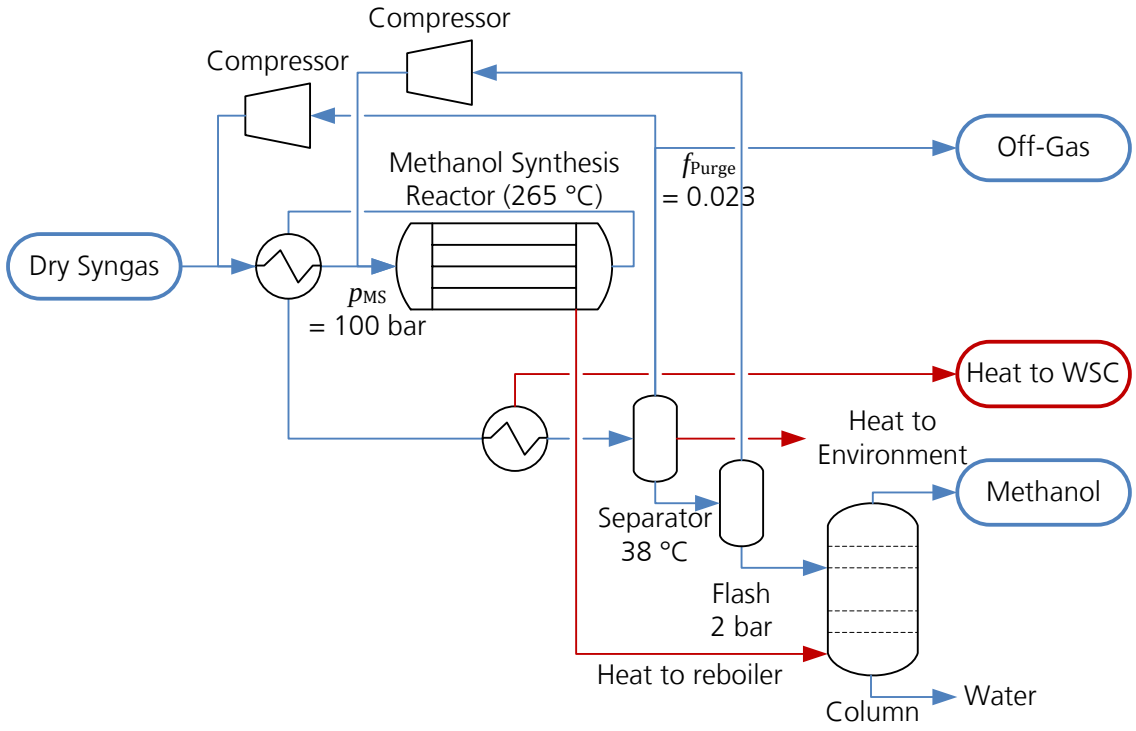

Figure 3-6: Methanol synthesis in the SOLME process

3.2.4. Water-Steam Cycle

The design of the water-steam cycle for the SOLME process is a challenging task because of the unusual type of heat source. The most similar heat source that is industrially used is the exhaust gas from gas turbines that provides heat to the heat recovery steam generator in CCGT plants.

The high pressure (HP) level of the WSC is chosen as 113 bar in accordance with literature on the WSC in CCGT's [49]. The exhaust steam of the HP turbine is reheated at 39.25 bar in order to allow for a utilization of the steam produced by the methanol synthesis reactor for the case that this steam is not required for the distillation column. In Figure 3-7 the temperature of the syngas flow as well as the four pressure stages in relation to the transferred heat are shown. It can be seen that the gradient of syngas temperature is significantly lower at low temperatures than at high temperatures. This is due to condensing water at temperatures below 300 °C. It can be seen that more than 25 % of the heat in the syngas are available below 150 °C and another 20 % between 150 °C and 250 °C. In order to make efficient use of this heat, two low pressure stages are

implemented into the WSC, LP1 and LP2. The pressures of the different stages and the inlet temperature of the corresponding turbines are given in Table 3-1.

Table 3-1: Steam Parameters in the different pressure stages of the WSC

Stage	Pressure in bar	Temperature in °C
HP	113	550 °C
MP	39.25	580 °C
LP1	4	220 °C
LP2	1	135 °C

In Figure 3-7 it can also be seen that from the syngas point of view, significantly higher temperatures could be reached in the WSC. However, temperatures in excess of 600 °C are not feasible due to material limitations. The condenser of the WSC operates at 0.06 bar and condensate outlet temperature of 38 °C. A schematic of the WSC with the central parameters for the different pressure stages is presented in Figure 3-8.

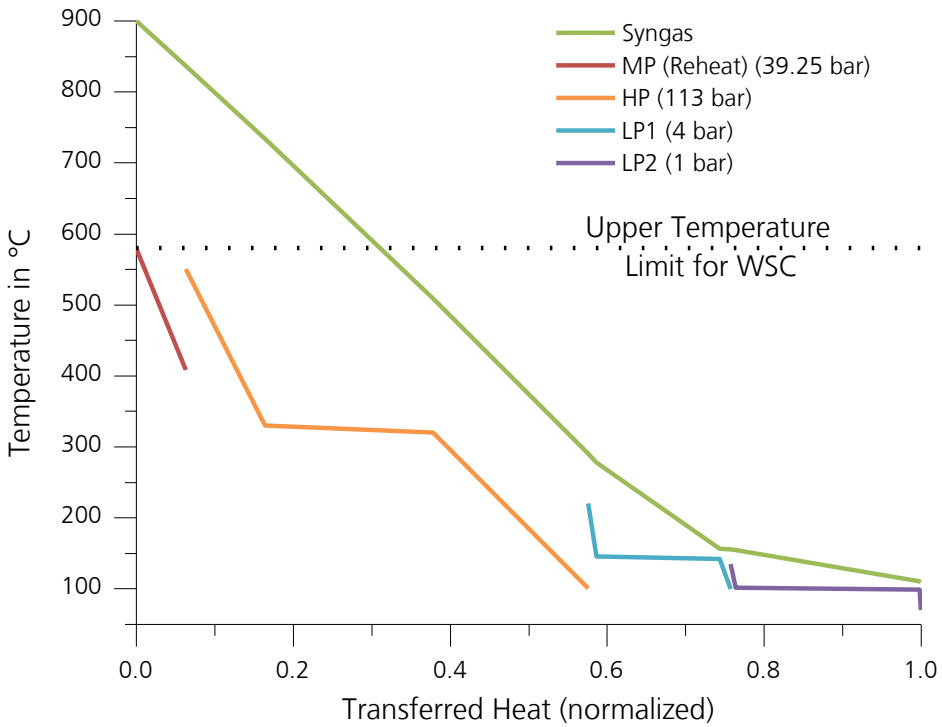

Figure 3-7: Temperature of hot and cold side over transferred heat in WSC for an upper syngas temperature of 900 °C and pressure of 26.5 bar

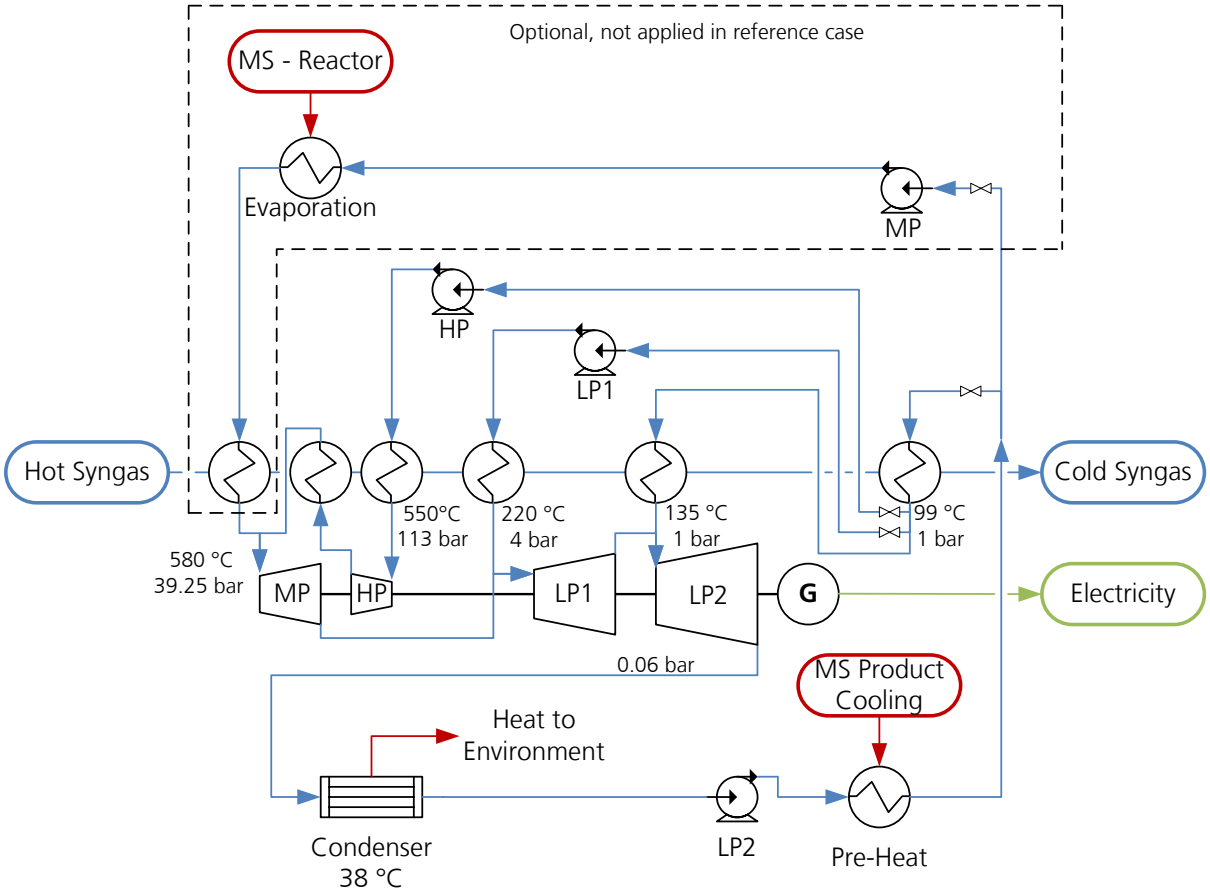

Figure 3-8: Water-Steam Cycle in the SOLME process

4. Development of process evaluation criterion

It was already mentioned in the introduction that the evaluation of the SOLME process is not meaningful with conventionally used criteria for efficiency. This is caused by the fact that the production of methanol is not primarily motivated by energetic considerations, but by the beneficial physical and chemical characteristics of the product. The same applies for most conceivable products in the world. In this chapter, a short review of available evaluation criteria is given and a new criterion is developed. Thereafter, the criterion is applied to a generic solar process. Furthermore, the criterion is applied to the relatively simple case of a solar hybrid gas turbine power plant in order to proof its applicability to such processes. Eventually it is presented how the criterion is applied to the investigated SOLME process. In section 6.6, the results obtained with the developed evaluation criterion are compared to the results the other evaluation criteria would have yielded.

4.1. Review of available evaluation criteria

There are two simple evaluation criteria that are commonly used for evaluation of energetic performance of processes: Firstly the energy balance and secondly the exergy balance. Both are meaningful tools in optimization of processes where the primary aim of the process is unambiguous. However, in a process such as the SOLME process, these balances cannot give meaningful results, because the production of methanol is a waste of energy and exergy, if purely considering these criteria. Therefore, in process optimization, the configuration that will appear most efficient from energetic or exergetic point of view might not be the most beneficial one from a producer's point of view.

Some more innovative evaluation criteria for systems using renewable energies were proposed in the past. Two of the most interesting ones are presented in the following two paragraphs.

Zhao et al. [50] proposed a possible solution for the problem of evaluation of hybrid solar-coal power plants: They used the collector area of a solar power plant (which represents solar energy input) as the variable input and compared its value for a hybrid solar-coal

power plant to the value necessary in a conventional solar power plant (parabolic trough type in this case) while producing the same amount of electricity. Eventually the rationale is that a certain amount of electricity has to be produced and it is assessed with which approach this can be achieved with a smaller solar collector area. Therefore, in their scheme it is investigated if the proposed process is capable of generating a certain amount of electricity with less collector area, i.e. more efficiently, than the state of the art. However this scheme is not applicable to production of different products like methanol and electricity in the state of the art and the proposed process and is therefore not applicable to the SOLME process.

Bai et al. [51] proposed an evaluation scheme where the energy savings ratio S as they call it is determined for evaluation of a hybrid process that produces methanol and electricity from biomass. In their evaluation scheme they use reference processes that produce the same amount of methanol and electricity as the proposed hybrid process. Subsequently they compare the energy balance of the proposed process and the reference processes. To do so they determine the difference between solar – and biomass energy input of the proposed process (E_{Bio} and E_{Solar}) with the solar – and biomass energy input into the reference system ($E_{\mathrm{Bio,Ref}}$ and $E_{\mathrm{Solar,Ref}}$). This difference is then put into relation of the energy input into the proposed process as shown in Eq. (4.1).

$$S = \frac{E_{\mathrm{Bio}} + E_{\mathrm{Solar}} - E_{\mathrm{Bio,Ref}} - E_{\mathrm{Solar.Ref}}}{E_{\mathrm{Bio}} + E_{\mathrm{Solar}}} \tag{4.1}$$

In essence, this is an expedient approach, because it provides information on which process consumes more energy to provide the same products. However, the weakness of this scheme is that no difference is made between the different kinds of energy. This is the case neither for the solar- and biomass energy input, nor the electricity and methanol output. All input streams are determined independently of each other, thus the ratio between biomass and the solar energy input can be very different between the investigated process and the reference process. This has two consequences: Firstly the scheme does not give support for a meaningful optimization, because the electricity and methanol are only considered as energy streams. The second consequence is related to the energy inputs. Results are possible, where one process consumes more solar energy than the other, and vice versa for

biomass energy. The resulting value of S will then imply that one process performs better than the other, not considering the different value of the energy streams.

As to the best of the authors knowledge no suitable evaluation criterion or scheme exists that can adequately be used for process optimization as well as absolute evaluation of renewable energy processes independent of the product, a criterion is developed in the following.

4.2. Definition of efficiency of a solar industrial process

When a conventional production process is adapted to be operated with the aid of solar energy, which will be called solarization of the process, the efficiency of solar energy utilization has to be assessed to allow for an evaluation and optimization of the solarization. In order to do so, it is important to recall the original purpose of utilization of renewable energies: Reduction of fossil-fuel consumption and the attributed greenhouse-gas emissions. Therefore, eventually the reduction of fossil-fuel emissions in relation to a relevant reference system ΔE_{Fuel} should be the principal measure for the evaluation of any kind of renewable energy application. This is in accordance with Sternberg and Bardow [52], who identified the reduction of greenhouse-gas emissions and fossil fuel depletion as the central targets for renewable energy utilization and therefore defined this also as the aim for energy storage systems for surplus electricity. However, in order to avoid scaling effects in evaluation and take into account the expenditure that has to be undergone to harness the renewable energy resource, the reduction of fossil fuel is put into relation with the amount the renewable energy resource used $E_{\mathrm{Renewable}}$, in this case solar energy. This will lead to the generic evaluation parameter h as shown in Eq. (4.2).

$$h = \frac{\Delta E_{\mathrm{Fuel}}}{E_{\mathrm{Renewable}}} \tag{4.2}$$

In order to ensure a meaningful evaluation, the reference amount of fossil fuel used in the production has to be determined carefully. Therefore, a crucial part is to define a reference system, which should represent the state of the art for the given production process. When comparing the fossil fuel consumption of the investigated (solarized) process to the

reference process, the difference in fossil fuel consumption can be compared and the value for h can be determined. However, the value will not provide information whether the investigated process provides the best use of the renewable energy. Therefore, in order to compare the efficiency of renewable energy utilization, the same amount and kind of renewable energy should also be supplied to the reference system. This should be done by taking into account a state of the art utilization process for this kind of renewable energy. In the example of solar energy, this might be photovoltaic or a solar power tower for electricity production. The resulting system of conventional production process and state of the art renewable energy utilization process will be called the reference system. Finally the resulting variable h gives the most important information for evaluation of the system: The system can be optimized by maximizing h, and for values of h greater zero, a benefit compared to the state of the art exists, for values below zero, no benefit exits.

The resulting definition of the efficiency of solarization of a process (based on (4.2)) used in this work is the difference of the fuel consumption in the reference system $E_{\mathrm{Fuel,Reference}}$ and the solarized system $E_{\mathrm{Fuel,Solarized}}$. In Figure 4-1, a general scheme of the solarized process and the reference system with input and output streams is shown. The solarized process produces the quantity *C* of the product from the quantity *A* of solar energy and *B* of fuel. It is also possible that the process produces (or consumes) electricity. This is taken into account for in the figure as the electricity output of quantity *D*. The sequence of scaling the different processes in the reference system can be clearly observed in the figure: The state of the art solar power plant produces electricity (*E*) from the same amount of solar energy consumed by the solarized process (*A*). Note that in selection of the reference solar power plant aspects such as capability of night time operation with heat storage should be taken into account, i.e. a process that produces electricity demand oriented should not be compared to a photovoltaic power plant where no storage can be implemented. The state of the art production process for the considered product produces the same amount of product as the solarized process (*D*) while consuming (*F*) fuel. If the process also produces or consumes electricity, this has to be taken into account as well. Finally the state of the art process for conversion of the given fuel into electricity (e.g. for natural gas a combined cycle gas turbine power plant (CCGT)) is taken into account in

order for the reference system to produce the same amount of electricity as the solarized process (*C*). In the case that the solar power plant produces more electricity than the solarized process, the fuel consumption of the power plant will be negative. Finally, the only difference in the overall balance of the solarized process and the reference system is the fuel consumption (ΔE_{Fuel} = *F*+*G*-*B*).

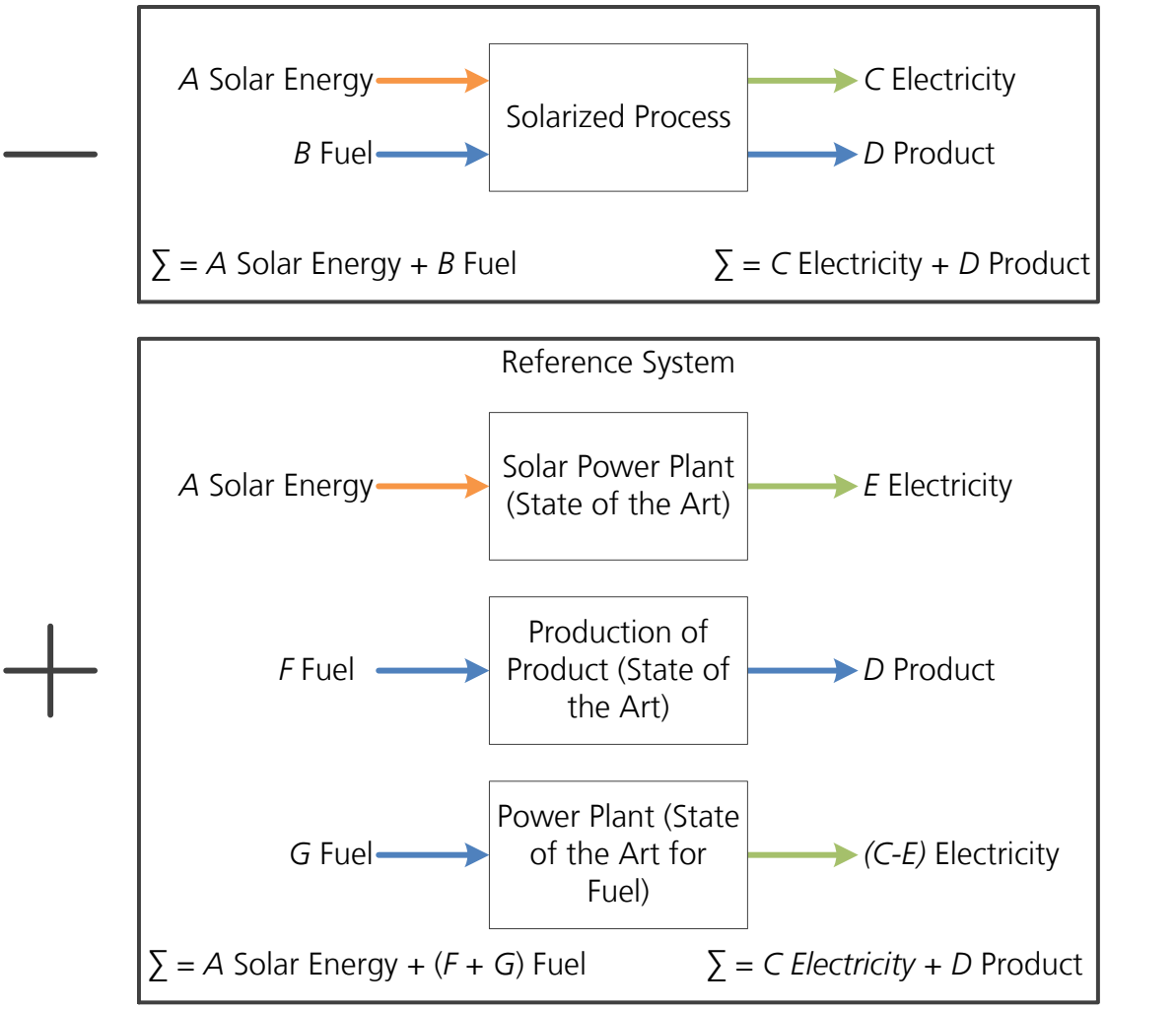

Figure 4-1: Scheme for definition of reference system for evaluation of solarized processes

The efficiency of the solarized process $h_{\mathrm{Solarization}}$ is defined as the reduction in fuel consumption ΔE_{Fuel} (LHV-basis) in relation to the solar energy input E_{Solar} (cf. eq. (4.3)). This parameter $h_{\mathrm{Solarization}}$ will be called *efficiency of solarization* and it allows for optimization of the process (by maximization) as well as for an assessment of the overall benefit of the system: If the value is below zero, there is no benefit but a detriment by the process, for values greater zero, a benefit exists. The defined efficiency of solarization is merely a relative parameter that indicates if and to what extent it is advantageous to solarize the process in focus or rather use the solar energy for electricity production and use the standard production process.

$$h_{\mathrm{Solarized}} = \frac{\Delta E_{\mathrm{Fuel}}}{E_{\mathrm{Solar}}} = \frac{E_{\mathrm{Fuel,Reference}} - E_{\mathrm{Fuel,Solarized}}}{E_{\mathrm{Solar}}} \tag{4.3}$$

The proposed scheme for evaluation can be applied to any kind of solarized process, independent of the energetic balance of the considered process. This is advantageous for evaluation of processes that are overall exothermic, but need solar energy due to exergetic considerations, like the methanol production process, where the reforming requires high temperature heat while the methanol synthesis releases large quantities of lower temperature heat.

As an advantage compared to the scheme proposed by Bai et al. [51], due to the sequential definition of the input and output streams in the reference system, an optimization of the considered process is possible without violating the principle target of the process, the production of a certain product. Furthermore, the proposed criterion specifically evaluates the efficiency of the secondary target of the considered process, the replacement of the fossil fuel with another energy input, such as solar energy. Furthermore, in the proposed evaluation scheme, the result can be converted into a reduction of GHG emissions if the specific GHG emissions of the reference fuel are known. In political debates, besides economics, this is often an argument to support a given technology.

4.3. Efficiency potential of generic solar industrial processes

Before an intensive numerical investigation is conducted in order to assess the efficiency of the solarization of a process, it should be investigated beforehand if the process has the

potential to be more efficient than the considered reference system. The systems are defined in accordance with the evaluation scheme previously introduced and depicted in Figure 4-2. At first, the efficiency of energy utilization in the process has to be determined. This is done by applying the previously presented evaluation scheme to a calculation with simple models that are the result the following assumptions:

- An ideal solar receiver (cf. section 2.2) converts the concentrated solar radiation into heat with the efficiency given in Eq.(2.14).
- The heat is then supplied to the process without any further losses.
- In the reference system, the process'heat demand is supplied by combustion of a fossil fuel without any losses.
- In the reference system, the solar energy is converted into electricity in a solar power plant. It is assumed that this power plant is a solar power tower with an ideal receiver exhibiting an efficiency as defined in Eq.(2.14).
- The upper temperature in the solar power plant is defined by the water steam cycle, assumingly 600 °C. The conversion of the heat into electricity in the solar power tower is restricted by the Carnot efficiency, which is used for calculation of conversion efficiency, ambient temperature serves as lower temperature, the water steam cycle temperature as upper temperature.
- Eventually, in order to yield identical products from both process scenarios, a CCGT can be considered (if the fuel is gaseous or liquid) to produce the same amount of electricity as the solar power plant (because the process has no electricity output in this consideration). As conversion efficiency, the Carnot efficiency is used again, but here the upper temperature of a state of the art CCGT can be used: 1300 °C.

The remaining 3 variables in the system are:

- Temperature of the industrial process T_{P}
- DNI from the sun I_{DNI}
- Concentration factor of the solar radiation supply C.

With the given data, the efficiency of solarization $h_{\mathrm{Solarization}}$ can be determined in dependence of those three variables. Details on the calculation are given in Appendix A.

The resulting values for $h_{\mathrm{Solarization}}$ for different concentration factors (C) over temperature are presented in Figure 4-2. It can be seen that for process temperatures below 900 °C, even relatively small values of C for point-focusing systems of 500 will yield values for $h_{\mathrm{Solarization}} > 0$, hence, have the potential to save fuel compared to the reference system. With concentration factors of 1000, even processes that operate above 1000 °C can be solarized with $h_{\mathrm{Solarization}}$ significantly above zero. Therefore, the results indicate that processes up to 1000 °C can potentially be solarized in solar power towers efficiently. With higher concentration ratios, this finding will even be true for processes with higher temperatures.

From those results, it becomes clear that solar reforming, which will most probably be carried out between 700 °C and 1000 °C, has the potential to achieve positive values for the efficiency of solarization with realistic concentration factors.

It has to be stated that these results only give an estimation of the thermodynamic potential. Hence the procedure is a suitable tool to assess the theoretical potential of a process to be solarized efficiently. However, from the considerations, no predictions on the performance of a real plant can be made.

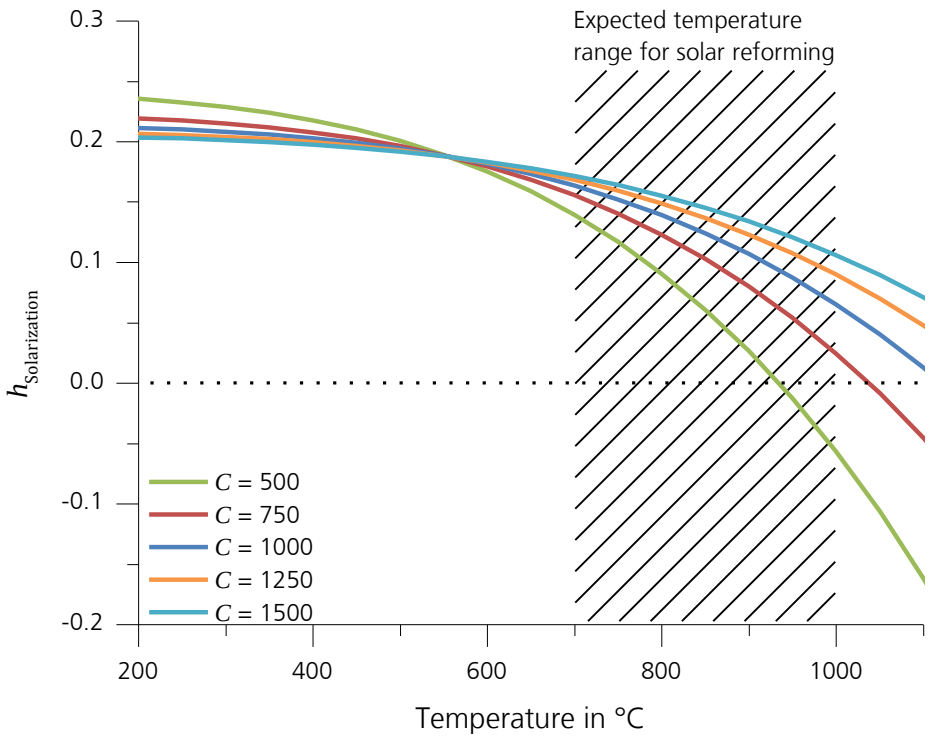

Figure 4-2: Efficiency of solarization over temperature for different concentration factors *C* in solar radiation supply, DNI of 1000 W/m² is assumed.

4.4. Sample application of evaluation scheme: Solar hybrid gas turbine

In order to give a more specific, but nevertheless simple example, as well as to illustrate its universal applicability, the proposed evaluation scheme is applied to a solar hybrid gas turbine (SHGT) process in the following. It should be noted that the presented evaluation is carried out with the aim of demonstrating the applicability of the evaluation scheme, rather than carrying out a comprehensive analysis of the SHGT process. In this demonstration, the receiver temperature is treated as an optimization parameter, i.e. the optimum temperature of the receiver in the SHGT is determined. The result of the optimization with the proposed evaluation scheme is compared to results obtained from an energetic optimization and the differences discussed. The energetic efficiency is defined in Eq. (7.5). It is the electricity production in relation to solar energy and natural gas energy input.

$$\eta_{\text{Energetic}} = \frac{P_{\text{El}}}{P_{Solar} + P_{NG}} \tag{4.4}$$

As reference system, in this investigation, a conventional combined cycle gas turbine power plant (CCGT) and a solar power tower with water steam cycle are selected. A simplified simulation of the CCGT is carried out with assumed values of the following parameters: The air stream is compressed to 30 bar and used for combustion of methane. The amount of methane consumption is adjusted in order to yield an inlet temperature to the gas turbine of 1300 °C. The hot flue gas is then expanded in a gas turbine. The isentropic efficiencies of the compressors and the turbine are set to 80 %. The exhaust from the gas turbine is cooled in a heat recovery steam generator (HRSG) to 170 C. The heat is converted into electricity in a water steam cycle (WSC) with an efficiency of 35 %. For the solar power plant, no losses in the heliostat field are taken into account. The receiver efficiency is calculated as shown in Eq. (2.14) with a temperature of 650 °C and an intercept flux density of 800 kW/m². The conversion from heat to electricity in the water steam cycle of the solar power plant is also 35 %.

In the SHGT, the air is compressed and then heated to the temperature $T_{\mathrm{Rec,SHGT}}$ in a solar receiver. Subsequently, some natural gas is added and combusted to achieve the same inlet temperature into the gas turbine as in the reference power plant (1300 °C). However, now the natural gas input is lower because some of the heat is already provided in the solar receiver. The rest of the SHGT is identical to the reference CCGT plant. The efficiency of the receiver of the SHGT is also calculated according to Eq. (2.14) with an intercept flux density of 800 kW/m². The receiver temperature is varied in order to find an optimum value.

In the proposed evaluation scheme, the reference solar power plant consumes the same amount of solar energy as the SHGT plant. From its efficiency, the amount of produced electricity is determined. As all parameters are fixed for the reference solar power plant, the energetic efficiency ($\eta_{\mathrm{Energetic}}$, cf.Eq. (7.5)) from intercept radiation to electricity is also fixed. It is 33.2 %. With this value, the difference in electricity production between the SHGT and the conventional solar power plant can be determined. The reference CCGT is scaled in order to close this gap so that the overall electricity production of the reference system is identical to the production of the SHGT. In the calculations an efficiency of the CCGT of 47 % was determined. From this, the natural gas consumption of the CCGT can

be determined. According to the previous definition, the efficiency of solarization h is the difference of natural gas consumption in relation to the solar energy input.

In the Figure 4-3 (left) the solar energy consumption of the SHGT and the electricity production of the reference solar power plant in dependence on the receiver efficiency are shown. It should be noted that according to the evaluation scheme, the reference solar power plant always has the same solar energy input as the SHGT plant. It can be seen that the solar energy input into the process is increased with increasing receiver temperature. This also causes an increase in electricity production of the reference solar power plant. On the right hand side of the Figure, the natural gas input of the SHGT that is required to achieve 1300 °C turbine inlet temperature is shown. Furthermore, gas input of the CCGT that is necessary to achieve the same total electricity production in the reference system as the SHGT is shown. Furthermore, the difference in natural gas consumption between the CCGT and SHGT is depicted in the figure. It can be seen that the natural gas input of both processes decrease with increasing receiver temperature. This is caused by the fact that the solar energy input is increased. It can also be seen in Figure 4-3 (right) that for temperatures below 1150 °C, h is positive. Hence, the SHGT consumes less natural gas than the CCGT. It can also be seen in the figure that h has a maximum for a receiver temperature of 700 °C.

In Figure 4-4 the resulting efficiency of solarization h as well as energetic efficiency $\eta_{\mathrm{Energetic}}$ of the SHGT are shown. It can be seen that both follow a similar trend: Decrease with increasing temperature. However, while the energetic efficiency strictly decreases with increasing temperature in the considered range, an optimum develops for the efficiency of solarization at 700 °C receiver temperature.

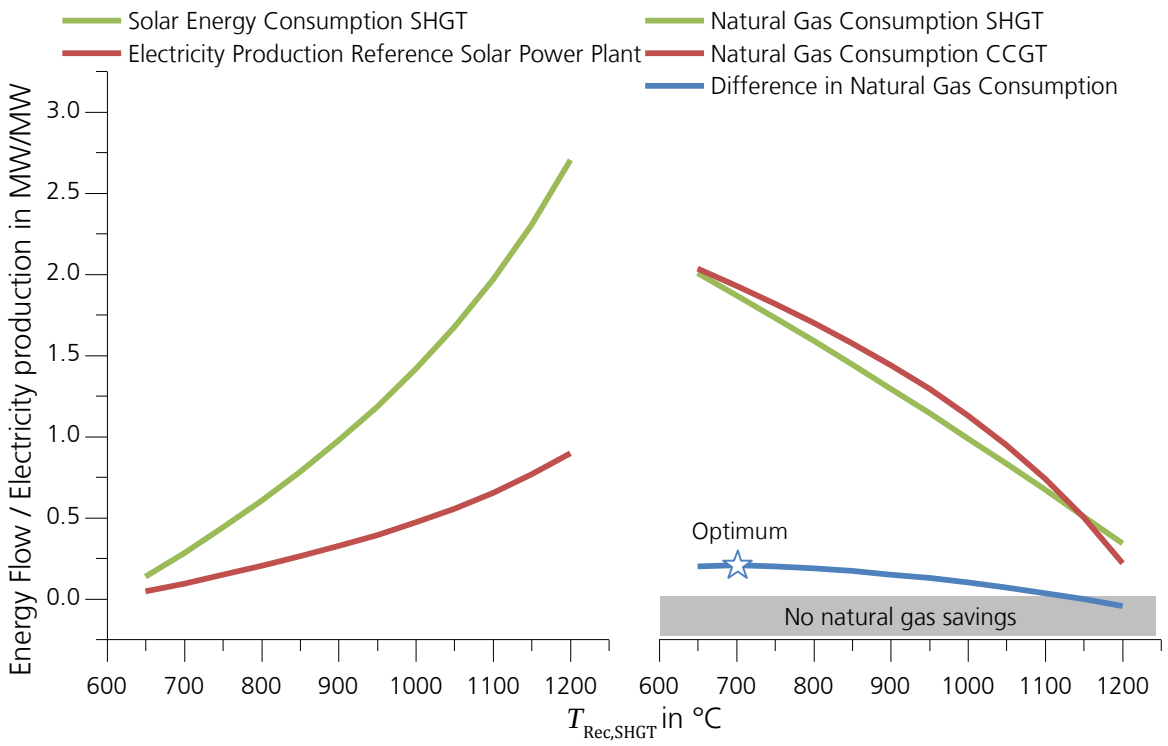

Figure 4-3: Energy inputs of SHGT (left) and reference processes (right) in relation to total electricity production

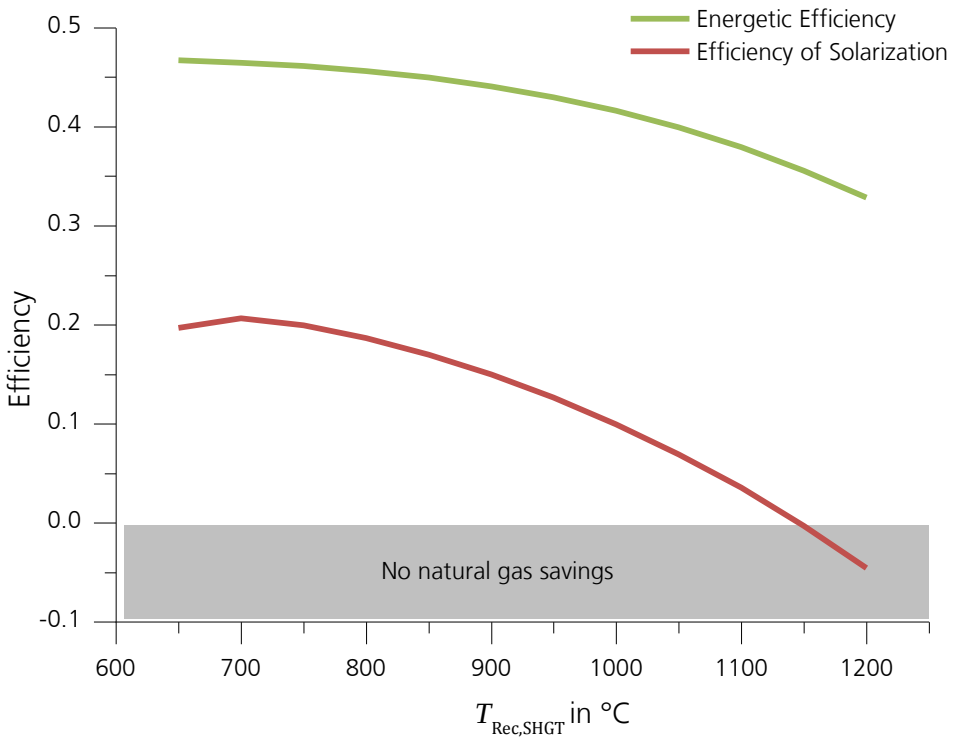

Figure 4-4: Efficiency of solarization and energetic efficiency (energy balance) of SGHT plant.

The diverging optimization results demonstrate the limited applicability of the energy efficiency of such a process for optimization. Because the conversion of solar energy into electricity is less efficient than the conversion of natural gas into electricity, the optimum configuration from an energetic point of view is not to use solar energy at all (which is the case when the receiver outlet temperature is further reduced). But as the utilization of renewable energy is the aim in such processes, those results are not productive. In contrast to that, the proposed efficiency of solarization allows for the determination of the process configuration that achieves the highest reduction in fossil fuel consumption. It can furthermore be used to determine if the investigated process makes more efficient use of solar energy than the reference technology. This is the case for the investigated SHGT process, because values greater zero are achieved for h.

4.5. Application of evaluation scheme to SOLME process

The reference system to be used for the evaluation of the SOLME process is a conventional methanol production plant and a solar power tower for electricity production. The methanol plant is scaled to produce the same amount of methanol as the SOLME plant and the solar power tower is scaled to consume the same amount of solar energy as the SOLME plant. A natural gas fueled CCGT power plant is used to produce such an amount of electricity that the SOLME and CCGT plants together produce the same amount of electricity as the conventional methanol plant and the solar power tower. This will be referred to as the external CCGT, in order to distinguish it from the internal CCGT that was described in section 3.2. In order to allow for good comparability, the reference methanol plant and solar power plant are modeled (cf. sections 6.1 and 6.2), rather than taking data from literature. This seems adequate, because for literature data, no sufficient data is provided to assess whether the data is applicable to the methanol plant considered in this work (i.e. specifications and assumptions). For the CCGT, a fixed efficiency is assumed. A flowsheet to illustrate the two systems that are compared in the evaluation scheme is depicted in Figure 4-5. In the figure, some exemplary data is given to show the magnitude of the different energy flows into and out of the processes. It can be seen that all outputs as well as the solar energy input are identical in both systems.

The efficiency of solarization of the SOLME plant h_{SOLME} is then calculated according to Eq.(4.5): It consist of the savings of natural gas input, on lower heating value (LHV) basis, in relation to the total solar energy input.

$$h_{\mathrm{SOLME,System}} = \frac{E_{\mathrm{NG,Reference}} - E_{\mathrm{NG,SOLME,System}}}{E_{\mathrm{Solar}}} = \frac{\Delta E_{\mathrm{NG}}}{E_{\mathrm{Solar}}} \tag{4.5}$$

In the example given in Figure 4-5, the resulting values of h_{SOLME} is 0.07. This means that 70 kWh of natural gas are saved per MWh of used solar energy when using the SOLME process instead of the reference processes. Therefore, in this illustration, the utilization of solar energy in the SOLME process is more efficient than the state of the art utilization in a solar power tower for electricity generation. The values shown in the figure are only exemplary. In the following two chapters, a detailed model of the SOLME process is developed and its performance is assessed in more detail and optimized with sensitivity studies.

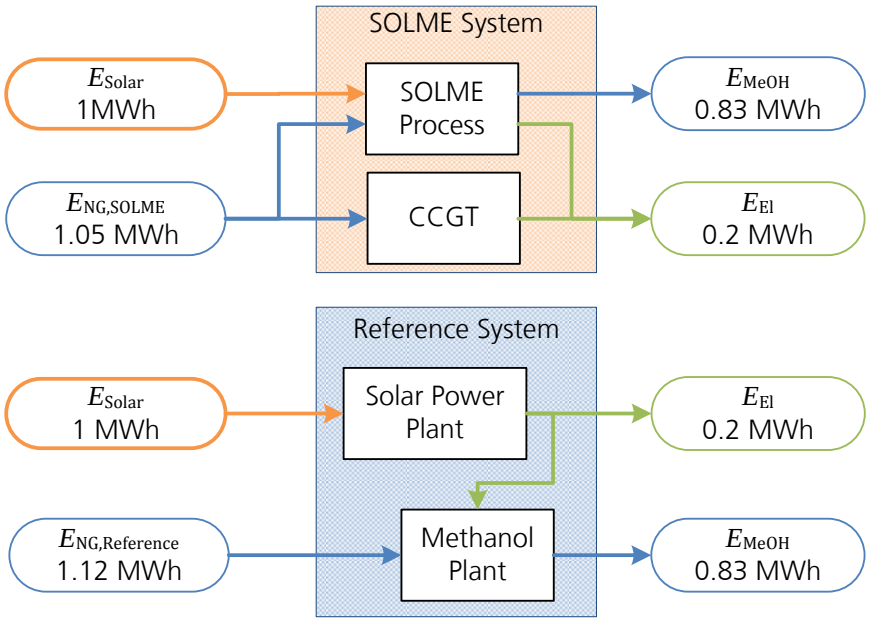

Figure 4-5: SOLME and Reference system considered for evaluation of efficiency of solarization

5. Modelling of the SOLME process

As explained in the process description, the overall SOLME process consists of a dynamic and a stationary part. The dynamic part consists of the heliostat field, the solar receiver, and TES, while the stationary part consists of the reforming and methanol plant. Furthermore, as the scope of this work covers the whole process from solar radiation and natural gas to methanol and electricity, many process steps have to be taken into account. The simulation of these different process steps has distinct demands and approaches. Therefore, it is not feasible to carry out the simulation with one single model in only one simulation software. The simulation is split into several steps being partly congruent with the process sections in the previous section. The splitting of the process model and the associated workflow are depicted in Figure 5-1. The DNI data is used for the layout of the heliostat field in the software *HFLCAL* [53]. Besides several other parameters, for the heliostat field layout, the design intercept radiation to the receiver $\dot{Q}_{\mathrm{IC,DP}}$ as well as the flux density onto the aperture of the receiver I_{AP} are central parameters to be set. In this work, the design intercept radiation will be 50 MW, while the flux density is varied. The value of 50 MW intercept radiation is chosen, because it represents a small commercial scale for solar power towers, as it could be expected for a first commercial SOLME plant. With the *HFLCAL* output, hourly values for the intercept radiation $\dot{Q}_{\mathrm{IC}}(t)$ for the entire year are generated. The receiver and the non-solar part of the SOLME plant is modelled in the software *ASPEN Dynamics*. This software is chosen, as it provides a good environment for modelling the process. Different methods for calculation of material properties are available as well as several models of common process units are already implemented in the model library. Furthermore it allows for the implementation of custom models in the *Aspen Custom Modeler*. The common process units are simulated with models from the implemented model library. However, no suitable model exists to simulate the air-heated reformer. Hence, a model is set up in *Aspen Custom Modeler*. For calculation of the material properties Peng-Robinson [54] method is used, as it is suitable for real gases.

The simulation of the SOLME flowsheet is carried out with normalized natural gas input and several process parameters, such as reforming temperature (T_{Ref}) and split fraction (f_{Split}). It

yields results for process simulation, such as the methanol and electricity output, but also results that are necessary as input for the simulation of the receiver: The hot-air-temperature (T_{HA}) and the return-air-temperature (T_{RA}). The SOLME flowsheet is carried out in a dimensionless way, and is scaled with the results from the simulations of the solar part.

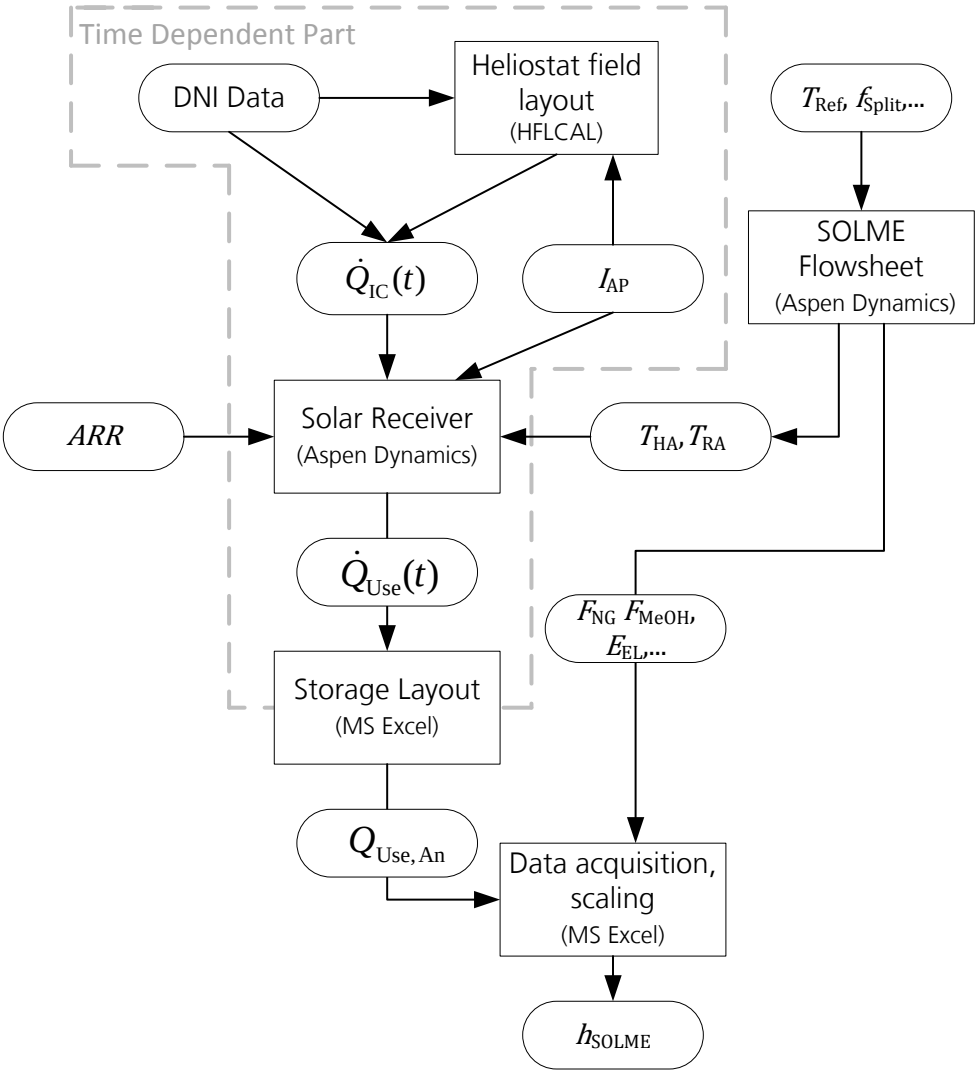

Figure 5-1: Workflow of SOLME simulation

Also the solar receiver is modeled in *Aspen Custom Modeler* and simulated in *Aspen Dynamics*. It is carried out as a quasi-stationary simulation, because the response to a change of intercept radiation of the receiver is nearly instantaneous. The annual operation of the receiver is carried out with the previously generated intercept radiation data and further input, such as I_{AP}, T_{RA}, T_{HA} and ARR. It should be noted that the flux density is assumed to be uniform over the receiver, hence it is the total intercept radiation divided by the aperture area. In the simulation, flux density and total intercept radiation are set, therefore, the aperture area is a result of the simulation. The receiver simulation yields hourly values for thermal energy supply throughout the year $\dot{Q}_{\mathrm{Use}}(t)$. With a simplified TES layout tool that is set up in *MS Excel*, the storage of solar heat and later release to the process is simulated. This allows for an increase in operating hours of the SOLME process compared to operation without storage. The TES layout yields a total annual amount of thermal energy supplied to the SOLME process $Q_{\mathrm{Use,An}}$ as the product of the amount of hours at which the nominal heat flow is delivered. With those results, the previously generated results from the SOLME flowsheet simulation can be scaled and evaluated in a tool set up in *MS Excel*. In this tool, also the efficiency of the process h_{SOLME} is calculated.

In the following sections, more detailed information on the modelling of the different sections is given.

5.1. Heliostat field

The heliostat field is designed and modelled in the software *HFLCAL*. This software is chosen, because it enables the layout and optimization of a heliostat field with low computational time while still taking into account the main loss mechanisms that occur in heliostat fields, such as beam error of heliostats, blocking and shading as well as atmospheric attenuation. In the software, data for a predefined heliostat is added and the software places a large number of heliostats, the gross field, in a defined pattern around the tower. This gross field should by far exceed the actually necessary heliostat field size. Some further parameters, such as aperture area and shape are defined and data for the DNI at the considered location can be imported. Subsequently HFLCAL performs calculations of the annual performance of the heliostats and chooses the ones with the highest annual

efficiency until the defined design intercept radiation is achieved. The possibility of carrying out the simulations of the solar receiver within HFLCAL is not used, because only limited variation of parameters can be carried out with this model. Therefore the solar receiver is modelled separately, as presented in the following section. For further information on the procedures and parameters HFLCAL uses, the user's guide [55] should be referred to. The heliostat field is designed to provide a layout intercept radiation of 50 MW at the location of In Amenas, Algeria (28 °N).Values for the parameters added in HFLCAL for heliostat field layout is given in Table A - 2 in the Appendix.

The resulting heliostat field (for a flux density of 700 kW/m² in receiver aperture) is depicted in Figure 5-2. The color scale indicates the efficiency of the individual heliostats. Lighter colors represent higher efficiency. The field is set up from 518 single heliostats, resulting in a total heliostat area of 62854 m². The numbers on the axes of the coordinate system indicate the dimensions of the field in meters. From the scale it can be seen that the area necessary for the heliostat field is a rectangle of 582 m in width and 574 m in length, for this configuration. This results in a total land area of 334 thousand square meters.

As in the simulation of the SOLME process the flux density of the receiver will be a parameter for optimization, it has to be varied in the layout of the heliostat field as well. For a given design power entering the receiver, the aperture size is varied in order to achieve the desired flux density. With decreasing aperture size, the *spillage* losses increase. Spillage losses are caused by sunrays that are redirected by the heliostats towards the receiver but miss the aperture. This is caused by several phenomena: Firstly, due to the finite shape of the sun, some heliostats, depending on their position in the field, may not be able to generate an image of the sun within the area of the aperture. Furthermore inaccuracies in heliostat production and field erection as well as in tracking of the sun path may cause spillage losses. When decreasing the aperture size of the plant, more heliostats have to be added to the field, in order to compensate for the increased spillage losses. Since HFLCAL adds heliostats to the field according to their annual performance, the new heliostats will achieve a lower annual efficiency than any of the heliostats previously added to the field. Hence their addition will decrease the annual efficiency of the field. Therefore, the flux density to be used is a matter of optimization, as also mentioned by Winter et al. [56] (p.

124): *"The aperture area is selected during system optimization to minimize the sum of radiative and spillage losses"*. Therefore, the optimum size of the receiver aperture cannot be determined independently of the process simulation.

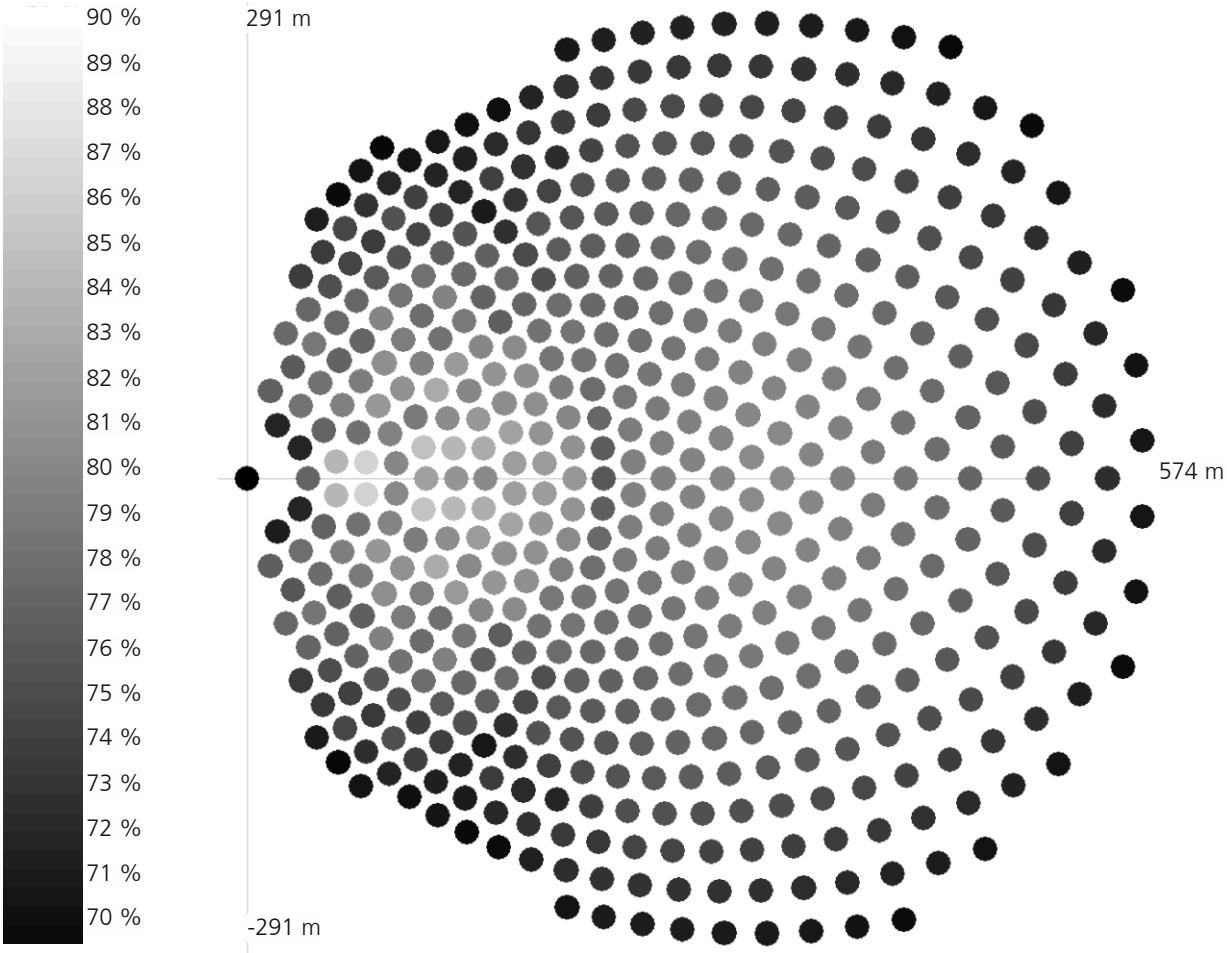

Figure 5-2: Heliostat field designed for SOLME process (at 700 kW/m² in Receiver-Aperture). Shade of heliostats represents annual efficiency according to scale on the left.

In order to take into account the change in field efficiency in the subsequent receiver-simulation runs with acceptable computational expense, the field efficiency for different flux densities is calculated with HFLCAL. Subsequently a polynomial function is fitted to predict the field efficiency for any flux density in the given range (400…1300 kW/m²). The resulting polynomial for the correction factor f_{Corr} of the heliostat field efficiency is given in Eq.(5.1). In Figure 5-3, the results provided by HFLCAL and the polynomial fit are shown and good agreement can be observed. The maximum deviation in prediction of the correction factor is $3.4 \cdot 10^{-4}$. This is an acceptable result for the polynomial fit, as it will cause deviations in the predictions of heliostat field efficiencies well below 0.1 %. The

correlation for the calculation of the heliostat field efficiency from flux density and the reference heliostat field efficiency (with intercept flux of 700 kW/m²) is given in Eq.(5.2). It should be noted that the correlation given in Eq.(5.1) is only valid for flux densities between 400 kW/m² and 1300 kW/m². The data for the generation of the fitted field performance correlation, as well as a plot of the HFLCAL results and results obtained with the fit, are given in Appendix B.2.

$$f_{\mathrm{Corr}} = 0.01 + 4.99 \cdot 10^{-5} \cdot I - 1{,}08 \cdot 10^{-7} \cdot I^2 + 2.25 \cdot 10^{-11} \cdot I^3 \tag{5.1}$$

$$\eta_{\mathrm{HF}}(I) = f_{\mathrm{corr}}(I) \cdot \eta_{\mathrm{HF,700kW/m^2}} \tag{5.2}$$

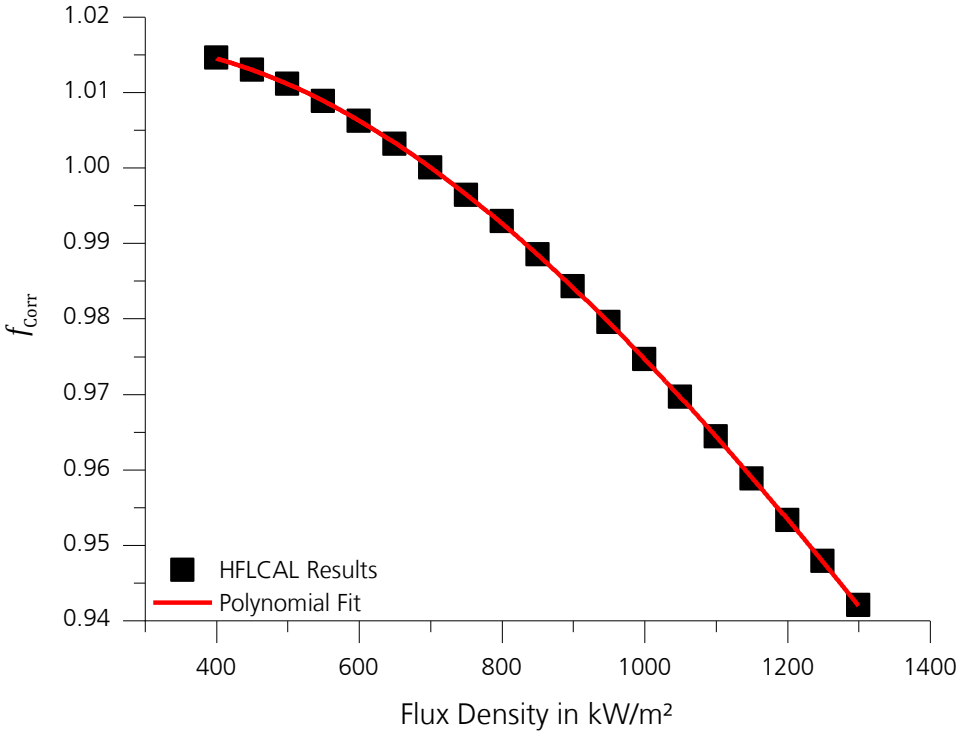

Figure 5-3: Comparison of HFLCAL results with polynomial fit for f_{Corr}

5.2. Solar receiver

As discussed above, the open volumetric receiver (OVR) is chosen as the receiver to provide heat to the SOLME process. Even though a model of the OVR is implemented into the software HFLCAL that is used for heliostat field layout, it cannot be applied for simulation of the investigated process, because only limited variation of few parameters is possible in HFLCAL. For example, a cavity-type geometry cannot be used and the model is only capable of calculating the performance with hot air temperature up to 700 °C, while higher temperatures are to be investigated in this study. Furthermore, no receiver model exist in the *Aspen Dynamics* model library, therefore a model is implemented with Aspen Custom Modeler.

The receiver, of which a principal sketch was shown in Figure 3-3, consists of a honeycomb absorber that is set up from small structures called cups. A photograph of such a cup is shown in Figure 5-4. The geometry of the absorber taken into consideration is that of the Hitrec II structure, as this is state of the art (cf. Avila-Marin [57]).

Figure 5-4: Hitrec II absorber cup

The concept of the OVR was already illustrated in Figure 3-3 and Figure 3-4. In the receiver model it is assumed that the intercept radiation provided by the heliostat field is evenly distributed on the absorber surface. The ratio of the flux density into the aperture of the receiver and the flux density of the absorber is equal to the ratio of the absorber surface A_{Abs} and the aperture area A_{Ap}, as shown in Eq.(5.3). Note that for a flat absorber the absorber surface is equal to the area of the aperture.

$$\begin{aligned} \dot{Q}_{\mathrm{IC}} &= A_{\mathrm{Ap}} \cdot I_{\mathrm{AP}} = A_{\mathrm{Abs}} \cdot I_{\mathrm{Abs}} \\ \Rightarrow \frac{A_{\mathrm{Ap}}}{A_{\mathrm{Abs}}} &= \frac{I_{\mathrm{Abs}}}{I_{\mathrm{Ap}}} \end{aligned} \tag{5.3}$$

In Figure 5-5 (left), a schematic front view of an absorber part is shown. It can be seen that it is a honeycomb structure that consists of several square channels with width s and strut thickness b. In the given geometry, the side length is 2 mm and the strut thickness is 0.8 mm. A rendered side view with information on the modelling procedure is shown in the same figure (right): The structure is modelled in similar a way as the *one-channel*-model presented by Pitz-Paal [58], where one representative strut (wall) and the adjacent channel, which the air flows through, are assumed to represent any other channel in the absorber. This indicates that no gradients perpendicular to the air flow are taken into account. The axial direction of the absorber structure is discretized. Furthermore, in the model, it is assumed that the intercept radiation does not penetrate into the absorber structure, but is absorbed or reflected at the front surface. This corresponds to cell 1 in the model (cf. Figure 5-5 (right)). The absorbed fraction of radiation is determined by the absorptivity of the receiver α_{Ap}, which depends on the absorptivity of the absorber structure and the geometry of the absorber (cf. eq. (2.17)). Furthermore, due to its temperature, the absorber emits thermal radiation from the front part. As assumed for absorbance of incoming radiation, the emittance of thermal radiation is assumed to occur from the front surface only. It is furthermore assumed that the absorptivity is not temperature dependent, therefore it is always equal to the emissivity. In the strut, the heat is transported towards the back of the absorber structure by thermal conduction. The air flowing through the channels is heated convectively by the struts, as shown for the first cell in Figure 5-5 (right).

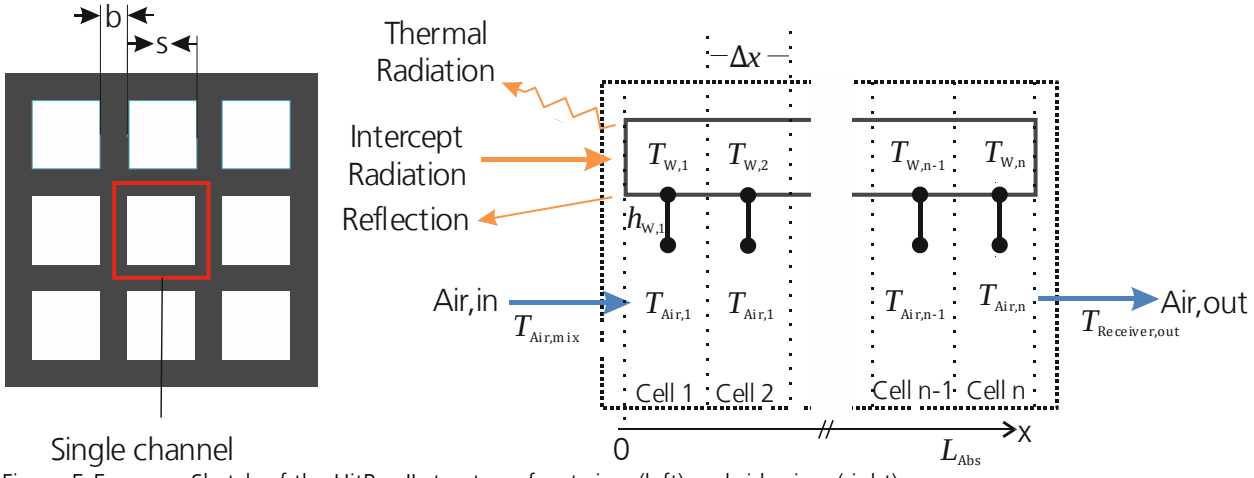

Figure 5-5: Sketch of the HitRec II structure: front view (left) and side view (right)

The equations for conductive heat transfer in the solid material and the convective transfer between solid and air are given in Eqs. (5.4) and (5.5). Note that the first equation describes the heat transfer between cell i-1 and cell i, it can therefore not be applied to cell 1. The temperature-dependent effective thermal conductivity $\lambda_{\text{eff,Abs}}$, which refers to the overall cross-section (not only the solid part) of the absorber is calculated with a correlation determined and used by Ahlbrink [59] through experimental data by DLR for this structure, which is presented in Appendix C.1 (made available by Ahlbrink [60]). Δx refers to the length of the cells in the model. The parameter a_{Abs} is the volume specific surface area of the structure, where heat transfer to the fluid occurs. It depends only on the geometry of the channels (cf. Eq. (5.6)); for the given structure its value is 1020.4 m^{-1}. A_{Abs} is the surface area of the absorber. The heat transfer coefficient $h_{\text{W},i}$ for laminar forced convective flow is determined by a Nusselt correlation originally proposed by Nonino et al. [61] and later used by Pitz-Paal [58] for the purpose of modelling a similar receiver structure. The correlation is given in Appendix C.1 in the form presented by Pitz-Paal [58]. The hydraulic diameter used for both, the calculation of the Nusselt number Nu, as well as for the Reynolds number Re, is the width of the channel s.

$$\dot{Q}_{\text{Cond},i} = -\lambda_{\text{eff,Abs}}(T_{W,i}) \cdot A_{\text{Abs}} \cdot \frac{T_{W,i} - T_{\text{W},i-1}}{\Delta x} \tag{5.4}$$

$$\dot{Q}_{\text{Conv},i} = a_{\text{Abs}} \cdot A_{\text{Abs}} \cdot h_{\text{W},i} \cdot \Delta x \cdot (T_{\text{W},i} - T_{\text{Air},i}) \tag{5.5}$$

$$a_{\text{Abs}} = \frac{4 \cdot s}{(s+b)^2} \tag{5.6}$$

The air for the circuit is modelled as a molar mixture of 21 % oxygen and 79 % nitrogen.

The energy balance for the first cell of the absorber wall, calculated with the previously stated assumptions, is shown in Eq. (5.7). It is the difference of the absorbed energy $\dot{Q}_{\alpha}$ (eq. (5.8)) and the losses due to re-radiation $\dot{Q}_{\varepsilon}$ (eq.(5.9)), conduction $\dot{Q}_{\mathrm{Cond},2}$ towards cell 2 and the convection to the air $\dot{Q}_{\mathrm{Conv},1}$. In the equation for the radiative heat losses (5.8), the effective absorptivity α_{Ap} of the aperture, which is determined through Eq.(2.17), is temperature-independent and therefore equal to its emissivity.

$$0 = \dot{Q}_{\alpha} - \dot{Q}_{\varepsilon} - \dot{Q}_{\mathrm{Cond},2} - \dot{Q}_{\mathrm{Conv},1} \tag{5.7}$$

$$\dot{Q}_{\alpha} = \alpha_{\mathrm{Ap}} \cdot \dot{Q}_{\mathrm{IC}} \tag{5.8}$$

$$\dot{Q}_{\varepsilon} = \alpha_{\mathrm{Ap}} \cdot \sigma \cdot A_{\mathrm{ap}} \cdot \left(T_{\mathrm{W},0} + 273.15\ \mathrm{K}\right)^4 \tag{5.9}$$

For the cells 2 to n-1, the energy balance is calculated by Eq.(5.10). The back side of the absorber is assumed to be adiabatic, therefore no thermal conduction out of the absorber is allowed to occur. This is ensured by the boundary conditions for cell n given in Eq.(5.11).

$$0 = \dot{Q}_{\mathrm{Cond},i} - \dot{Q}_{\mathrm{Cond},i+1} - \dot{Q}_{\mathrm{Conv},i} \quad , \quad i = 2, \dots, \mathrm{n} - 1 \tag{5.10}$$

$$0 = \dot{Q}_{\mathrm{Cond},n} = \dot{Q}_{\mathrm{Conv},n} \tag{5.11}$$

The air flow that is returned to the receiver is assumed not to cool the receiver structure but being ejected in front of the receiver at T_{RA}, where it mixes with air at ambient temperature $T_{\mathrm{Air,Amb}}$. In the investigation of Ahlbrink [59] the cooling of the receiver by the return air is taken into account, which leads to severe losses when the ARR is low. This can also be seen in the data presented in Figure 5-6, where results of the receiver model with - and without this effect are presented. For the open volumetric cavity receiver (OVCR), it is assumed that the air return concept is changed, so that no cooling of the receiver by the return air occurs, hence reducing the thermal losses.

The mixed air that is a result of mixing of return air with ambient air, enters the receiver with a temperature between T_{RA} and $T_{\mathrm{Air,Amb}}$. The temperature of the mixed air is determined by the ARR. In the receiver model used here, the temperature of the mixed air is derived through the fluid properties from its enthalpy $h_{\mathrm{Air,mix}}$, which is determined by

mixing the enthalpy of the return air h_{RA} and the enthalpy of the ambient air $h_{\mathrm{Air,Amb}}$, according to Eq.(5.12).

$$h_{\mathrm{Air,mix}} = ARR \cdot h_{\mathrm{RA}} + (1 - ARR) \cdot h_{\mathrm{Air,Amb}} \tag{5.12}$$

The air enters the absorber structure with the temperature $T_{\mathrm{Air,Mix}}$, which therefore represents $T_{\mathrm{Air},0}$ in the absorber model. No thermal conduction in the air is considered, as this is taken into account in the effective thermal conductivity of the absorber structure (cf. Appendix C.1). Therefore, the energy balance only consists of the change in enthalpy of the air and the convective heat transfer, as presented in Eq.(5.13). The equation is valid for cells 1 to n.

$$h_{\mathrm{Air},i} - h_{\mathrm{Air},i-1} = \dot{Q}_{\mathrm{Conv},i-1} \tag{5.13}$$

The velocity of the air in each cell is determined from the total volume flow of the air through the receiver divided by the total area of channels in the absorber, i.e. the open cross section of the total absorber area. The volume flow is determined from the molar flow and the molar density of the air.

The efficiency of the receiver is defined as the useful heat flow it provides in relation to the total intercept radiation delivered to it by the heliostat field. The useful power is measured by the enthalpy increase of the HTF in the receiver. Even though this is common practice, for OVR, this is not completely unambiguous, as the enthalpy increase of the fluid can be measured from the absorber inlet (i.e. h_{mix}) or the receiver inlet (i.e. h_{RA}). The difference is that in the first option, the losses due to incomplete air return are not taken into account in the receiver balance, which they are in the latter. In this study, the useful energy provided by the receiver is defined as the enthalpy increase of the fluid from receiver inlet to its outlet, as shown in Eq. (7.5). Hence, the losses due to incomplete air return (ARR-loss, $\dot{Q}_{\mathrm{ARR}}$) are considered to be a receiver loss. In Eq.(5.15) the definition of the ARR loss is given. It is defined as the molar specific enthalpy difference ($h_{\mathrm{RA}} - h_{\mathrm{mix}}$) of the air multiplied with the total molar flow of the air in the system F_{Air}.

$$\dot{Q}_{\mathrm{use}} = F_{\mathrm{Air}} \cdot (h_{\mathrm{HA}} - h_{RA}) \tag{5.14}$$

$$\dot{Q}_{\mathrm{ARR}} = F_{\mathrm{Air}} \cdot (h_{\mathrm{RA}} - h_{\mathrm{mix}}) \tag{5.15}$$

It should be noted that the air return ratio is an input parameter in this model and not calculated. Therefore, only its influence onto the receiver's efficiency can be investigated and its value not be determined. For calculation of the plants efficiency, values for the ARR have to be obtained from other sources or appropriately assumed.

In the simulations, the number of cells in the OVR model is set to 300 as a further increase in number of cells has sown not to have a significant impact on the results.

Due to lack of experimental data a comprehensive validation of the model is not possible. However, as far as possible, validation with data from the software *FreeGreenius* was carried out. In the software a model of the open volumetric receiver is implemented and values for design point efficiency can be retrieved. This was carried out for an air return ratio of 0.6, hot air temperature of 700 °C and return air temperature of 150 °C and varying flux density onto the receiver. The data provided by *FreeGreenius* is based on a model where the return air is preheated in the receiver. This is not taken into account in the presented model, because it causes significant thermal losses for an air return ratio below 1. However, for validation the preheating was taken into account in the receiver model. The resulting receiver efficiency for varying flux density is presented in Figure 5-6. A good agreement between the results from *FreeGreenius* and the results obtained with the OVR model that takes into account the pre-heating of the air can be observed. It can also be seen that the receiver efficiency of the OVR without pre-heating of the return air is significantly higher. Therefore, in this work, the pre-heating of the air before ejecting it in front of the receiver is not taken into account. Note that due to the limited range of values for the parameters in *FreeGreenius,* a validation towards higher hot air temperatures or cavity geometry is not possible.

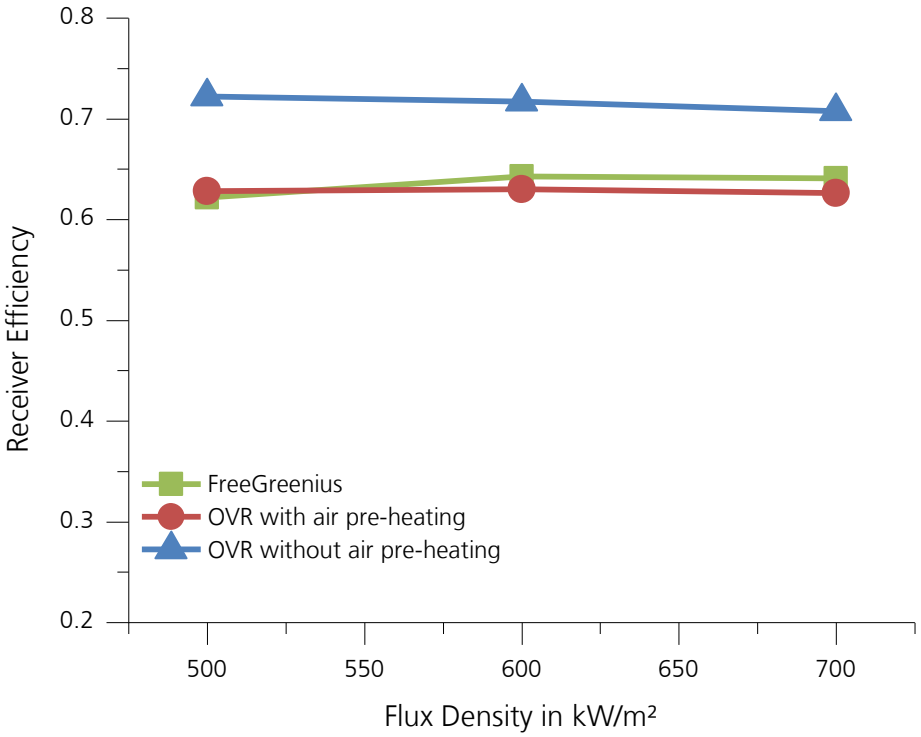

Figure 5-6: Comparison of the results for receiver efficiency for varying flux density of the Freegrenius and the OVR model with and without preheating of the air for validation.

5.2.1. Determination of optimum flux density onto receiver

In order to reduce the computational time for determining the optimum flux for operation of the SOLME process, the characteristics of the receiver are investigated prior to the process simulation. The main parameters influencing the receiver efficiency besides the flux density are air return ratio (ARR), the hot air temperature (T_{HA}), the return air temperature (T_{RA}) as well as the ratio of aperture to absorber area (C_{Cav}) When these parameters are fixed, no interactions with the subsequent process occur, and an efficiency map of the receiver with regard to the flux can be obtained.

Therefore, simulations are carried out with a variation of all of the mentioned parameters. As all parameters are varied independently, a large number of simulations are carried out yielding a correspondingly large amount of results. For clarity, it is only mentioned that the results of variation of air return ratio and the return air temperature are not presented in the following, because even though they influence the absolute value of the receiver efficiency, they do not influence the location of optimum flux for receiver operation. The results of the remaining parameter variation are shown in Figure 5-7, on the left side for a

receiver without cavity, on the right for a receiver with cavity C_{cav} = 0.637. Note that the scale of the abscissa is different on the two sides. Furthermore, the correction factor for the energy provided by the heliostat field presented in section 5.1 is applied here. It can be seen that the energy provided by the receiver, which is proportional to the receiver efficiency, increases when the flux density is increased above 400 kW/m². When further increasing the flux density an optimum develops, above which the energy provided by the receiver decreases. It can be seen that this optimum moves towards higher flux densities, when the hot air temperature is increased. It is also higher for the cavity receiver than for the flat receiver. Another general trend that can be observed is that for low flux densities (< 700 kW/m²) the receiver efficiency increases with decreasing temperature, within the considered range.

In the receiver simulations carried out in this work, the optimum flux density for the given geometry and hot air temperature that is obtained from the data in Figure 5-7 will be used. In Appendix D, a table with the values to be used is presented.

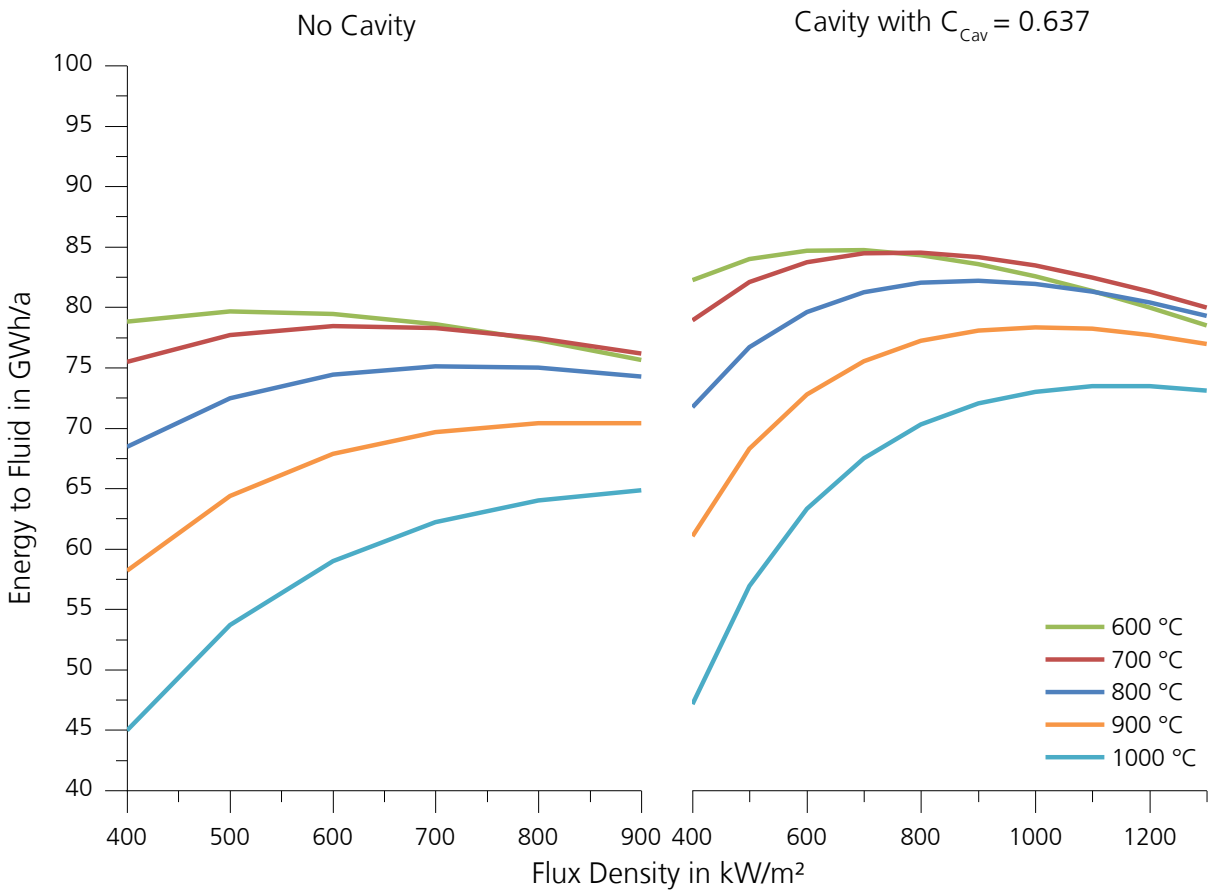

Figure 5-7: Influence of flux density on energy transferred to fluid for different T_{HA} for a receiver without cavity (left) and a receiver with cavity (right). Note the different scale of the abscissa left and right.

5.3. Thermal energy storage

For simulation of the thermal energy storage (TES), a simple model based on energy balances is implemented. It is noted that the TES does not influence the results of the simulation regarding thermodynamics, but only the results of the economic investigation that is carried out in chapter 7. This is due to the fact that the TES is not implemented out of thermodynamic considerations but due to economic reasons. Hence, a meaningful layout is only possible when economics are taken into account. In the thermodynamic process investigation in chapter 6, an ideal storage without any losses is assumed. In the economic investigation in chapter 7, the storage layout is carried out and the its resulting efficiency is applied.

The structure of the model is presented in Figure 5-8. The structure represents the calculation for the time interval Δt. In the time interval the receiver provides the heat flow

of $\dot{Q}_{\mathrm{Use}}(t)$ that is previously calculated with the receiver model. If it is larger than the nominal heat flow required by the process $\dot{Q}_{\mathrm{Process,nominal}}$, the excess heat is given to the storage, as long as the storage is not full. If the heat provided by the receiver is smaller than the heat required by the process, the missing heat is taken from the TES, if it contains a sufficient amount of energy. If this is not the case, the process is shut down.

The nominal heat required by the process is determined by division of the maximum heat flow the receiver provides by the solar multiple (SM). The solar multiple, just as the maximum storage size $Q_{\mathrm{Storage,Max}}$, is an input parameter. As can be seen in Figure 5-8, if the storage is full, not all of the heat provided by the receiver can be made use of. If this is the case, energy from the receiver is wasted, causing a decrease in the efficiency of the TES. The simulation of the TES is carried out with a time interval Δt of one hour, as this is the time interval of the DNI data that is used as input for receiver simulation. The storage is calculated for the entire year and remaining energy content at the end of the year is provided at the first time interval of the year in order to allow for a valid energy balance. Therefore, an iterative calculation has to be carried out. The simulation is carried out in *MS Excel*, as this software allows for coupling with the receiver and process model in *Aspen Dynamics* and provides all required operations.

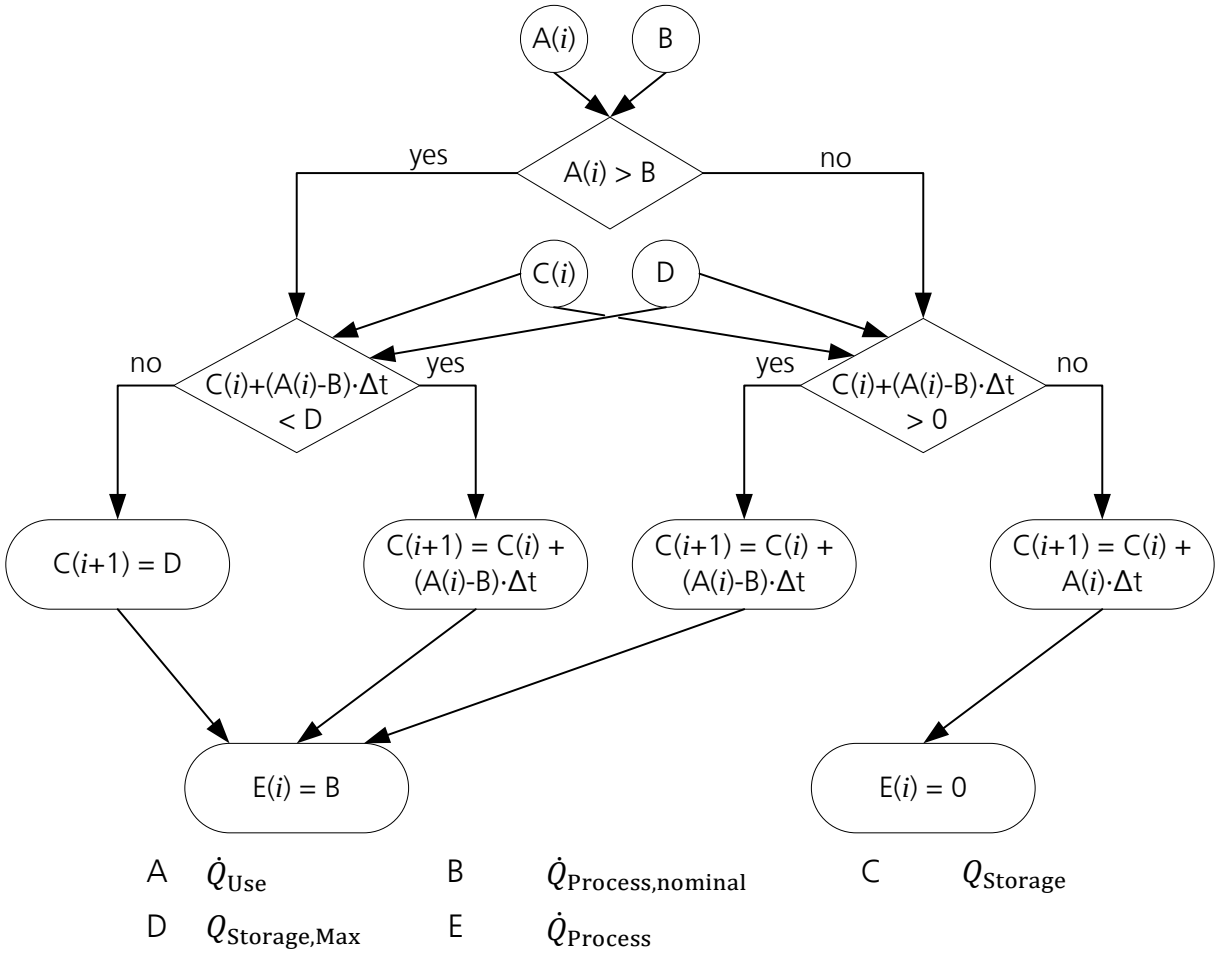

Figure 5-8: Structure of thermal energy storage model.

The central results of the simulation of the TES are its efficiency and the amount of hours it allows for operation of the process by supply of the nominal heat load. As no thermal losses of the receiver are taken into account, the efficiency is only influenced by the amount of energy that cannot be stored because the TES is already full.

5.4. Air-heated reformer

For the air heated reformer (AHR), a jacketed tube, which is shown in Figure 5-9, is assumed, where the reactants flow through the inner tube and hot air flows through the annulus. In order to model the AHR, the heat transfer between the two countercurrent flows and the simultaneous reaction in the inner tube has to be modelled. This type of model does not exist in the model library of Aspen Dynamics, therefore a model is developed in the Aspen Custom Modeler. Wesenberg [46] presented in her work a model

of a gas-heated reformer, which follows a similar concept as the AHR. The main differences are that in the gas-heated reformer, hot syngas serves as heat transfer fluid and it only serves for pre-reforming of the reactants with a target conversion of approximately 30 %. The gas-heated reformer model from Wesenberg [46] is used as a basis for the AHR model. However, in order to allow for low simulation time, the model is simplified. It is also adjusted to achieve a close to complete conversion. The model is identical to the model used in the work presented by von Storch et al. [62].

The model of the AHR is carried out as a pseudo-homogeneous plug-flow (i.e. 1-D) model. Therefore, as no separate solid catalyst phase is modelled, the diffusive limitations in the kinetics cannot be determined, but effectiveness factors have to be implemented, when intrinsic kinetics are used. Furthermore, only one of the jacketed reactor tubes is modelled, as it is assumed to represent any other tube in the bundle. All fluid properties used in the simulation of the reactor tube are retrieved from the Aspen Properties, with the Peng-Robinson properties method.

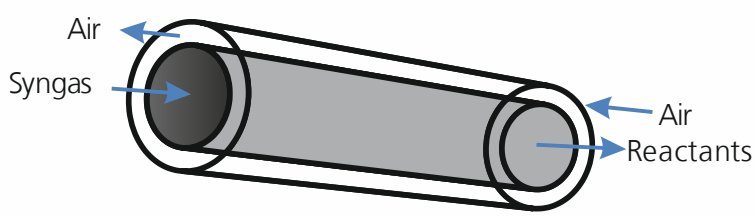

Figure 5-9: Sketch of AHR tube

The reforming reaction is modelled with the kinetics determined by Xu and Froment [63] for a nickel-based catalyst. In their kinetic model, the reactions given in Eqs. (2.1), (2.2) and (2.4) occur, here they will be referred to as reaction 1, reaction 2 and reaction 3 respectively. The correlations they determined are given in Appendix D. As the presented model is a pseudo-homogeneous model, but the kinetics that are used are intrinsic (i.e. not taking into account diffusional limitations), an effectiveness factor for the catalyst pellet has to be used. The effectiveness factor is necessary, as not all the catalyst mass in the pellet can promote the reactions as intrinsic kinetics imply, because for catalyst inside the pellet, diffusional limitations are the limiting mechanism. Wesenberg [46] presented results for the effectiveness factors η_{r_i} of the catalyst pellets for each reaction obtained from her simulations of the reformer tube with a heterogeneous model. Average values retrieved from her results are used for the effectiveness factor. The values are 0.055 for reaction 1 and 3 and 0.09 for reaction 2. The effective rate of reaction $r_{i,\mathrm{eff}}$ is the product of the rate calculated from intrinsic kinetics r_i and effectiveness factor (cf. eq.(5.16)).

$$r_{i,\mathrm{eff}} = r_i \cdot \eta_{\mathrm{r},i} \tag{5.16}$$

The species that are present in the reactor are the ones that are present in the natural gas plus the water added to the reactor, as well as the reaction products. Commonly these are CH_4, CO_2, CO, H_2O, H_2 and N_2. In Eqs. (5.17) and (5.18) the material balance for CH_4 and CO_2 respectively are shown. In the equations it can be seen that the derivative for the conversion X of the species inlet flow F over reactor length z equals its formation or consumption in the reactions . The conversion of both species is defined in relation to the natural gas flow at the reactor entrance, as shown in Eqs. (5.19) and (5.20). While the conversion of CH_4 describes the disappearance of the substance, the conversion of CO_2 describes the formation of the substance. Only two independent reactions occur in the reactor tube. Therefore, equations for determination of the conversion of two substances are sufficient to describe the gas composition in the tube at any location, if the composition at reactor inlet is known. The mass of the catalyst in the tube is represented by the density of the catalyst bed $\rho_{\mathrm{Cat,Bed}}$ (i.e. solid material per tube volume) and the cross sectional area of the tube $A_{\mathrm{tube,c}}$.

$$\frac{\partial X_{\mathrm{CH_4}}}{\partial z} \cdot F_{\mathrm{CH_4}} = \rho_{\mathrm{Cat,Bed}} \cdot A_{\mathrm{tube,c}} \cdot (r_{1,\mathrm{eff}} + r_{3,\mathrm{eff}}) \tag{5.17}$$

$$\frac{\partial X_{CO_2}}{\partial z} \cdot F_{CH_4} = \rho_{\mathrm{Cat,Bed}} \cdot A_{\mathrm{tube,c}} \cdot (r_{2,\mathrm{eff}} + r_{3,\mathrm{eff}}) \tag{5.18}$$

$$X_{\mathrm{CH_4}}(z) = \frac{F^0_{\mathrm{CH_4}} - F_{\mathrm{CH_4}}(z)}{F^0_{\mathrm{CH_4}}} \tag{5.19}$$

$$X_{CO_2}(z) = \frac{F_{\mathrm{CO_2}}(z) - F^0_{\mathrm{CO_2}}}{F^0_{\mathrm{CH_4}}} \tag{5.20}$$

The equations for the calculation of the molar flow of the remaining species in dependence of $X_{\mathrm{CH_4}}$ and $X_{\mathrm{CO_2}}$ and the species' flow at reactor inlet is given in Eqs. (5.21) to (5.24). The determination of the total molar flow in the reactor is the sum of the molar flow of all species, which can be simplified to the equation given in Eq. (5.25).

$$F_{\mathrm{CO}}(z) = F^0_{\mathrm{CO}} + F^0_{\mathrm{CH_4}} \cdot (X_{\mathrm{CH_4}}(z) - X_{\mathrm{CO_2}}(z)) \tag{5.21}$$

$$F_{\mathrm{H_2O}}(z) = F^0_{\mathrm{H_2O}} - F^0_{\mathrm{CH_4}} \cdot (X_{\mathrm{CH_4}}(z) + X_{\mathrm{CO_2}}(z)) \tag{5.22}$$

$$F_{\mathrm{H_2}}(z) = F^0_{\mathrm{H_2}} + F^0_{\mathrm{CH_4}} \cdot (3 \cdot X_{\mathrm{CH_4}}(z) - X_{\mathrm{CO_2}}(z)) \tag{5.23}$$

$$F_{\mathrm{N_2}}(z) = F^0_{\mathrm{N_2}} \tag{5.24}$$

$$F_{\mathrm{Total}}(z) = F^0_{\mathrm{Total}} + F^0_{\mathrm{CH_4}} \cdot (2 \cdot X_{\mathrm{CH_4}}(z)) \tag{5.25}$$

The heat transfer from the air to the reactants, or the catalyst, occurs by convection from the air to both the inner wall as well as the outer wall of the annulus, $r_{\mathrm{an,in}}$ and $r_{\mathrm{an,o}}$ respectively. From the outer wall of the annulus, heat is transferred radiatively to the inner tube. From the inner wall of the annulus, which is also the outer wall of the reactor, the heat is transported by conduction to the inner wall of the reactor $r_{\mathrm{w},i}$, where the reactants are heated convectively. The heat transfer mechanisms are illustrated in Figure 5-10.

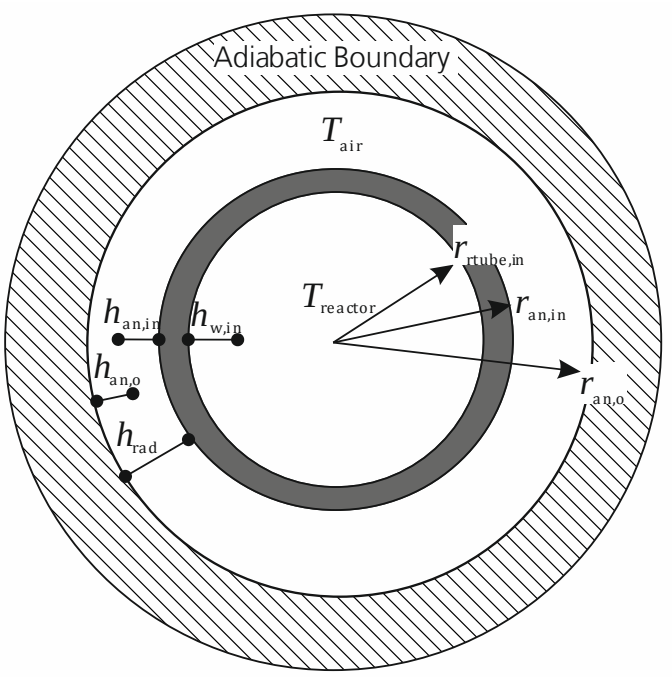

Figure 5-10: Cross-section of the AHR with illustration of heat transfer mechanisms

The hot air enters the annulus with the temperature T_{HA}, the heat transfer coefficient for the heat transfer towards the two annulus walls is determined with a Nusselt correlation for a concentric annulus from VDI-Heat-Atlas (German version) [64], chapter Gb, originally proposed by Petukov and Roizen [65]. The correlation is merely a factor to be used with the Nusselt number for fully developed turbulent flow from VDI-Heat-Atlas (German version [64], chapter Ga, originally proposed by Gnielinski [66]). It is dependent on the Reynolds and Prandtl number and the corresponding correction factor for the present boundary condition. For this model the boundary condition 3 (cf. [64], chapter Gb) is chosen: Heat transfer occurs to both inner and outer wall, with the same wall temperature. This seems valid despite the fact that the outer wall is adiabatic towards the environment. The outer wall emits heat radiatively to the inner wall and because it is in thermal equilibrium has to be heated convectively by the air flow. The same wall temperature for inner and outer wall of the annulus cannot be perfectly satisfied, however, the temperature difference is expected to be small. The pressure drop in the annulus is calculated according to the procedure proposed in VDI-heat atlas [67], chapter L1: The regular pressure drop correlation for turbulent flow through pipes is used, but with the hydraulic diameter as the

characteristic length (also in the Reynolds number). The correlations are given in Appendix F.1.

The radiative heat exchange between the outer and the inner tube is calculated with view factors for a closed geometry, assuming only one-dimensional heat exchange. This is only valid for constant wall temperature in axial direction, which does not apply for the present case. However, due to the low axial temperature gradient expected in the reformer (approx. 33 K/m) and the low thickness of the annulus, this is expected to be acceptable. The heat transferred radiatively between the inner and the outer annulus wall $\dot{Q}_{\mathrm{rad,An}}$ is given in Eq.(5.26) [68].

$$\dot{Q}_{\mathrm{rad,An}}(\mathrm{z}) = \frac{1}{\frac{1}{\varepsilon_{\mathrm{Tube}}} + \frac{A_{\mathrm{An,o}}}{A_{\mathrm{An,in}}} \cdot \left(\frac{1}{\varepsilon_{\mathrm{Tube}}} - 1\right)} A_{\mathrm{An,in}} \cdot \sigma \cdot \left(\left(T_{\mathrm{An,in}}(z) + 273.15\right)^4 - \left(T_{\mathrm{An,o}}(z) + 273.15\right)^4\right) \tag{5.26}$$

The conductive heat transfer through the reactor tube wall (i.e. inner annulus wall to reactor wall) is modelled with the Fourier equation for a cylindrical shape. Again only radial heat transfer is modelled; axial heat transfer is neglected due to the low axial temperature gradient.

The heating of the gases inside the reactor tube is modelled with correlations for a pseudo-homogeneous flow, i.e. no separate solid phase is modelled for the catalyst. For the heat transfer coefficient of the inner reactor tube wall (at $r_{\mathrm{w,in}}$), a correlation proposed by Peters et al. [69] and validated for the purpose of modelling a particle filled (packed bed) reactor tube by Wesenberg [46]. The correlation is given in Appendix F.2. In the equation, the ratio of the equivalent diameters of the catalyst pellets (d_{Particle}) and the reactor tubes inner diameter ($d_{\mathrm{Tube,in}}$) as well as the particle Reynolds number, with the particle diameter as the characteristic length, and the Prandtl number are used. The data for the catalyst is retrieved from the data sheet of a broadly applied catalyst by Haldor Topsøe [70]. The same catalyst was considered in several other models of reforming reactors, e.g. by Wesenberg [46] and Pedernera et al. [71]. The diameter used is the equivalent diameter of a sphere with the same surface per unit volume, in this case 10.95 mm.

When calculating the heat transfer coefficient from the Nusselt correlation for the gas flow through a packed bed, the thermal conductivity of the packed bed has to be used. This is the case because the flow and particle characteristics significantly influence its thermal behavior [72]. The thermal conductivity of the packed bed is calculated according to the Zehner/Bauer/Schlünder model proposed for this purpose in VDI-Heat Atlas [67], sub-section D6.3.4. The model is recited in Appendix F. For calculation of the thermal conductivity of - and the pressure drop through - the packed bed, the porosity has to be known. The porosity is calculated for the reactor tube according to the correlations given in VDI – heat atlas [64] in chapter Mh (German version) for Raschig-rings with the dimensions of the catalyst considered. The model for the porosity takes into account the influence of the wall on the particle bed and hence on the porosity. However, as the reformer model does not take into account radial gradients, only the mean value for the porosity is used. The correlation is given in Appendix F. The calculated mean value is 0.481; this value agrees well with the value used by Pedernera et al. [71], 0.489 (calculated from given data for pellet density and bulk density).

The pressure drop in the reactor is determined with the correlation proposed by Hicks [73], and also used by Wesenberg [46]. It is given in Appendix F.2.

5.4.1. Validation of AHR Model

No experimental data is available yet for validation of the AHR model. However, Wesenberg [46] had the possibility to compare parts of her model with experimental data and published sufficient data of her model to allow for validation of the AHR model with the results obtained with her model. In order to do so, the input flows for reacting gas and heating gas were set identical to the flows in her model. It should be mentioned that in her model a hot syngas flow is used for heating the reaction, while in this work air will be used. The resulting mole fractions for the different species in the reactor over reactor length are presented in Figure 5-11. A very good agreement can be seen throughout the entire reactor length.

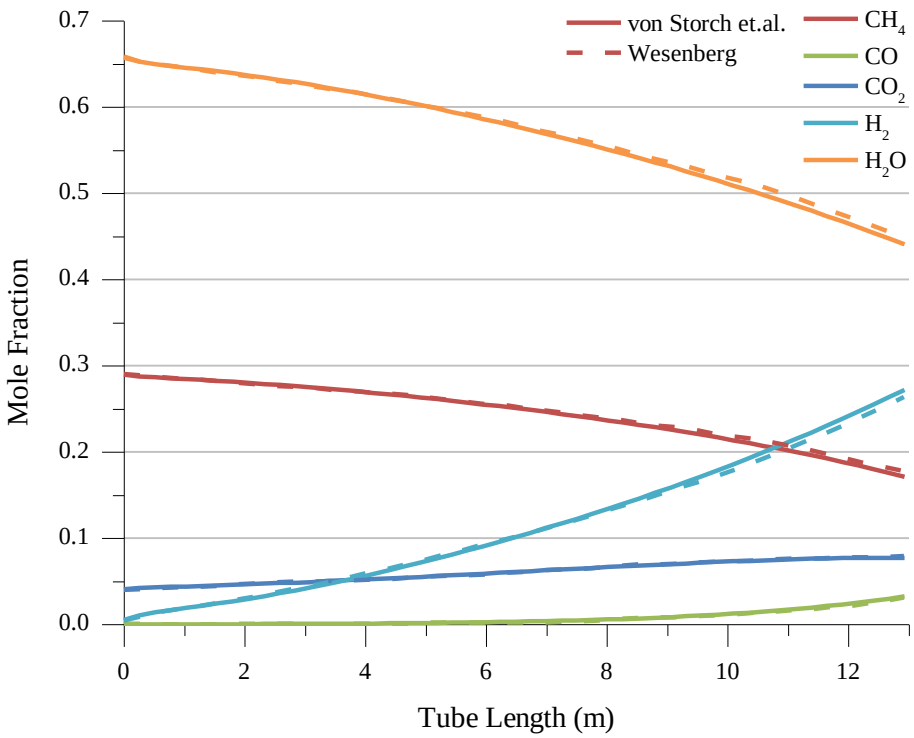

Figure 5-11: Comparison of results presented by Wesenberg and obtained by AHR. The validation was already published in [74].

5.4.2. Air as heat transfer medium for the reforming reaction

In order to set the operating conditions of the AHR, it is reasonable to assess the maximum performance achievable by a reforming system that is heated by hot air. In order to do so, the reactants' heat demand to achieve chemical equilibrium at a given temperature and the capability of the air to provide the necessary heat are determined. In order to do so, neither heat transfer coefficients nor reaction kinetics should be taken into account, but ideal heat transfer and instantaneous chemical reactions should be assumed. However, a simple energy balance of the reactor will not give meaningful results, as it might suggest results that are not feasible in reality. This is illustrated by Figure 5-12. On the left hand side of the figure the temperature of an air flow as well as the temperature of the reactants in the reactor are shown over the transferred heat, the air flow is $F_{\mathrm{Air}} = 4.5 \cdot F_{\mathrm{Total}}$. Note that a countercurrent flow is assumed, therefore the air enters from the right with high temperature and is cooled by heating the reactants. As can be seen, even though the overall energy balance gives reasonable results, the heat transfer is not possible in the depicted form, because at some parts of the AHR, the air is colder than the reactants. This

so called *internal crossover* is caused by varying effective thermal capacity of one of the participants in the heat transfer, i.e. the temperature is strongly non linearly dependent on the transferred heat. This phenomena can also occur in simplified modelling of heat exchangers with phase change. On the right hand side of the figure, the same configuration is shown, but the air flow is adjusted to give feasible results. It can be seen that either the air flow can be reduced to $F_{\mathrm{Air}} = 3 \cdot F_{\mathrm{Total}}$, so that a small temperature difference is achieved at the cold *lower* end of the reactor, resulting in low return air temperatures. However, the inlet temperature of the air has to be 1200 °C in order to achieve this (cf. dotted line in Figure 5-12, right). This high air inlet temperature will lead to receiver temperatures in the same range and reduce receiver efficiency significantly. Alternatively, the air flow can be increased to e.g. $F_{\mathrm{Air}} = 5.5 \cdot F_{\mathrm{Total}}$ (cf. solid line in Figure 5-12, right) and a low temperature difference can be set at the hot *upper* end of the reactor, resulting in an increased outlet air temperature. Due to the paramount influence of the receiver temperature on its efficiency (cf. Eq. (2.13)), the receiver temperature is expected to be one of the dominating factors for overall process performance. In order to take this into account, in process simulation, the upper temperature difference $\Delta T_{\mathrm{Upper}}$ at the hot side of the AHR, is one of the optimization parameter.

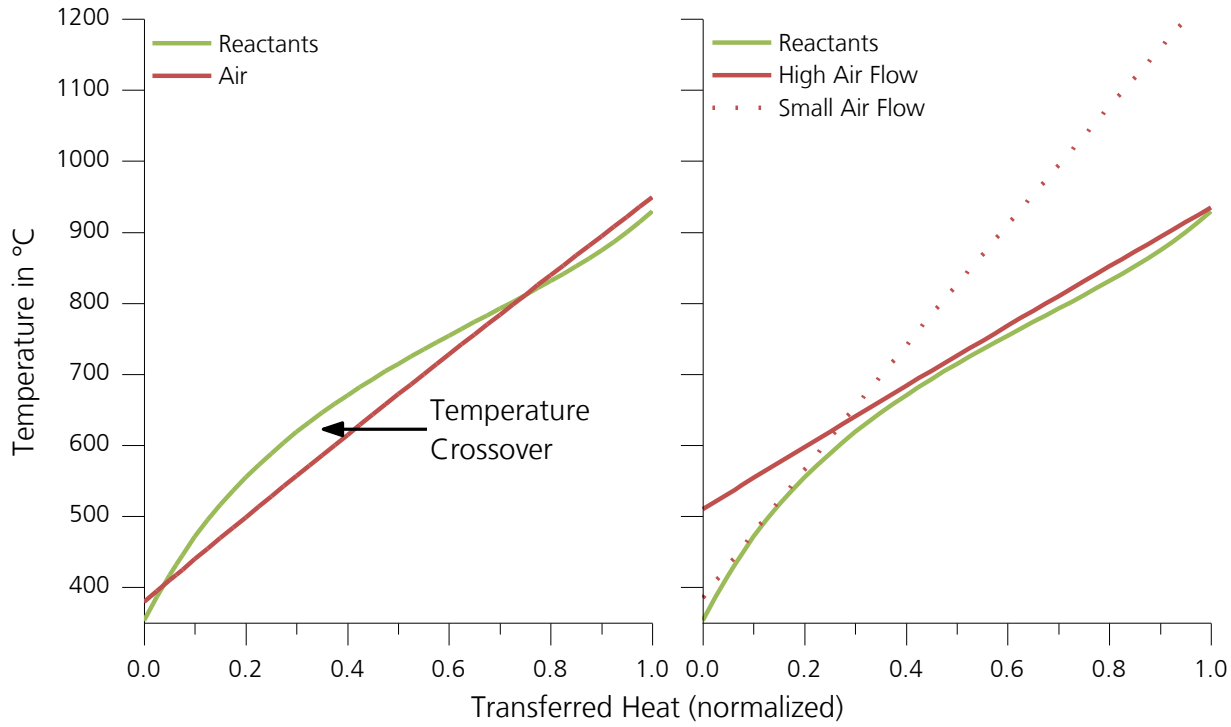

Figure 5-12: Temperature over transferred heat in the air heated reformer (exemplary values), with invalid temperature crossover (left) and two adjusted air flows to prevent temperature crossover (right). Reactants flow is 1 mol/s, reactants pressure is 26.4 bar.

The issue presented in this figure furthermore indicates that even for simplified modelling of the reactor, a discretization of the heat transfer is necessary in order to prevent the model to yield non-logical results that might not always be identifiable as such.

5.4.3. Adaption of model to conditions in SOLME process

The gas-heated reformer presented by Wesenberg [46] is not designed to achieve complete conversion of the natural gas, but only approximately 30 %. In contrast, in the AHR, a close-to complete conversion of the natural gas is desired in order to achieve a high yield of methanol in the process. Therefore, the residence time of the reactants in the reforming reactor should be increased to allow for both the reaction and the heat transfer to occur to the required extent.

In order to determine the appropriate residence time for the reactants in the AHR, simulations of the AHR are conducted: A natural gas flow of 10 kmol per hour is introduced into the reactor and the number of reactor tubes is varied. In this example, the reactor pressure is set to 26.4 bar, the steam to natural gas ratio is set to 2. The ratio of air

flow to reactants flow is 5.5 and the hot air temperature is set to 900 °C (identical to the conditions that were used in preparation Figure 5-12 (right, dashed line)). Due to compression of the natural gas to the reforming pressure and the evaporation and superheating of the steam by heat transfer from the hot air that leaves the reactor, the reactant mixture has a temperature of 390°C when entering the reactor. The upper temperature difference in the reactor in dependence of the number of tubes is shown in Figure 5-13. It can be seen that in order to achieve upper temperature differences below 30 K more than 100 reactor tubes are necessary, in order to achieve 15 K temperature difference 500 reactor tubes are necessary. It is expected that the optimum upper temperature difference will be in this range in order to achieve high receiver efficiency. Due to the low velocities in the reactor, Reynolds numbers below 100 for the air flow and below 10 for the gas flow result. Hence laminar flow can be assumed in both parts of the AHR, but some of the equations used in the model assume turbulent flow. Therefore, the model has to be adjusted to be valid for the present laminar flow conditions.

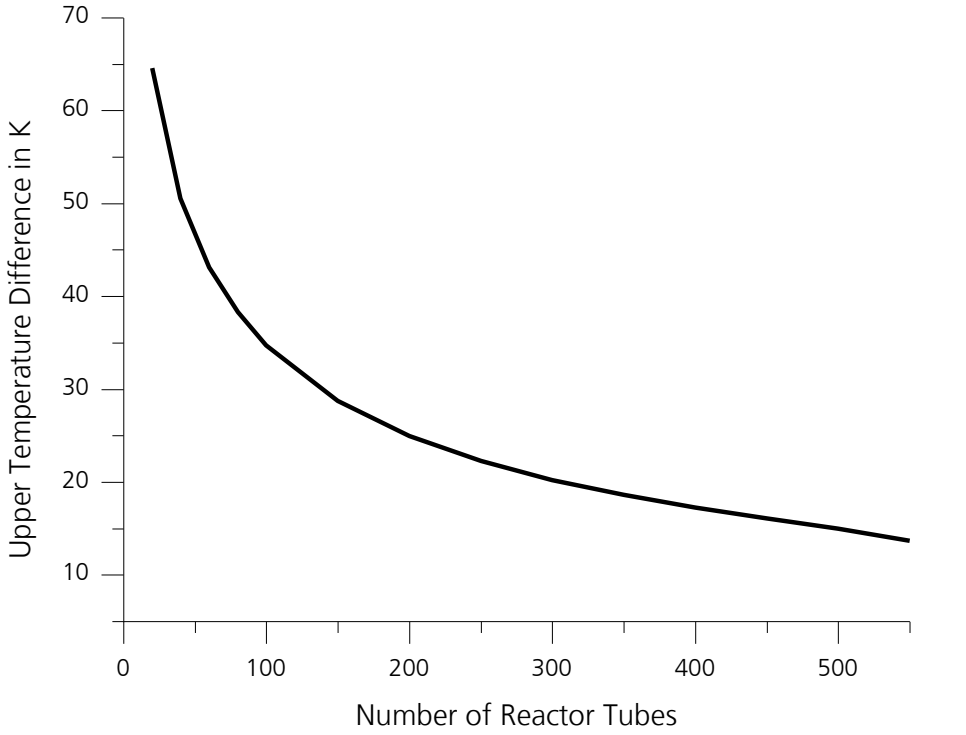

Figure 5-13: Upper temperature difference in AHR for 10 kmol/h of reactants and 55 kmol/h of hot air in dependence of number of reactor tubes

For laminar flow in the in the annulus (i.e. $Re_{\mathrm{An}} < 2300$), the corresponding correlation for calculation of the Nusselt number given in VDI heat atlas [67] chapter G2. The correlation is presented in Appendix F.1. The pressure drop in the annulus at laminar conditions is calculated by a general pressure drop equation (depicted in Appendix F.1) with the friction factor for laminar flow, as suggested in VDI-Heat Atlas [67], Chapter L1.

The heat transfer and pressure drop inside the reactor tube do not have to be adjusted, because the original correlations are valid at the low Reynolds numbers present. The correlation used for calculation of the Nusselt number is valid for Reynolds numbers below 8000. The validity of the correlation used to calculate the pressure drop in the packed bed is given for $Re/(1-\psi) > 300$. Even though this is not the case in the given example, the equation is used due to lack of a more appropriate one. It should also be noted that the pressure drop in the reactor tube for conditions with Reynolds numbers at the lower end of validity, is below 0.01 bar. For smaller Reynolds numbers, an even smaller pressure drop can be expected. Due to the low magnitude of the expected pressure drop and the corresponding negligible influence on process performance, it is not a matter of further investigation in this work.

Rout and Jakobsen [75] claim that the utilization of a pseudo-homogeneous reforming reactor model will lead to severe deviation in the results from reality due to the fact that effectiveness factors vary throughout the reactor. However, they assume a state of the art reforming reactor that is heated by combustion on the outside with resulting high heat fluxes through the reactor walls. For the conditions given in the present example of the AHR, the actual effectiveness factors have a negligible effect on the results of the simulation, as shown in Figure 5-14. In the figure the conversion of CH_4 and the product outlet temperature for different values of the effectiveness factors for steam reforming (SR), water gas shift (WGS) and their combination (SR+WGS) are shown. One effectiveness factor is varied at a time, the other ones are kept at the originally set value. The conditions are identical to the conditions in the example given above in Figure 5-13 for an upper temperature difference of 15 K. It can be seen that the results are nearly constant for values of the effectiveness factor down to 10^{-3}. The variation in conversion and temperature are below $8.1 \cdot 10^{-4}$ (0.13 %) and 0.3 K respectively. This means that for values above the lower

limit of 10^{-3} for the effectiveness factors, the effective rate of reaction is fast enough, so that only heat transfer into the reactor is limiting the progress of the reaction. The effectiveness factors reported by Rout and Jakobsen [75] are always well above 10^{-3}, hence no distortion of the results due to application of a pseudo-heterogeneous model are expected. Furthermore, this indicates that the actual value of the rate of reaction does not influence the results of the model, but chemical equilibrium is reached in the reactor at all times. Therefore it seems adequate to omit the calculation of rate of reaction in order to reduce computational time of the model and calculate composition in the reactor model with the assumption that chemical equilibrium is achieved. The results of the model with and without kinetics are compared and no deviation is detected. These findings are supported by Rostrup-Nielsen et al. [7], who state "The activity of the catalyst is rarely a limiting factor" (p.82), even for gas-fired reformers with higher heat fluxes.

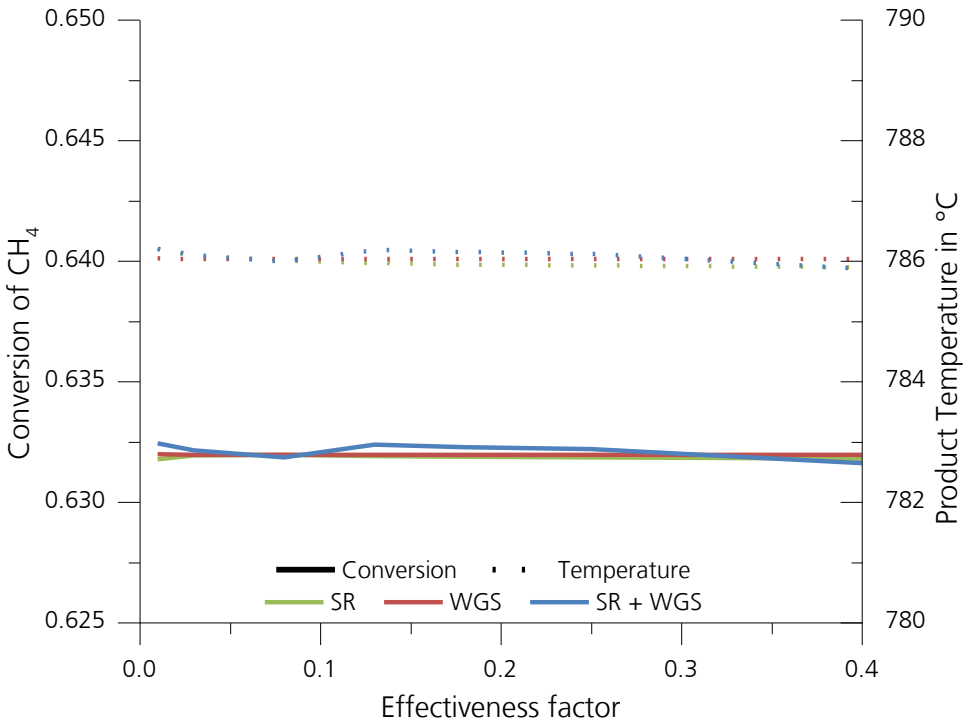

Figure 5-14: Influence of effectiveness factors on AHR results for conversion of methane and product temperature.

5.5. Methanol Synthesis

In order to enable low simulation times, a model is designed that uses some simplifications in simulation of the methanol synthesis reactor. In the model, the chemical equilibrium is calculated for the two reactions that occur in the reactor: The methanol synthesis reaction (Eq. (5.27)) and the water-gas-shift (Eq. (2.2)).

$$3\mathrm{H_2} + \mathrm{CO_2} \rightleftharpoons \mathrm{CH_3OH} + \mathrm{H_2O} \qquad \Delta H^0_{\mathrm{R,298K}} = -49\frac{\mathrm{kJ}}{\mathrm{mol}} \qquad (5.27)$$

In the reactor model a desired outlet temperature is set and the heat necessary to reach the temperature and chemical equilibrium at the temperature are calculated. This method seems valid for the simulation of a boiling water reactor, because the reaction is cooled isothermally by boiling water and the temperature can be controlled well. A temperature difference between reactor outlet and boiling water and a temperature approach to the chemical equilibrium can be assumed. The values are set in accordance with Luyben [48]: The outlet temperature of the reactor is set to 265 °C, the pressure of the cooling water is set to 39.52 bar, to allow for boiling at 252 °C. For the Methanol synthesis reaction, a temperature approach of 10 K is assumed (i.e. the chemical equilibrium is calculated for 275 °C). Furthermore, a pressure drop of 2.5 bar is assumed.

Due to utilization of this simplified model, an intensive investigation of the methanol part of the SOLME process is not possible, as heat transfer and flow through the reactor are not modelled in detail. However, this is not the central aspect of this work and the methanol synthesis in the SOLME process is in essence not different from the industrially practiced methanol synthesis, where sufficient data is published to retrieve the values that are set in this model to meaningful values (e.g. [48]).

The separator, flash and compressor units in the methanol synthesis part are simulated with models from the Aspen Dynamics library. In Aspen Dynamics, there is no appropriate model to simulate the distillation column that determines the necessary heating and cooling demand of a column to separate a mixture. Therefore, the distillation column is beforehand simulated in Aspen Plus which provides an appropriate model. This is possible, because the inlet composition of the column does not vary significantly when the process parameters

are changed. Then values for the heat demand of the column in relation to the methanol product flow are generated and the heat demand is implemented into the Aspen Dynamics flowsheet of the SOLME process. The heat demand of the distillation column is 16.3 kWh per kmol of purified methanol produced at a temperature above 100 °C. The cooling demand can be provided by water from the ambient, hence it will not influence the process performance significantly. Therefore, even though the distillation column is not actually implemented into the flowsheet of the SOLME plant, its implications on process performance are taken into account.

6. Process Simulation and Results

In simulation of the SOLME process, the overall plant, including heliostat field, receiver, reforming and methanol synthesis is simulated. The most central results transferred to the data acquisition tool in *MS Excel* are the total solar energy onto the heliostat field, the input natural gas, the power transferred to the air in the receiver, the methanol production rate and the electricity production. From this data the reference system (methanol plant and solar power plant), as well as the external CCGT in the SOLME system, can be scaled to achieve the identical output of methanol and electricity with the identical input of solar energy onto heliostat field. The reference methanol plant and the reference solar power plant are presented in the two sections 6.1 and 6.2, the CCGTs in the SOLME system, both the internal one for off-gas utilization as well as the external one for additional electricity production are simulated by an assumed fuel-to-electricity efficiency of 60 %. However a sensitivity study is carried out later on to assess the sensitivity of the results on this assumption.

The natural gas composition is identical for the SOLME process, the reference methanol plant and the CCGT. It is presented in Table 6-1, it is the same composition that was used in previous studies [43, 74]. It can be seen that the considered natural gas exhibits a high carbon dioxide content. This is set intentionally, as there are a number of natural gas or methane sources with high carbon dioxide content (i.e. molar fraction > 0.1). Finn and O'Brien [76] discussed the significant costs of the different possibilities of avoiding the emission of carbon dioxide content in these CO_2-rich natural gas resources. In the methanol production (both SOLME and the reference process, CO_2 is a useful reactant, hence it does not have to be separated from the methane.

Table 6-1: Natural gas composition of natural gas into processes

Component	Molar fraction
CH_4	0.760
CO_2	0.209
H_2	0.013
N_2	0.018

The process model that was presented in chapter 5 used for simulation of the SOLME process and the performance data is retrieved into the data acquisition. An optimization of the process is carried out as well as a variation of some crucial parameters in order to assess the results sensitivity on changes in the assumed values.

The distinction between some of the terms used in this and the subsequent chapter should be emphasized in order to ensure comprehensibility. The term *SOLME process* refers to the process that was developed within this work and explained in detail in section 3.2. In contrast to that, the term *SOLME system* refers to the system of the SOLME process and the external CCGT power plant introduced in section 4.4. The *reference system* refers to the system of the two reference processes that were also introduced in section 4.4: The conventional methanol production via steam reforming of natural gas (*reference methanol plant)* and the state of the art solar power plant (*reference solar power plant*).

6.1. Reference methanol plant

The reference methanol plant is in principal similar to the SOLME, introduced in section 3.2. Only the manner of heat supply is different and causes some changes in the process. The heat is supplied by combustion of additional natural gas. The temperature cross-over that was discussed for air as heat transfer medium in section 5.3 is not a problem for heating by combustion. Thus, the reforming in the reference plant is modelled with the same model used for the methanol reactor in the SOLME process. This means that the chemical equilibrium is calculated for the given outlet temperature for the SR and the WGS reaction. In order to keep the natural gas consumption to a minimum, the hot syngas is used for pre-heating the reactants and the off-gas from the methanol synthesis is also combusted to

heat the reforming reactor. Not the entire syngas can be used to heat the reactants, because its heat content exceeds the pre-heating demand of the reactants. Therefore, a certain fraction (less than 10 vol.-%) is used to heat a WSC for electricity production. The reboiler in the distillation column is heated by the heat generated in the methanol synthesis reactor.

In the simulation of the methanol plant, the reforming temperature and reforming pressure are varied, in order to find optimal values for process efficiency. The methanol production efficiency is defined as the output of methanol in relation to the natural gas input. Here also electricity supply to the process by additional combustion of natural gas has to be taken into account.

The simulation results show that an increase in reforming temperature causes a monotonous increase in efficiency of the methanol synthesis. Therefore, the reforming temperature is set to the upper limit of 1000 °C. This value agrees with the data given by Aasberg-Petersen et al. [23]. The reforming pressure yielding optimum overall efficiency is 68 bar. The reformer outlet composition at these compositions corresponds to a value of 2.047 for the parameter M that was defined in Eq.(7.5). Therefore, a good agreement with the mentioned literature regarding the syngas composition for methanol synthesis is achieved (cf. ref. [25]).

The resulting efficiency of the process, which is defined as the lower heating value of the product in relation to the lower heating value of the input natural gas is 65 %. This agrees well with the value of 67 % reported by Wang and Huang [77] for the efficiency of methanol production, therefore the generated results can be considered realistic. Some more key results for the methanol plant are given in Table 6-2. All values in the parameters are normalized to one mole of methanol product.

Table 6-2: Natural Gas demand of reference methanol plant (normalized to 1 mole of purified methanol)

As reactant	1.182 mole
For heat supply	0.218 mole
For electricity generation	0.005 mole (21 kJ_{El})

Total demand $(F_{\mathrm{NG}_{\mathrm{Reference}}}/F_{MeOH})$	1.405 mole

6.2. Reference solar power plant

The reference solar power plant is assumed to be located at the same location as the SOLME plant, therefore the same data for solar irradiation (DNI-Data) can be used. Furthermore the same type of receiver as in the SOLME process is used. This does not only indicate that an open volumetric receiver is used, but that the shape of the absorber and the air return ratio of the reference solar power plant are set to the same values as in the SOLME process. This seems appropriate, because if, for instance, an air return ratio of 0.9 is achieved for the SOLME process, it should also be achieved in the reference solar power plant.

The receiver in the reference solar power plant is designed to deliver a hot air temperature of 650 °C. It is assumed that the return air temperature is 120 °C. The heat production of the receiver is then determined with the same receiver model that is used in simulation of the SOLME process. The intercept flux to be used for the simulation was determined with the performance map presented for the heliostat field - receiver system in Figure 5-7. This yielded a flux density of 550 kW/m² for a flat absorber and 700 kW/m² for a cavity type absorber. The mean annual power block efficiency $\eta_{\mathrm{PB,ref}}$ is assumed to be 35 %. In the ECOSTAR Report [78], an annual efficiency of 30.6 % for the power block was stated. In order to take into account potential improvements of the power block, a higher value than in the literature is used. However, in order to assess the results' sensitivity on changes of this assumption, a variation of this value up to 40 % is also carried out. The annual solar to electric efficiencies for the calculations in dependence of air return ratio and absorber shape are given in Table 6-3 for both assumptions of power block efficiency. Note that losses that might occur in the heat storage are not included and results should be scaled with the annual efficiency of the heat storage.

Table 6-3: Results for annual solar-to-electric efficiency of the reference solar power plant

	Annual Efficiency (solar to electric)			
	$\eta_{\mathrm{PB,ref}}$ = 35 %		$\eta_{\mathrm{PB,ref}}$ = 40 %	
ARR	Flat	Cavity	Flat	Cavity
0.6	17.2 %	18.4 %	19.7 %	21.1 %
0.9	18.1 %	19.3 %	20.7 %	22.1 %

6.3. Procedure of optimization and parameter study

The varied process parameters and the range of values are given in Table 6-4. Furthermore, in the right column a reference value is given for some of the parameters. If no other information is given, this value is used in the simulations. The first parameter in the table is the absorber shape, which was already discussed in detail in chapter 3. The remaining parameters, except for the number of tubes in the AHR n_{Tubes}, were also already introduced in chapter 3. In order to avoid scaling effects, the number of tubes are defined in relation to the mole flow of reactants per second through the reactor.

Another important parameter that is varied is the air return ratio. The variation of this parameter is carried out to assess its influence on the optimum process configuration and the potential benefit its increase has on process performance. It is not an optimization parameter, because it cannot be adjusted freely, but a maximization is aimed for. Two values are selected: 0.6 as reference or assumed current state and 0.9 as potential improvement.

Table 6-4: Varied parameters and ranges of values in simulation

Parameter	Unit	Range of Values	Reference Value
Absorber Shape	-	Flat or Cavity	-
$\boldsymbol{p_{\mathrm{Ref}}}$	bar	1…70	given in Table 6-5
$\boldsymbol{T_{\mathrm{Ref}}}$	°C	850…1000	-
$\boldsymbol{f_{\mathrm{Split}}}$	-	0 – 1	-
$\boldsymbol{S/NG}$	-	2…3	2
$\boldsymbol{\Delta T_{\mathrm{Upper}}}$	K	10-90	30
$\boldsymbol{n_{\mathrm{Tubes}}}$	1/(mole/s)	2…32	16

The initial values for the reforming pressure are set in dependence of the temperature such that a composition corresponding to a value of M close to 2.05 is achieved. This depends on the ratio of steam to natural gas flow S/NG in the reactor feed. The pressures that are determined for $S/NG = 2$ as well as the resulting value for M are given in Table 6-5. If not stated otherwise, those values are used for the simulations. However, in order to assess if an optimum value of 2.05 for M is valid for the SOLME process, a parameter variation of the reforming pressure is also carried out.

Table 6-5: Initial values for reforming pressure in dependence of reforming temperature for steam to natural gas ratio of 2 and the resulting value for M

$\boldsymbol{T_{\mathrm{Ref}}}$	$\boldsymbol{p_{\mathrm{Ref}}}$	$\boldsymbol{M}$
in °C	in bar	-
850	15.8	2.049
900	26.4	2.050
950	42.5	2.050
1000	66.0	2.050

The values for S/NG are limited to values > 2 in order to avoid catalyst damage by coking. Sun and Edwards [79] investigated the carbon formation in mixed reforming reactors and showed that even for a molar ratio of H_2O to CO_2 to CH_4 of 1.5/1.0/1.0, carbon formation will occur at temperatures below 780 °C. Even though, the reforming temperature will be higher than this value, the reformer inlet temperature will in most configurations be significantly lower. Therefore, the steam fraction is kept high enough in order to avoid the

possibility of coking in the catalyst. This is in good agreement with the procedure suggested in literature on reforming (e.g. [8, 14]).

Some interactions between parameters are expected and the results are presented accordingly. The first set of parameters expected to have interacting influence on the efficiency of the SOLME process are the reforming temperature and split fraction that together determine the hot air temperature and return air temperature, which in turn significantly influence the receiver efficiency. In the same set of simulations it is also investigated if the flat – or the cavity absorber achieves a higher overall efficiency.

Furthermore, the number of tubes in the AHR representing the heat transfer area in the reactor is expected to have an influence on the optimum value of $\Delta T_{\mathrm{Upper}}$ because it will assumingly influence the return air temperature. Therefore again a dependence on the receiver configuration is expected. Furthermore, an interaction with the steam to natural gas ratio is expected, as the return air temperature is decreased when more steam has to be evaporated. The optimum steam to natural gas ratio is expected to be a function of the air return ratio, as this determines the influence the return air temperature imposes on the receiver efficiency.

6.4. Results and discussion

For better comprehensibility, the results are structured in several blocks, according to the varied input parameters and the expected interactions explained above.

6.4.1. Split fraction, reforming temperature, receiver shape

At first, the results for the efficiency of the SOLME system in dependence of f_{Split} and variation of the reforming temperature are shown. The results for an air return ratio of 0.6 are shown in Figure 6-1 and Figure 6-2 for a cavity and flat absorber respectively

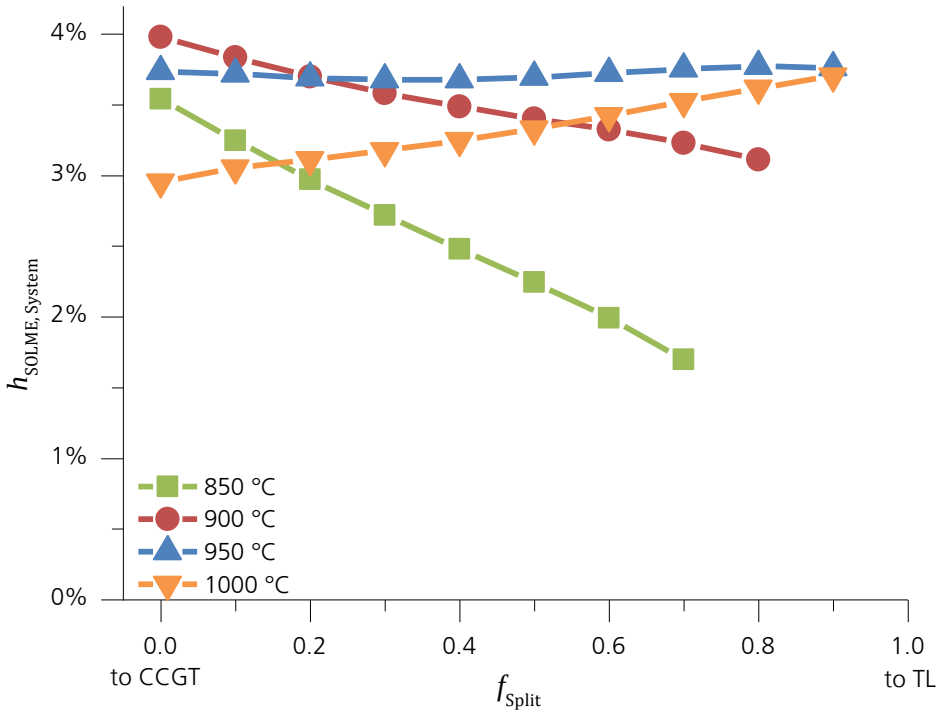

Figure 6-1: Efficiency of SOLME for a cavity absorber with air return ratio of 0.6 in dependence of split fraction for off-gas and reforming temperature.

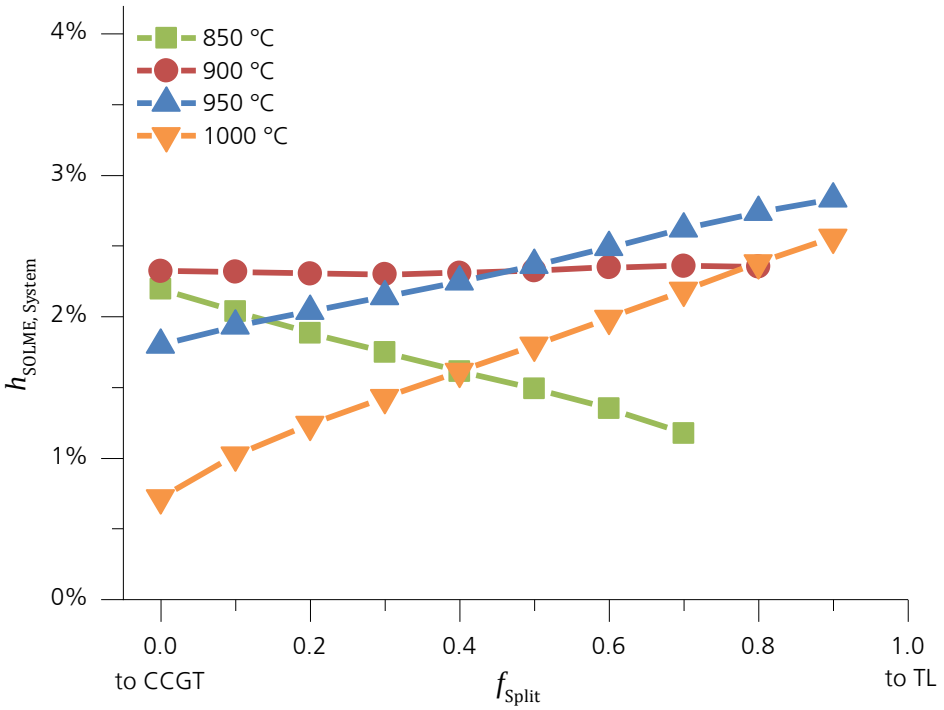

Figure 6-2: Efficiency of SOLME for a flat absorber with air return ratio of 0.6 in dependence of split fraction for off-gas and reforming temperature.

In the results it can be seen that the split fraction of off-gas has a significant influence on the efficiency $h_{\mathrm{SOLME,\ System}}$. It can also be seen that the influence depends on the reforming temperature. For both absorber geometries, the efficiency is linearly dependent on the split fraction. The gradient of this linear dependence increases with increasing reforming temperature. However, for a given reforming temperature, neither the gradient nor the absolute values are the same for the two different absorber geometries. The gradient of a given temperature is higher for the flat absorber than for the cavity absorber. In general, higher values for $h_{\mathrm{SOLME,\ System}}$ are achieved with the cavity absorber than for the flat absorber. With a cavity absorber, an efficiency close to 4 % is achieved at 900 °C reforming temperature and a split fraction of 0. For higher split fractions the optimum temperature is increased to 950 °C. At 950 °C the efficiency is nearly independent of the split fraction and values around 3.7 % are achieved. In contrast to that, for the flat absorber a maximum efficiency of 2.8 % is achieved for a temperature of 950 °C and a split fraction of 1.

The results indicate that for the flat absorber it is beneficial to use a higher fraction of the off-gas for a temperature lift rather than for electricity production in the CCGT. This is caused by the poorer performance of the flat receiver at high temperatures.

In Figure 6-3 the hot air and return air temperature are shown in dependence of the split fraction for a reforming temperature of 900 °C. The receiver efficiencies for the cavity and the flat absorber are also shown. Furthermore, the efficiency of the SOLME system is shown with a fixed receiver efficiency assumed in order to illustrate its dependence on the split fraction independent of receiver efficiency. It can be seen that the hot air temperature of the receiver decreases with increasing split fraction, causing the receiver efficiencies for both cases to be increased. It is not clearly visible in the graph, but for the flat absorber the increase in receiver efficiency is stronger than for the cavity absorber. The difference between the receiver efficiency with air return ratio of 0.9 and 0.6 is 0.0463 at f_{Split} =0 and 0.0421 at f_{Split} = 0.8).

The efficiency of the non-solar part of the SOLME process drops for an increasing split fraction, because less of the off-gas is used for the highly efficient conversion into electricity in the CCGT. In the case of the flat absorber the increase in receiver efficiency can

compensate the reduction in efficiency of the non-solar part of the SOLME at 900 °C, causing the overall efficiency to be nearly independent of the split fraction. For the cavity absorber this is not the case, therefore a reduction of overall efficiency occurs for an increase of split fraction.

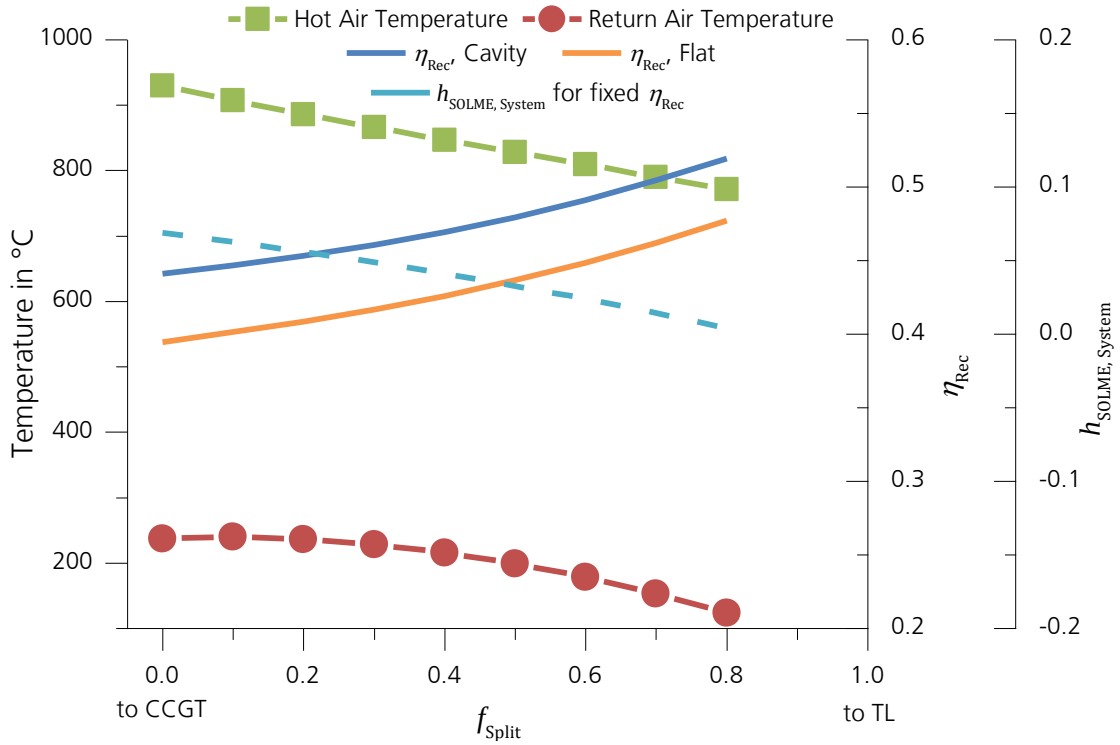

Figure 6-3: Hot air - and return air temperature and receiver efficiencies in SOLME process for flat and cavity absorber and non-solar $h_{SOLME,System}$ (fixed η_{Rec}) over split fraction.

In Figure 6-4, the results for the efficiency of the SOLME system with a receiver with cavity geometry and air return ratio of 0.9 is shown in dependence of split fraction and for varying reforming temperatures. For comparison, the results obtained with the same receiver with air return ratio of 0.6 for reforming temperatures of 900 °C and 950 °C are taken from Figure 6-1. It can be seen that a concave curve results for the higher air return ratio with an optimum value for the split fraction that is neither 0 nor 1 for some of the reforming temperatures. The maximum value of 5.23 % is achieved with a reforming temperature of 900 °C and a value of 0 for the split fraction. However, at 950 °C and a split fraction of 0.2 the efficiency of 5.18 % is only slightly lower. It can be observed that for some values the process efficiency is higher for the case with the lower air return ratio. This is caused by the fact that the air return ratio of the reference solar power plant is adjusted accordingly. From this behavior it can be concluded that for some configurations, the reference solar power plant benefits more from the increase of air return ratio than the SOLME plant.

For those data sets, where the efficiency with a certain reforming temperature and split fraction is higher in the case of lower air return ratio, the conclusion can be drawn that the increase in air return ratio is more beneficial for the reference solar power plant than for the SOLME process.

In summary a clear benefit can be observed from the utilization of a cavity type receiver. Furthermore an increased air return ratio will in general increase process efficiency. The optimum split fraction and reforming temperature depends on the receiver type that is used and on the air return ratio that is achieved. However, for a cavity-type absorber low split fractions between 0 and 0.2 and reforming temperatures between 900 °C and 950 °C seem most advantageous. Due to the clear benefit of a cavity-type absorber, only the results for the cavityreceiver will be presented in the following.

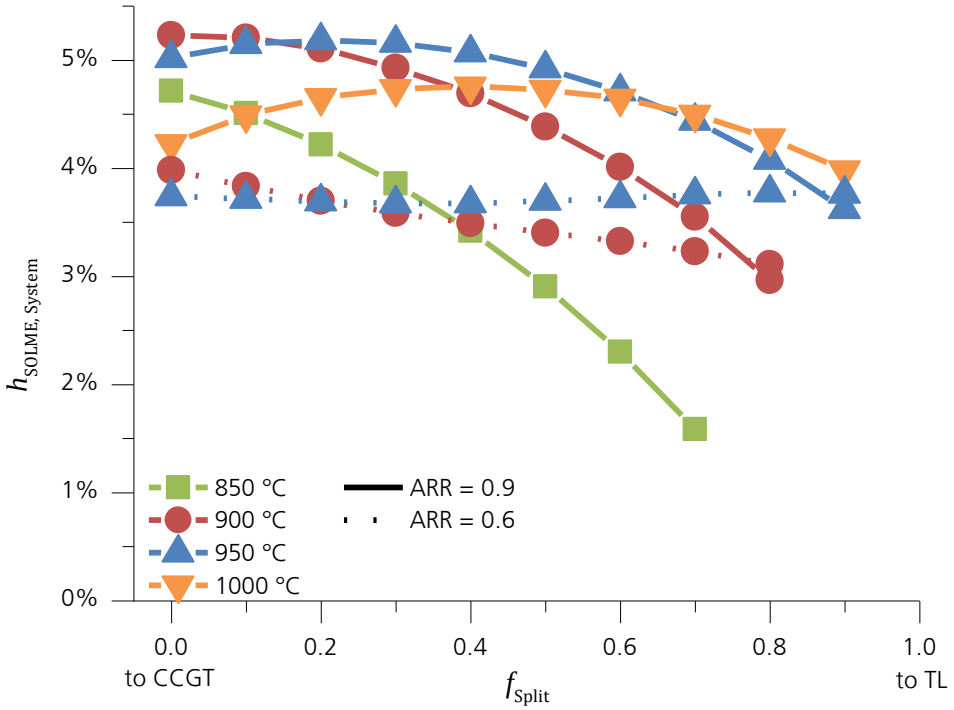

Figure 6-4: Efficiency of SOLME with cavity type receiver in dependence of f_{Split} for different reforming temperatures and $ARR = 0.9$ and $ARR = 0.6$.

6.4.2. Reforming pressure, air return ratio

In Figure 6-5, the influence of the reforming pressure on the SOLME efficiency is shown for an air return ratio of 0.6 and 0.9 at a reforming temperature of 900 °C and a split fraction of 0. It can be seen that for both air return ratios, the efficiency increases with increasing pressure for pressures below 17 bar. From 17 bar to 24 bar the process efficiency is nearly independent of process pressure. Above 25 bar the efficiency begins to drop slightly. Correspondingly, at values of M between 2.10 and 2.06 the highest overall efficiency is achieved. It should be noted that for a given composition of the reactants and reforming outlet temperature, the product composition M is only dependent on reforming pressure. In comparison to the values recommended by literature ($M \approx 2.05$), optimum process efficiency is achieved with higher values for M (or lower pressures correspondingly) independent of the air return ratio. The decrease in process efficiency for reforming pressures above 24 bar, or correspondingly values of M below 2.06, is caused by the increased heat demand of the distillation column that is supplied by additional cooling of the air. This heat demand is also shown in Figure 6-5. The additional cooling of the air at

elevated pressure is necessary, because the conversion of methane is reduced with increasing pressure, causing an increase of inert species in the methanol reactor that consume some of the heat released by the methanol synthesis. As a consequence the heat supply by the methanol reactor does not suffice to supply the distillation column, causing an increasing additional heat demand with increasing pressure.

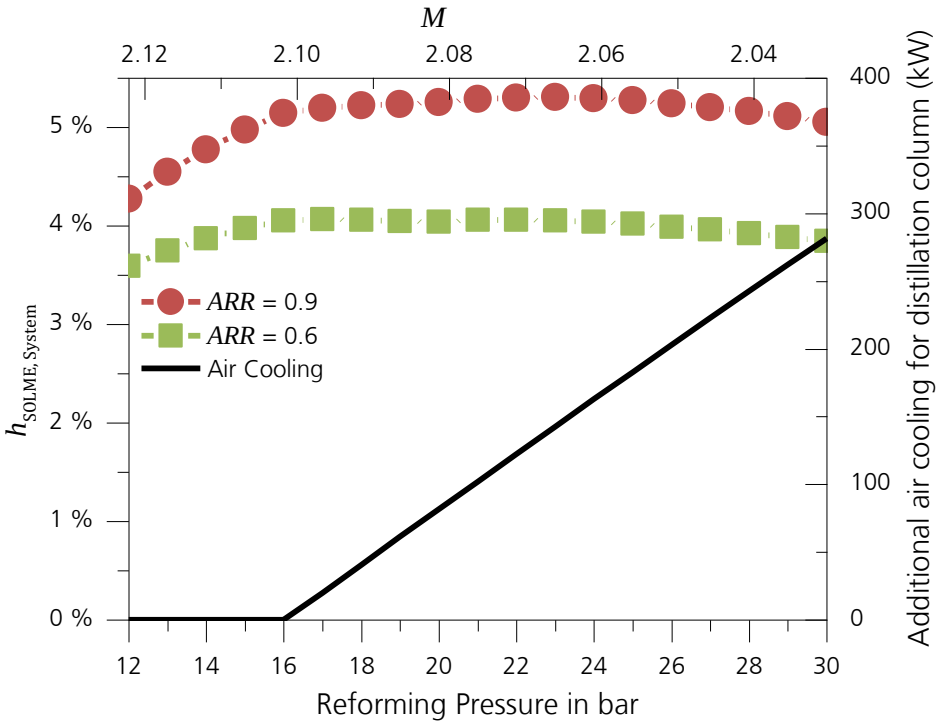

Figure 6-5: Efficiency of SOLME process in dependence of reforming pressure and air return ratio. Reforming temperature is 900 °C, split fraction is 0.

The general trend of increasing process efficiency for increasing pressure is caused by a reduction in total compression work. This occurs because it is energetically cheaper to compress the natural gas input than the syngas, because the volume flow is lower. However, the conversion of methane is reduced with increasing pressure, causing a reduction of methanol yield and an increase in electricity production by combustion of off-gas and an increase in overall flow in the methanol synthesis reactor. Beyond the effect of increased electricity production, the amount of off-gas that is used for heat supply in the secondary reformer is increased for a given split fraction (if the split fraction is > 0).

Besides the heat supply to the distillation column, the evaporation temperature of the reactant water influence the return air temperature. The evaporation temperature of the water is set by the reforming pressure. It is increased by increasing pressure. The conflicting influence of the increasing evaporation temperature and the cooling for heat supply of the distillation column cause a maximum in return air temperature and minimum in receiver efficiency at 24 bar reforming pressure, corresponding to a value of M = 2.06. This can be observed in Figure 6-6.

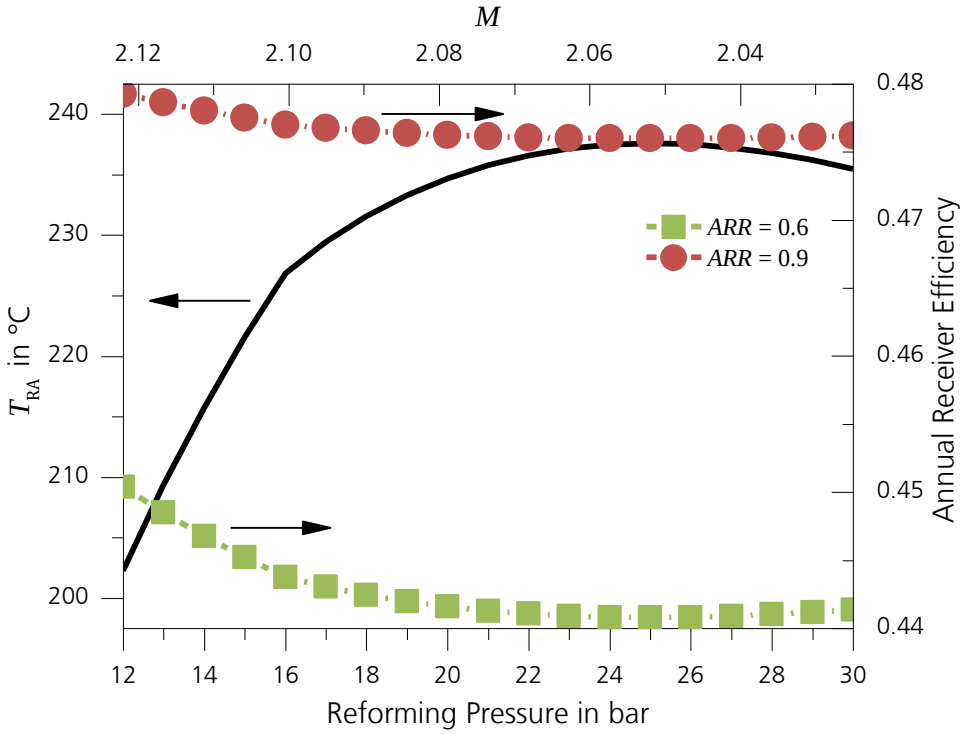

Figure 6-6: Return air temperature and receiver efficiency in dependence of p_{Ref} for air return ratio of 0.6 and 0.9

In Figure 6-7 the influence of the split fraction on the value of optimum pressure for overall process efficiency is illustrated. It can be seen that the influence of the pressure is similar for both values of split fraction when air return ratio is 0.9. For the air return ratio of 0.6 this is not the case; the optimum pressure is clearly shifted towards higher values when the split fraction is increased.

When the split fraction is 0, the hot air temperature is independent of reforming pressure. When the split fraction is significantly higher than zero, the heat supply to the secondary reformer is increased with pressure, because the overall amount of off gas is increased due to decreased methanol yield. This causes a reduction in hot air as well as return air temperature. When the air return ratio is low, this causes a significant increase in receiver efficiency, this effect is not as significant for high air return ratios. For low air return ratios, this overcompensates the reduction in methanol production, shifting the optimum pressure towards higher values. For the higher air return ratio the opposite is the case in the presented configuration, because the receiver efficiency is less sensitive on changes in hot air temperature.

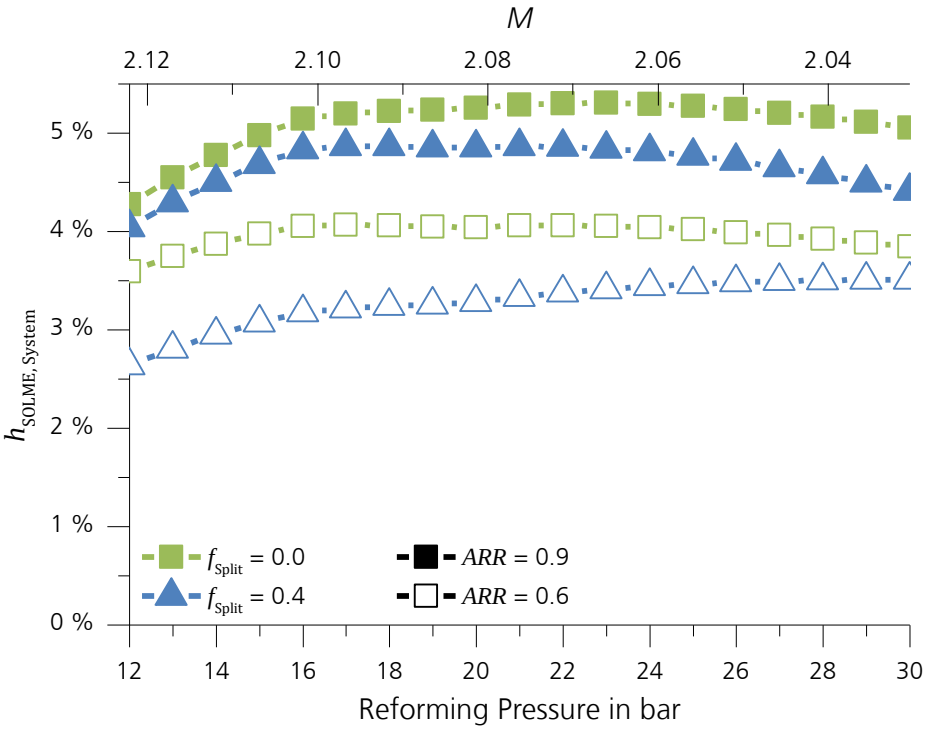

Figure 6-7: Influence of reforming pressure on SOLME efficiency in dependence of split fraction

In general, it can be stated that the optimum reforming pressure corresponds to a lower value of M than the value of 2.05 proposed by Huber et al. [25] when the split fraction is zero or air return ratio is high. A reforming pressure corresponding to values of M between 2.1 and 2.06 should be chosen. However, for low air return ratio and high split fractions a pressure that corresponds to an M of 2.05 seems adequate.

In order to take these results into account in the further investigations, for the case which has shown highest efficiencies so far (ARR = 0.9, T_{Ref} = 900 °C, f_{Split} = 0), a reforming pressure of 23 bar is set. This corresponds to a value of 2.065 for M. It should be noted that a variation of pressure within reasonable limits, i.e. corresponding to $2.1 > M > 2.05$ has a minor influence on overall efficiency.

6.4.3. Steam to natural gas ratio

The influence of the steam to natural gas ratio (S/NG) on process efficiency is illustrated in Figure 6-8. In the figure, the efficiency is shown in dependence of split fraction for air return ratios of 0.9 and 0.6 respectively. In general the same behavior as seen in Figure 6-1 and Figure 6-4 can be recognized: A decreasing trend for increasing split fraction. It can also be seen that the course of the plot is not significantly influenced by the steam to natural gas ratio, only the absolute values are influenced. It can furthermore be seen that the efficiency decreases with increasing S/NG for an air return ratio of 0.9. This shows that for an air return ratio of 0.9, the lower limit of 2.0 for S/NG should be chosen (the limit was set in sub-section 6.4.3). For an air return ratio of 0.6 the opposite is the case. The consequence for the lower air return ratio of 0.6 is further investigated.

In Figure 6-9 the efficiency of the process in dependence of the air return ratio is shown for three different values of the steam to natural gas ratio. As expected from the previous results, an increase in air return ratio causes an increase in process efficiency independent of steam to natural gas ratio. However, it can be seen that the gradient of the process efficiency with respect to air return ratio depends on steam to natural gas ratio, causing an intersection of the curves, below which higher steam to natural gas ratios are beneficial, while above lower steam to natural gas ratios are beneficial.

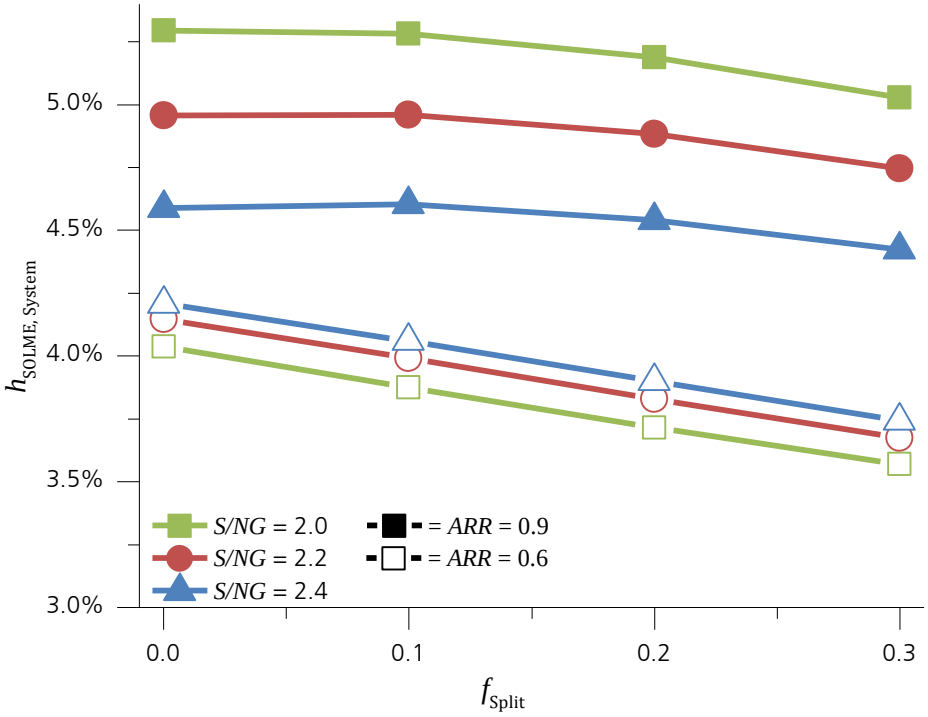

Figure 6-8: Influence of steam to natural gas ratio on process efficiency with varying split fraction and air return ratio for 900 °C reforming temperature

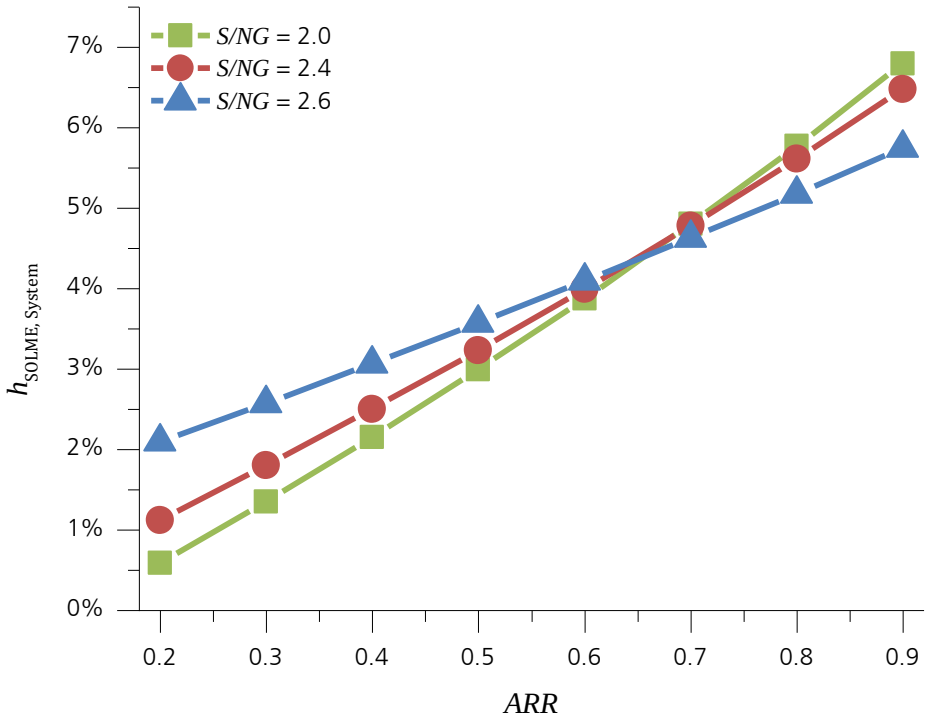

Figure 6-9: Influence of air return ratio on process efficiency in dependence of steam to natural gas ratio

The characteristic of process efficiency in dependence of steam to natural gas ratio as shown in Figure 6-9 is caused by the fact that more water has to be evaporated when S/NG is increased. This causes a decrease in return air temperature. The excess water that is evaporated before entering the reforming reactor is later cooled and partly condensed in the water steam cycle causing an increase in electricity production. However, the efficiency of converting the energy content of the air to electricity is low and competes with the recovery of the energy content in the air through recycling it to the receiver. At high air return ratios a large part of the energy content of the air is recovered. Therefore it is more beneficial not to cool the air further for electricity production at low efficiency. When the air return ratio is low, a large part of the energy stored in the air is lost to the environment and it is more beneficial to convert the energy to electricity (even at low efficiency) than to return it to the receiver. As can be seen in Figure 6-9, the threshold above which a low steam to natural gas ratio is advantageous is approximately 0.65. It should be noted that the efficiency of the reference solar power tower used for determination of the process efficiency should also be adjusted with varying air return ratio, because an improvement of the air return ratio would also apply for the reference solar power plant. However, for better comparability of the effects in the SOLME process, it is kept constant at the value that was determined for an ARR of 0.6 (which is 18.43 %) for the results presented in the figure.

From the results it becomes clear that the steam to natural gas ratio should be chosen in dependence of air return ratio. An interaction with the number of tubes in the AHR can be assumed, because this also strongly influences the return air temperature (for a given upper temperature difference in AHR, cf. sub-section 5.4.2). The interaction of the number of tubes, with upper temperature difference in the AHR $\Delta T_{\mathrm{Upper}}$ and the steam to natural gas ratio is assessed in the Figure 6-10 and Figure 6-11. In Figure 6-10, the efficiency of SOLME is shown in dependence of the steam to natural gas ratio for different number of tubes and $\Delta T_{\mathrm{Upper}}$ for an air return ratio of 0.6. In Figure 6-11, the same is shown for an air return ratio of 0.9. Note that not for all configurations the full range of steam to natural gas ratio from 2.0 to 2.8 can be investigated. For high $\Delta T_{\mathrm{Upper}}$ and high S/NG, the outlet air temperature is too low to provide enough heat to the distillation column and operation is

not feasible. Therefore, for high values of $\Delta T_{\mathrm{Upper}}$, the steam to natural gas ratio cannot be set as high as for lower values of $\Delta T_{\mathrm{Upper}}$. In Figure 6-10 it can be seen that the highest considered values for $\Delta T_{\mathrm{Upper}}$ achieve the highest efficiencies for an air return ratio of 0.6. This effect will be investigated in more detail in the following sub-section (6.4.4).

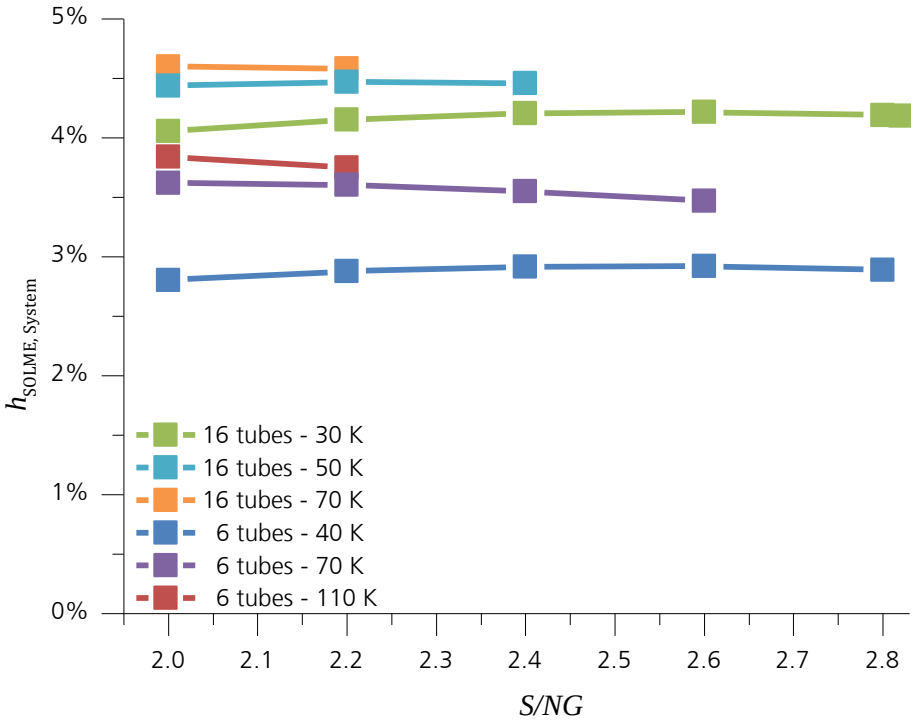

Figure 6-10: Efficiency of SOLME in dependence of steam to natural gas ratio in the reformer for different values number of tubes and upper temperature difference in AHR, air return ratio of 0.6. (Legend: n_{Tubes} in 1/(mole$_{NG}$/s) – ΔT_{Upper} in K)

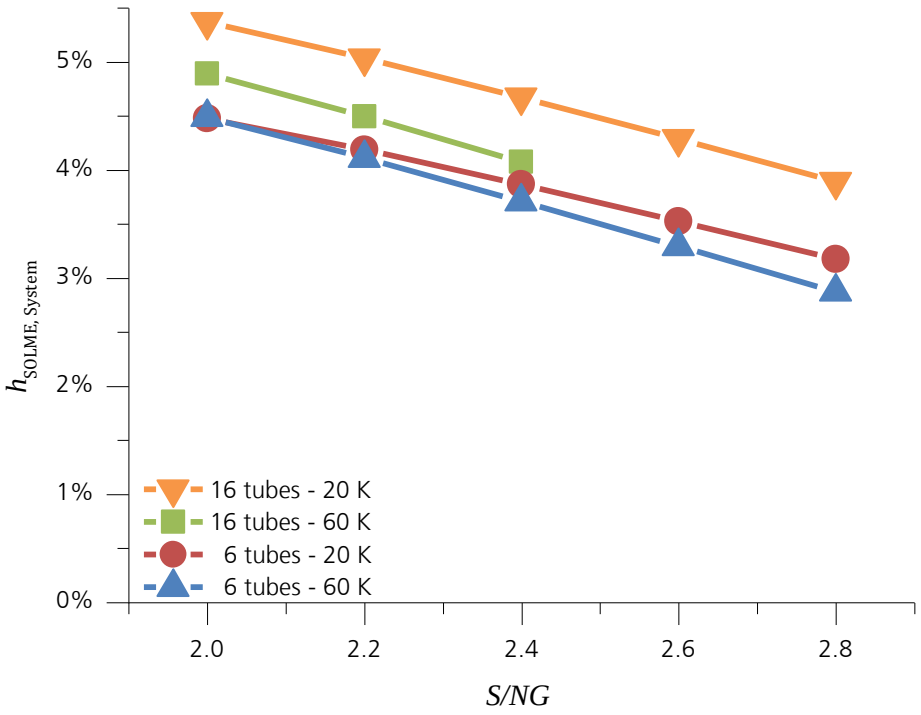

Figure 6-11: Efficiency of SOLME in dependence of steam to natural gas ratio in the reformer for different values number of tubes and upper temperature difference in AHR, air return ratio of 0.9. (Legend: n_{Tubes} in 1/(mole$_{NG}$/s) – ΔT_{Upper} in K)

In Figure 6-10 it can be seen that for the parameters that were also used as basis for Figure 6-9 (16 tubes/(mole$_{NG}$/s) and 30 K for ΔT_{Upper}), an optimum of 2.6 evolves for the steam to natural gas ratio. It can furthermore be seen that this optimum is shifted towards lower values of *S/NG* when increasing the upper temperature difference. This trend is limited by the lower limit for the steam to natural gas ratio of 2.0. At the same time, an increase of the upper temperature difference in the AHR causes an increase in efficiency. Therefore, it can be concluded that for an air return ratio of 0.6 a steam to natural gas ratio of 2.0 is optimal, but the corresponding optimum upper temperature difference is yet to be determined.

In Figure 6-11, it can be seen that for any configuration, the steam to natural gas ratio of 2.0 is optimal, when an air return ratio of 0.9 is achieved. However, it can be seen that the upper temperature difference in the AHR can have a significant influence on the overall efficiency. Its optimum value in dependence of the number of tubes is determined in the following sub-section.

6.4.4. Number of tubes in AHR and upper temperature difference

In Figure 6-12 and Figure 6-13, the efficiency of SOLME in dependence of the upper temperature difference in the AHR is shown for different number of tubes for an air return ratio of 0.6 and 0.9, respectively. As basis for both figures a steam to natural gas ratio of 2.0 and split fraction of 0 was set. In both figures it can be seen that for a given upper temperature difference, an increase in number of tubes increases the efficiency. However, the increase in efficiency per tube is decreased with increasing number of tubes. It is therefore expected that the optimum number of tubes will be determined in the economic investigation that is carried out in chapter 7. It is expected that the optimum number of tubes is reached when the gain in efficiency and the corresponding increase in production cannot compensate the cost increase caused by the increase of reactor size.

From the results for an air return ratio of 0.6 it can be seen that the efficiency of SOLME increases with increasing upper temperature difference in the AHR. At a certain value of the upper temperature difference, an optimum is achieved, above which the efficiency drops. This applies for all investigated number of tubes in the reformer. The optimum value for the upper temperature difference is shifted towards lower values with increasing number of tubes. This is caused by the fact that with a higher number of tubes, more heat can be transferred from the air to the reactants, causing a lower exit temperature for a given upper temperature difference.

In Figure 6-13, the results for an air return ratio of 0.9 are shown. In general the same behavior as for the case with the air return ratio of 0.6 can be observed. However, the optimum values for $\Delta T_{\mathrm{Upper}}$ are lower and the influence on overall efficiency is not as strong when the air return ratio is 0.9.

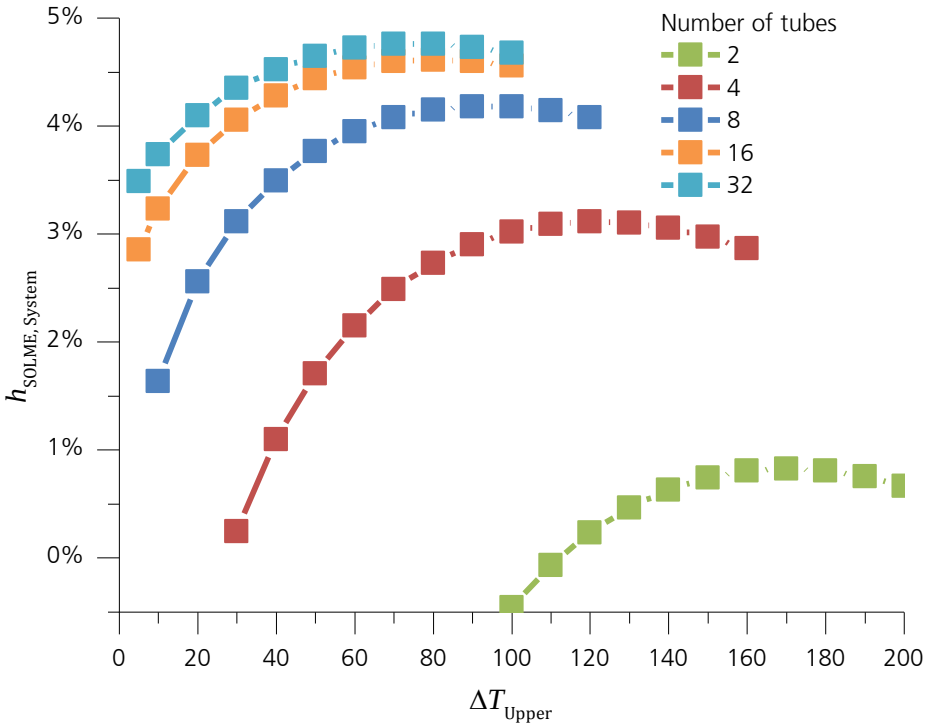

Figure 6-12: Process efficiency in dependence of upper temperature difference and number of tubes in the AHR with an air return ratio of 0.6

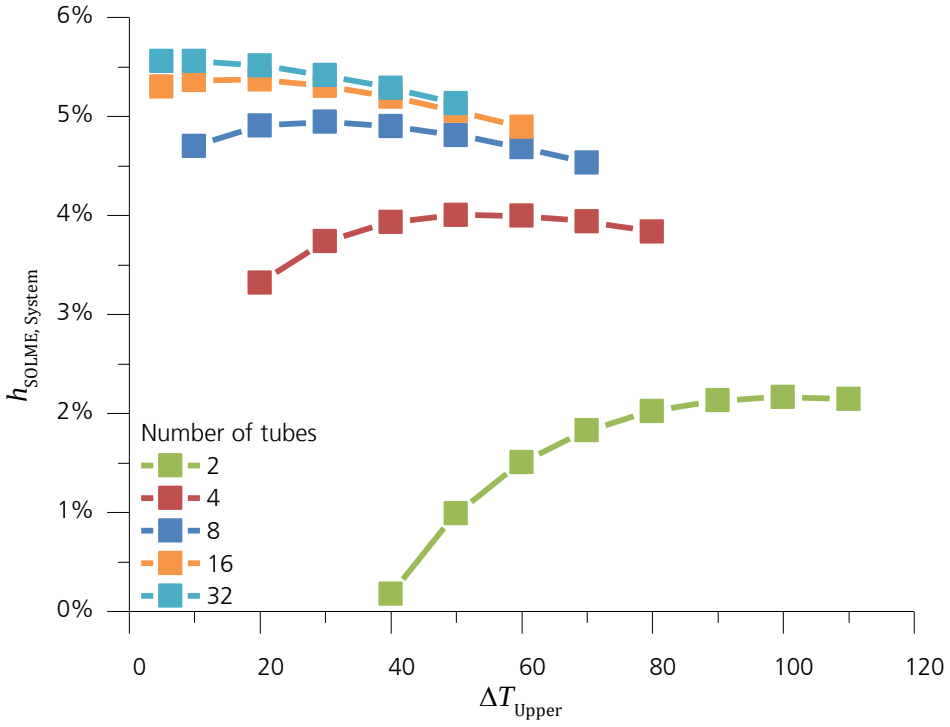

Figure 6-13: Process efficiency in dependence of upper temperature difference and number of tubes in the AHR with an air return ratio of 0.9

From the results presented above, optimum values for the upper temperature difference in dependence of the number of tubes in the AHR and the air return ratio can be determined. Those values can be used in the economic investigation when assessing the optimum size of the AHR. The optimum values of upper temperature difference in the AHR in dependence of number of tubes that are used in the further simulations are given in Table 6-6.

Table 6-6: Optimum values for upper temperature difference in dependence of number of tubes in AHR for air return ratio of 0.6 and 0.9

Tubes	ΔT_{Upper} in K	
per $mole_{NG}$/s	$ARR = 0.6$	$ARR = 0.9$
2	170	100
4	120	50
8	90	30
16	80	20
32	70	10

6.5. Sensitivity on input parameters

In the simulation of the SOLME process some assumptions were made with respect to the determination of the defined process efficiency $h_{\mathrm{SOLME,\ System}}$ that cannot be considered as definite. In order to understand the influence of potential errors in the assumed values, sensitivity studies are carried out with regard to these parameters. Those assumptions are the efficiency of the combined cycle gas turbine power plant (CCGT), both the internal one as well as the external one, as well as the efficiency of the power block of the reference solar power tower. The first was assumed to be 60 %, the latter 35 %.

Regarding the CCGT it is commonly known that the technology exists to achieve an efficiency of 60 % in favorable ambient conditions. However, for a CCGT that is located in a desert with high ambient temperatures and dry cooling, a decrease in efficiency can be expected. Maulbetsch and DiFilippo [80] state in their report that CCGT's have lower efficiencies when they are located in a desert compared to the coast and furthermore that dry cooling and high ambient temperatures (hot day conditions) will lead to lower

efficiencies. The values for the efficiency of a CCGT that results from the relative efficiency changes they give are presented in Table 6-7. The efficiency that results for a reference efficiency of 60 % are also given in the table. The values presented in the table indicate that an efficiency of 55.9 % is the lowest to be expected for a state of the art CCGT power plant in desert conditions with dry cooling and hot ambient temperature. Therefore the sensitivity study is carried out for values between 55 % and 60 %.

Table 6-7: Relative and absolute efficiency of CCGT for different conditions, according to Maulbetsch and DiFilippo [80]

Conditions	relative efficiency	absolute efficiency
Coast, wet cooling (reference)	100 %	60.0 %
Desert, wet cooling	99.6 %	59.8 %
Desert, dry cooling	96.7 %	58.0 %
Desert, dry cooling, hot day	93.1 %	55.9 %

In the sensitivity study, a distinction is made between the external and the internal CCGT, as introduced in section 3.2. While the internal CCGT has to be located in the vicinity of the SOLME process, the external CCGT could be located anywhere in the world, as it is only taken into consideration so that the overall electricity output is identical to the one of the reference system. Therefore, the efficiencies of the two CCGTs are varied independently in the sensitivity analysis.

The results for variation of the CCGT efficiency are presented in Figure 6-14. It can be seen that the process efficiency increases monotonously with increasing CCGT efficiency. It can be seen that the increase is more significant when both the internal as well as the external CCGT efficiency are varied compared to the case with variation of the internal CCGT only. The results show that even for the lowest value of the CCGT efficiency that is considered (55 %) the efficiency of the SOLME system is well above zero, even with an ARR of 0.6.

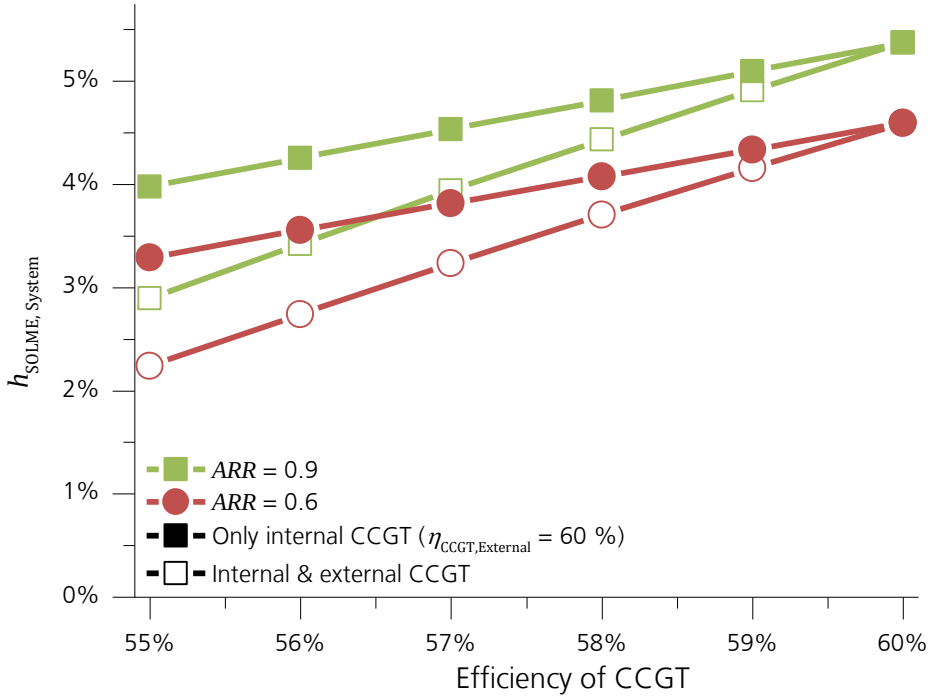

Figure 6-14: Influence of variation of CCGT efficiency on process efficiency

In Figure 6-15 the results for a variation of the efficiency of the power block in the reference solar power tower are presented. In order to give results for a coupled variation of the results, the variation is shown with an efficiency of the CCGT (internal and external) of 60 % as well as for 55 %. The efficiency of the SOLME system decreases with increasing efficiency of the power block of the reference solar power plant, independent of air return ratio or CCGT efficiency. Within the considered range of values, the sensitivity of SOLME efficiency with respect to changes in power block efficiency is more drastic than the sensitivity on changes in CCGT efficiency. It can be seen that for the lower efficiency of the CCGT and an efficiency of the power block above 37 % the efficiency of the SOLME system drops below zero when the air return ratio is 0.6. For an air return ratio of 0.9 the efficiency of the SOLME system drops below zero for an efficiency of the power block above 38 %. However, as stated above, in the ECOSTAR report [78], a value of 30.6 % was suggested. This would correspond to an efficiency of SOLME between 7 % and 10 %, depending on efficiency of CCGT and air return ratio. This shows that it can be expected to be well above zero for most real combinations of these parameters.

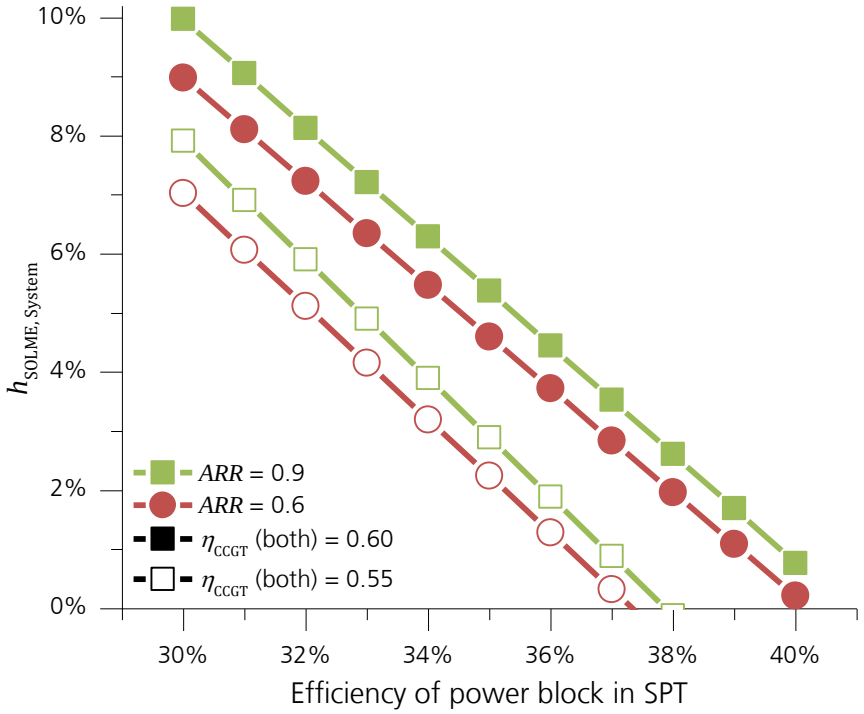

Figure 6-15: Influence of the variation of the efficiency of the power block of the SPT on process efficiency, solely as well as coupled with a variation of CCGT efficiency.

6.6. Comparison of results with different evaluation criteria

In order to further assess the validity of the defined and used evaluation criterion, the results obtained are compared to other evaluation criteria. Namely these are energetic efficiency η_{Energy} and the energy savings ratio S by Bai et al. [51] that were both already introduced in chapter 4. The comparison is carried out with a configuration that was already shown in Figure 6-4: The performance of the process in dependence of the split fraction with a reforming temperature of 950 °C. In Figure 6-16, the results for h_{SOLME}, S and η_{Energy} are presented for varying split fraction. A diverting behavior of the three evaluation criteria can be observed. While η_{Energy} increases with increasing f_{Split}, the contrary is the case for S. h_{SOLME} increases slightly at first until it reaches a maximum, above which it decreases.

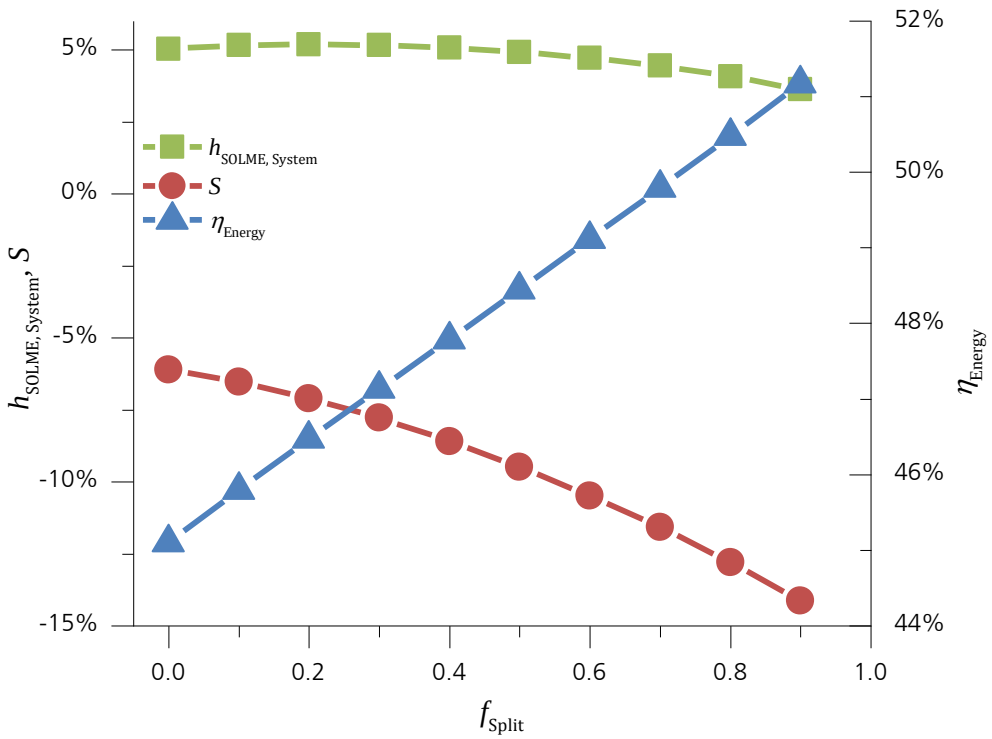

Figure 6-16: Comparison of different evaluation criteria

The results of the different evaluation criteria lead to different conclusions. Firstly the energetic efficiency suggests that a high value for f_{Split} is most beneficial and does not allow for evaluation whether it is more beneficial to use this process than a conventional solar power plant. Secondly, the energy savings ratio by Bai et al. [51] suggests that small values of f_{Split} are optimal and that the SOLME process does not provide a benefit compared to the reference technologies. Thirdly, the efficiency of SOLME as it was previously defined in this work gives an optimal value for f_{Split} of 0.2 and suggests that the SOLME process is more efficient than the reference technologies.

The energetic efficiency η_{Energy} increases with increasing split fraction, because less electricity is produced in the SOLME plant. Electricity production usually causes high thermal energy losses, the energetic efficiency of electricity production processes is usually low. In the case of the SOLME plant it is more energy efficient to use the energy of the off-gas to provide heat to the reaction rather than produce electricity with it. However, the high value of electricity compared to the enthalpy increase in the reforming reactor is not considered in the energy efficiency.

In energy savings ratio S the energy consumption (solar + natural gas) of the SOLME process is compared to the energy consumption of the reference system that produces the same amount of electricity and methanol. It should be noted that unlike in the evaluation scheme applied in this work, no additional CCGT is taken into account in the SOLME system. Instead the reference solar power plant is scaled down to supply the same amount of electricity as the SOLME process. Therefore, a different amount of the solar energy is used in the reference system than in the SOLME process. This causes a difference in the ratio of solar energy input to natural gas energy input between the SOLME process and the reference processes. More specifically, this ratio is significantly lower in the reference system than in the SOLME process as can be seen in Figure 6-17. It can also be seen that in both cases the share of solar energy input is reduced for increasing split fraction. This is also the reason why the lowest possible value for f_{Split} gives a maximum values for S. In the SOLME plant more of- gas is combusted for efficient electricity generation that has to be compensated in the reference system by an increase of electricity production from solar energy that is relatively inefficient. This scheme does not take into account the different value of different types of energy flows. It is merely a comparison of the two separate energy balances of the SOLME process and the reference processes.

This discussion shows the advantages of the proposed evaluation scheme of the efficiency of solarization. In this scheme the different value of the energy streams are taken into account and the optimization yields a configuration that makes most efficient use of the different input energy streams. This is accomplished by scaling of the reference processes to yield the same product but also consume the same amount of solar energy. The last factor is important, as the aim of the evaluation is to find the most beneficial way of utilizing solar energy.

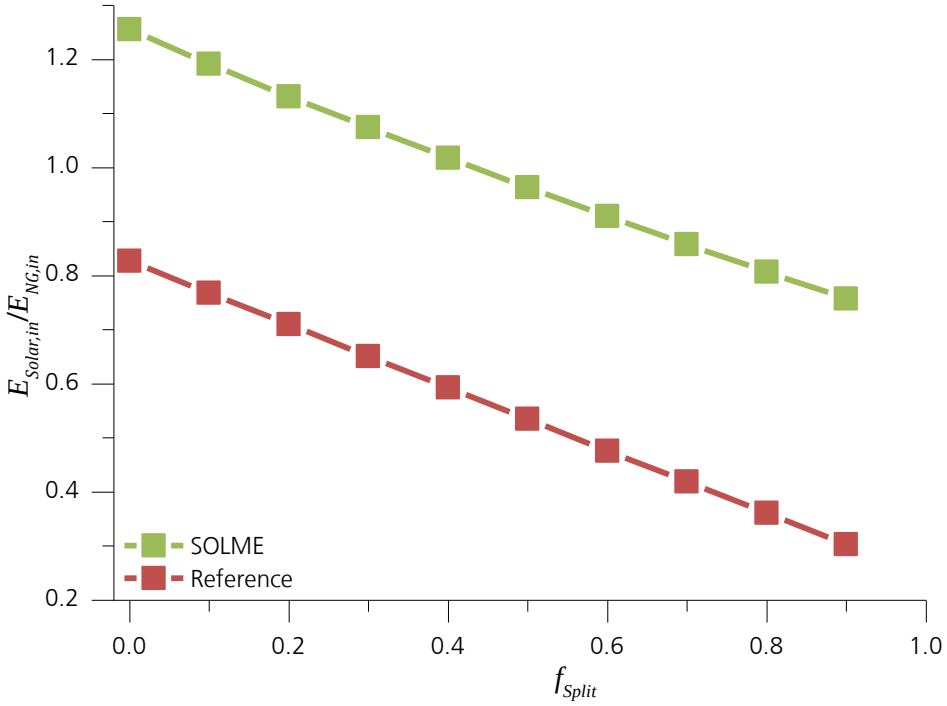

Figure 6-17: Ratio of input solar energy to input natural gas energy in SOLME and reference processes in evaluation scheme by Bai et al. [51].

6.7. Summary and conclusion of process simulations

By sensitivity study of several parameters a favorable configuration was determined with high efficiency. As no formal optimization of the process was carried out, the configuration cannot be called optimal. However, due to the large number of varied parameters with consideration of several interactions in parameter variation, it can be expected that the determined configuration is close to the optimum. Hence the determined value for h is expected to be close to the maximum value.

The air return ratio cannot be set freely, but its maximization is aimed for in receiver design. Therefore, two values of the air return ratio were used and the optimum configuration determined for both. The two values, 0.9 and 0.6 are chosen to represent an upper and lower limit for future open volumetric cavity receivers, respectively. It was shown that an absorber with cavity geometry is advantageous for the process. Therefore a flat absorber was not taken into account further. It was also shown that there is no thermodynamic

optimum for the number of tubes in the air heated reformer, but that an increase causes a continuous benefit. The optimum number of reactor tubes is expected to be determined through economic optimization in the next chapter.

The optimum process conditions for 16 tubes per mole of natural gas input per second into the reformer are given in Table 6-8 for an air return ratio of 0.9 and 0.6.

Table 6-8: Optimum values for the investigated parameters for air return ratio of 0.9 and 0.6

Parameter	Optimum Value for	
	ARR = 0.9	ARR = 0.6
Reforming temperature ($\boldsymbol{T_{Ref}}$)	900°C	900°C
Reforming pressure ($\boldsymbol{p_{Ref}}$),$\boldsymbol{M}$	23 bar (2.065)	23 bar (2.065)
Steam to natural gas ($\boldsymbol{S/NG}$)	2.0	2.6
Split fraction ($\boldsymbol{f_{Split}}$)	0	0
Upper temperature difference in AHR ($\boldsymbol{\Delta T_{Upper}}$)	20 K	40 K

The efficiency of the SOLME process with the two air return ratios 0.9 and 0.6 are 5.37 % and 4.34 % respectively. In a sensitivity study, the values for efficiency of the power block in the reference solar power plant, as well as the efficiency of the CCGT that is considered in the SOLME process were varied. The study has shown that only for a combination of the most disadvantageous conditions the efficiency of SOLME will drop below zero. These disadvantageous conditions are a combination of low efficiency of CCGT and high efficiency of power block in the reference solar power plant. For a broad range of more optimistic values for these two parameters, efficiencies well above zero are obtained.

7. Economic Investigation

It was already mentioned that a comprehensive investigation and optimization of the SOLME process is not possible, if economic aspects are not taken into account. For instance the implementation of heat storage to increase the operating hours is not driven by thermodynamic considerations but rather economic or strategic ones. Furthermore, as shown in detail in sub-section 6.4.4, the number of tubes representing the heat transfer area, is to be determined by economic investigation. This is the case because no thermodynamic optimum exists for this parameter.

In order to allow for the layout of an adequate heat storage for the SOLME process and assess the realistic size of the air-heated reformer an economic investigation and optimization of the process is carried out in the following. This will allow for a realistic prediction of the efficiency as well as the cost of the SOLME process. Furthermore this enables the determination of the realistic reduction of carbon dioxide emissions to be expected by the SOLME process.

7.1. Methodology

As discussed in the report on cost of generating electricity by the International Energy Agency, Nuclear Energy Agency and Organization for Economic Co-operation and Development [81], the levelized cost of electricity ($LCOE$) is a useful tool for comparison of the economic performance of two different technologies. However, it is not trivial to apply this method for economic evaluation to the SOLME process, because not only electricity, but also methanol is produced. Within this economic investigation, this is taken into account by subtraction of the revenue from methanol disposition from the total annual cost of the SOLME system and determining the $LCOE$ based on the remaining annual costs. This appears logical, as one of the aims of this work is to compare the economics of the SOLME plant and system to CSP utilization for electricity production. This can then be carried out by comparing the $LCOE$ of the SOLME system to the $LCOE$ of the reference solar power tower.

Another problem in the assessment of the economic performance of the SOLME system is the determination of the methanol price. Even though prices for methanol on the world market can be retrieved, e.g. 416 $ per metric ton in North America from www.methanex.com [82], those prices are subject to several factors, such as crude oil price and margin for the producer as well as pay-back time of the investment for the plant. The latter is especially critical, as pay-back times for investment in a methanol plant is in the range of few years, compared to solar power plant where it is usually well above a decade. Therefore, in order to allow for good comparability, the price of methanol production ($LCOM$) is determined for the reference methanol plant with a pack-back time that is identical to the pay-back time of the SOLME plant for fair comparability. The reference cost for electricity ($LCOE_{\mathrm{Reference}}$) is determined for the reference solar power plant. It should be noted that the electricity supply for the reference methanol synthesis is provided by the reference solar power plant at a predetermined price. This internal price for electricity will not influence the overall result, but will only influence the distribution of the overall process costs between the $LCOM$ and the $LCOE_{\mathrm{Reference}}$.

Eventually, the cost of electricity from SOLME ($LCOE_{\mathrm{SOLME}}$) is determined by applying the $LCOM$ to the methanol produced in the SOLME process for calculation of the corresponding revenues. This procedure is illustrated in Figure 7-1. In the upper part of the figure the reference system is illustrated. It can be seen that the electricity demand of the reference methanol plant $E_{\mathrm{El,Ref\,MeOH}}$ is sold at the price $C_{\mathrm{El,Ref,int}}$. The $LCOE_{\mathrm{Reference}}$ is then calculated by division of the difference between total annual cost of the reference solar power tower C_{SPT} and revenues from electricity sales to the methanol plant divided by remaining electricity for disposition E_{El}, as shown in Eq. (7.1).

$$LCOE_{\mathrm{Reference}} = \frac{C_{\mathrm{SPT}} - E_{\mathrm{El,Ref\,MeOH}} \cdot C_{\mathrm{El,Ref,int}}}{E_{\mathrm{El}}} \tag{7.1}$$

Subsequently the $LCOM$ is calculated for the reference methanol plant by division of the annual cost for the methanol plant $C_{\mathrm{Ref,Meth}}$, including the cost for electricity, by the amount of methanol produced m_{MeOH}. The $LCOM$ is calculated on a mass basis for better comparability with literature data. The unit used is dollars per metric tons.

The levelized cost of electricity from the SOLME process ($LCOE_{\mathrm{SOLME}}$) is calculated as shown in Eq. (7.2), by summation of the total cost of the SOLME process as well as the external CCGT (i.e. the total cost of the SOLME system) and subtraction of the revenues from methanol disposition at the previously calculated $LCOM$. Finally, the resulting annual costs that can be attributed to the electricity production are divided by the total net electricity production E_{El}. It should be noted that in the determination of the net electricity production of both the reference solar power plant as well as the SOLME plant, parasitic electricity consumption is taken into account. In accordance with the ECOSTAR report [78], 0.0065 kW of parasitic electricity consumption per square meter of heliostat area are assumed. For the considered plant, a total heliostat area of 62,854 m² (519 heliostats of 121 m² each) is used. This causes an average parasitic consumption of 408.6 kW during operation of the solar part of the plant.

$$LCOE_{\mathrm{SOLME}} = \frac{C_{\mathrm{SOLME}} + C_{\mathrm{CCGT}} - m_{\mathrm{MeOH}} \cdot LCOM}{E_{\mathrm{El}}} \tag{7.2}$$

This procedure is very similar to the one applied for h that was used for evaluation of the process in chapter 6. Again, all but one of the input and output streams are identical. Again, there are two results that depend on each other ($LCOE_{\mathrm{SOLME}}$ and $LCOM_{\mathrm{SOLME}}$). Therefore, one has to be fixed in order to determine the other. In determining h, one was determined by process simulation of SOLME (the methanol production) and the other was set by the simulation of the reference system. In contrast to that, in the economic investigation, the second result ($LCOE_{\mathrm{SOLME}}$) can be determined directly once the $LCOM$ is determined. The $LCOE_{\mathrm{Reference}}$ is then only determined in order to compare the economic results for the SOLME system to the results of the reference system.

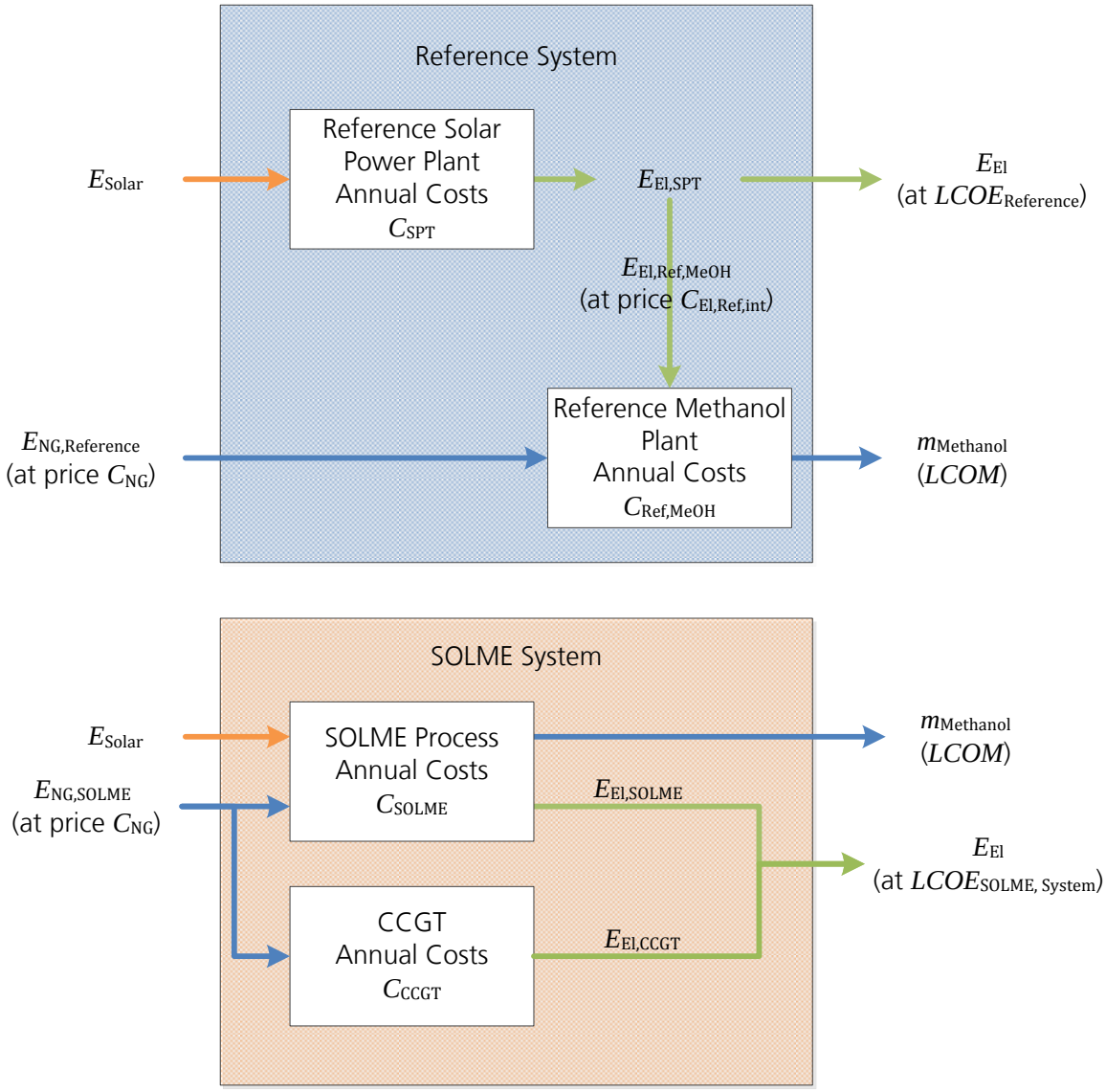

Figure 7-1: Illustration of methodology for economic evaluation of SOLME process

The annual costs of the different processes consist of the annuity of the original investment of the plant ($C_{Annuity}$), the generic operating and maintenance cost ($C_{O\&M}$) that are calculated as a factor of the annuity. As well as cost for natural gas (C_{NG}) and water (C_{Water}) that are necessary as reactants in the methanol production. All costs that are retrieved from literature are converted to prices of 2014 with the chemical engineering cost index (CEPCI). The CEPCI data is retrieved from [83] for the years 1999 to 2006 and from [84] for the years 2006 to 2014. The data is given in Appendix G.1. Furthermore, if necessary, the data from literature is converted from Euro to $US with the average exchange rate applicable for that year that is retrieved from [85]. The annual operating and maintenance cost of the

reference solar power plant, as well as all CSP – related parts in the SOLME plant (i.e. heliostat field, receiver, tower and TES) are, in accordance with Hernández-Moro and Martínez-Duart [86], estimated to be 2 % of the original investment cost of the corresponding process parts. For the methanol synthesis part of the SOLME process, the reference methanol plant and the CCGT in the SOLME system, annual operating and maintenance costs are estimated to be 0.5 % of the original investment cost, due to lack of more accurate information. The annual cost for demineralized water as reactant is estimated with data by Ulrich and Vasudevan [87] (utility cost calculation, p. 417) to be 0.35 mio. $ (for approximately 30,000 cubic meters of water per year). The cost for natural gas is set to 0.012 $/kWh (3.5 $/MBtu) in accordance with the data published for Henry Hub in Louisiana for May 2015. However, the natural gas price will be subject of a sensitivity study in the simulation. The interest rates and payback time of the investment are set to 8 % and 30 years respectively. As already mentioned in sub-section 7.1.1, the payback time for chemical plants is usually significantly lower than the value applied here. However for the solar plants this value is realistic and for the SOLME plant only one payback time can be set. In order to achieve a fair comparison it has to be set the same for the SOLME plant. Therefore the resulting value for $LCOM$ will be significantly lower than the real prices for methanol and the determined value should only be used within this study and not considered a realistic value. The given assumptions used are summarized in Table 7-1.

Table 7-1: Assumptions for calculation of system costs

Interest Rate	8 %
Payback time	30 years
O&M	
CSP – related components	2 % of investment/year
Other components	0.5 % of investment/year
Cost for demineralized water	0.35 mio. $/year
Natural Gas Price	0.012 $/kWh

From the explanation above it becomes clear that the determination of the $LCOM$ and the $LCOE$'s is carried out in a simplified way. For instance, the operation and maintenance cost are estimated in relation to investment cost, rather than determining the different cost factors that occur in operation and maintenance. Furthermore, land cost and insurance cost are not taken into account. However, due to the structure of the economic evaluation scheme, the factors are neglected both for the SOLME plant as well as the reference plant, therefore potential errors occur in both calculations, causing a shift in the $LCOE$ and $LCOM$ for both systems, still allowing for a good comparability. It should be emphasized that the absolute value of the calculated $LCOE$'s are not the desired result, but the difference between the $LCOE_{\mathrm{Reference}}$ and $LCOE_{\mathrm{SOLME}}$ is of central interest. Furthermore, it is to be noted that in order to allow for comparability of the results, the same heat storage is used both in the SOLME plant as well as in the reference solar power plant. This is done in order to ensure similar operating hours for both plants. A solar power plant with storage to allow for 4000 operating hours per year is cheaper than one that is capable of providing electricity for 7000 hours per year, but the value for the electricity grid is higher for the latter. But this higher value due to higher operating hours is not easily expressed in an amount of money. The straight-forward solution to this is to ensure the same operating hours for both systems.

7.1.1. Economic optimization of SOLME process

The procedure elaborated above allows for a comparison between the economic result of the SOLME system and the reference system. However, it does not give information on the absolute economic performance of the processes with the chosen input parameters. For instance, for an infinitely high solar multiple and infinitely large heat storage, the economic performance of the SOLME system might be better than of the reference system, but in general the performance will be very poor. In order to circumvent these unrealistic results, an economic optimization of the SOLME process is carried out prior to the assessment of the relative economic performance of the SOLME system.

In this optimization, an arbitrary but realistic value for the LCOM is set and the resulting $LCOE$ for the SOLME plant is determined (i.e. the external CCGT is not taken into account).

By minimization of the $LCOE$, the economic performance of the SOLME process is optimized. The parameters varied in the optimization are given the following:

- Solar multiple SM
- Storage Size $Q_{\mathrm{Storage,Max}}$
- Number of tubes in the AHR n_{Tubes}

One of the parameters is varied at a time, while the other two remain constant. The two parameters that are not varied are set to the reference value. The reference values are:

- Number of tubes: 6 tubes per mole of natural gas per second
- Storage capacity: 150 MWh
- Solar multiple: 3.4

In order to ensure that the optimum configuration is not influenced by the assumed value of $LCOM$ in this procedure, the optimization is carried out for different values of $LCOM$ and it is assessed whether different optimum configurations result. The four values of $LCOM$ that are used are 120, 150, 180 and 210 $/t. It should be noted that these values are significantly lower than the 416 $/t that were stated above, because the pay-back time of 30 years is significantly longer than the common pay-back time of only a few years.

The result of the optimization is the process configuration that gives the best economic result for the SOLME process. For this configuration the economic performance compared to the reference system is then determined.

7.1.2. Determination of investment costs

For the investment cost of the CSP-related process units, diverging information can be found in literature, as there is no industry standard available. However, the data used in this work was chosen carefully to be applicable to the investigated cases. In Table 7-2, the component costs of the main units attributed to the CSP plant are given. Most of the cost data is scaled with the size of the plant. However, this is not the case for the tower. The cost stated in the reference is directly used. This appears justifiable, as the main driver for tower cost is its height. On the one hand, the height would be decreased because the

heliostat field in the investigated process is approximately 40 % smaller than the field considered in the ECOSTAR Report. On the other hand, the considered site is further south in this work (28°N here vs. 37°N in the ECOSTAR report), which will lead to an increase in tower size.

Table 7-2: Unit costs for CSP related components

Component	Source	Value and basis in source	Value used in this work
Tower	ECOSTAR Report [78]	2 mio. €$_{2003}$ (104,580 m² heliostat field)	3.55 mio. $
Heliostat Field	Vogel and Kalb [88]	100 $_{2002}$/m² (in mass production)	146.64 $_{2014}$/m² 9.22 mio. $
Receiver	ECOSTAR Report [78]	115 €$_{2003}$/kW$_{th}$	204 $/kWh$_{th}$
Storage	ECOSTAR Report [78]	60 €$_{2003}$/kWh$_{th}$	106 $/kWh$_{th}$

The costs for the water steam cycle (or power block) in the SOLME plant, the reference solar power plant as well as the reference methanol plant are determined with data from the ECOSTAR Report [78]. They give a bare module price for a power block of 10 MW electric capacity of 600 €/kW$_{el}$ for 2003, this corresponds to 1064.4 $/kW$_{el}$ in 2015. As commonly done they give a scaling factor for variation of capacity. For building the same plant five times, they give an exponential factor of 0.93. Since this does not seem realistic for an actual adjustment of the plant size, the exponential factor of 0.6 is used, as recommended by Ulrich and Vasudevan [77]. The bare module cost of a power block or water-steam-cycle $C_{\mathrm{BM,PB,ref}}$ with nominal electric capacity of $P_{\mathrm{PB,ref,el}}$ in MW is calculated according to eq. (7.5).

$$C_{\mathrm{BM,PB,ref}} = 10{,}000\ \mathrm{kW} \cdot 1064.4 \frac{\$}{\mathrm{kW}} \cdot \left(\frac{P_{\mathrm{PB,ref,el}}}{10\ \mathrm{MW}}\right)^{0.6} \tag{7.3}$$

For many of the common process units used in the different processes Ulrich and Vasudevan [87] give data for determining the unit costs. In general a distinction has to be made between the purchase price C_{P}, the bare module price C_{BM}, the total module cost C_{TM} and finally the grass roots capital cost C_{GR}. The definition of the different quantities is given in the following:

- C_{P} is the cost of the component at the manufacturer.
- C_{BM} is the cost of the installed unit.
- C_{TM} includes fees and contingency.
- C_{GR} of a component or plant includes auxiliary facilities. It is the total Investment.

Ulrich and Vasudevan [87] give graphical data for determination of the bare module price of the different components. Furthermore they give general estimates for determination of the grass roots capital cost of the plant. In eq. (7.4)(7.5), it is shown how the grass roots capital cost is estimated from the bare module price. Factors for conversion of bare module price to total module price F_{TM} and grass roots capital F_{GR}.

$$C_{\mathrm{GR}} = C_{\mathrm{TM}} \cdot F_{\mathrm{GR}} = C_{\mathrm{BM}} \cdot F_{\mathrm{TM}} \cdot F_{\mathrm{GR}} \tag{7.4}$$

Polynomial fits are generated from the graphical data to be able to calculate the cost of the units automatically when the component size changes. The polynomial fits are presented in Appendix G.2. The values used for the total module price factor as well as the grass roots capital factor, both based on data by Ulrich and Vasudevan [87] are given in Table 7-3.

Table 7-3: Factors for determination of total module price and grass roots capital

F_{TM}	1.18
F_{GR}	1.30

In determination of the cost of the CCGT's, both the internal one in the SOLME process as well as the external one, it is assumed that not a CCGT is built for these low capacities, but that the gas is combusted in a larger CCGT and only the capacity used for the SOLME system is considered in determination of the cost. Therefore, in calculation of the cost of the CCGT, a plant of 200 MW size is considered, as that is the upper limit of validity of the data by Ulrich and Vasudevan [77] and it is assumed that a real CCGT of a capacity in this range or even higher would be built. The resulting bare module cost of the CCGT is 1020 $ per kW electric capacity in 2004.

The cost of the distillation column for purification of the methanol in the SOLME plant as well as the reference methanol plant is calculated with the procedure presented by Luyben [48]. He gives effective values for the heat transfer coefficients in the condenser and boiler

of the column with which the area can be estimated. He also gives a correlation that allows for calculation of the cost of the reboiler and condenser in dependence of the heat transfer area. Furthermore, he gives a correlation for determination of the height and diameter of the column itself and the corresponding cost. The correlations and data are given in Appendix G.3.

7.2. Results and discussion

In the following two sub-sections the results of the optimization are presented and the economic performance of the SOLME system is evaluated by comparison to the economic performance of the reference system. Subsequently, the sensitivity of the results on changes in some of the major assumptions is assessed. In addition to that the economic performance of the SOLME process alone is assessed. In order to do so, a reward for the reduction of carbon dioxide emissions is assumed. The reduction in carbon dioxide emissions are determined by the reduction in natural gas consumption by the SOLME process compared to the reference methanol plant. Finally, a summary of the overall results of the economic investigation is given.

7.2.1. Optimization Results

In the figures below the results for the levelized cost of electricity of the SOLME process (i.e. without the external CCGT) in dependence of the numbers of tubes (Figure 7-2), the storage capacity (Figure 7-3) and the solar multiple (Figure 7-4) is shown. In each of the figures four curves are shown that each represent an assumed value for the cost of methanol. For the results in all three figures, a receiver with an air return ratio of 0.9 was used.

In all three figures it can be seen that the four curves are parallel. This shows that the optimum value for the corresponding parameter is independent of the chosen value for the cost of methanol. Furthermore, in all three figures the levelized cost of electricity decreases with increasing value of the corresponding parameter until a minimum is reached above which the costs start to increase again. However, it should be noted that for the number of

tubes in the AHR as well as the solar multiple, the minimum $LCOE$ is flat, i.e. only minor increases occur when those two parameters are varied.

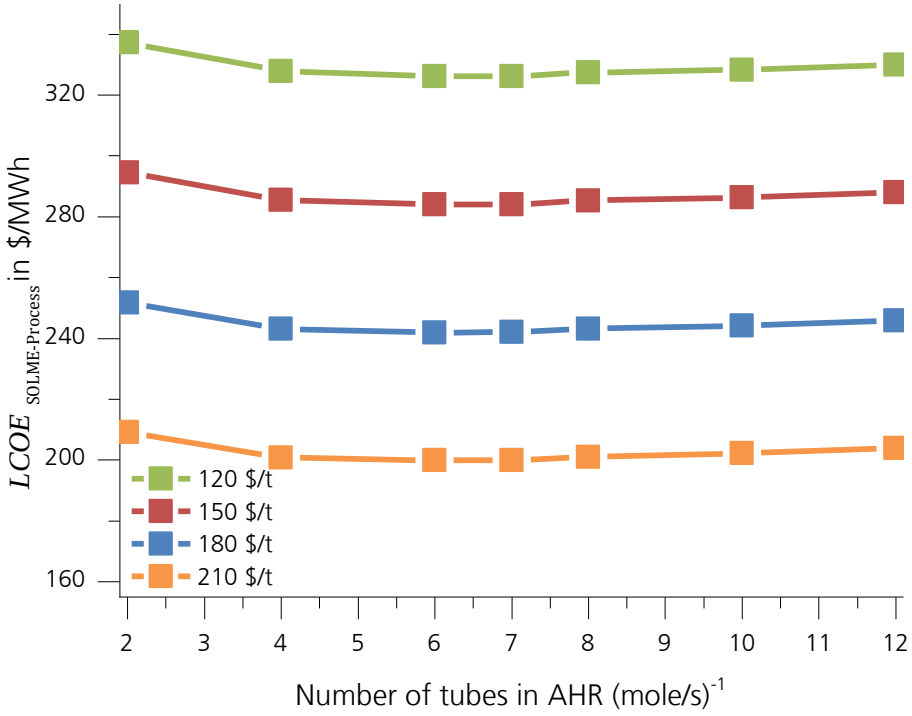

Figure 7-2: LCOE of SOLME Process in dependence of number of tubes in AHR with different values for LCOM

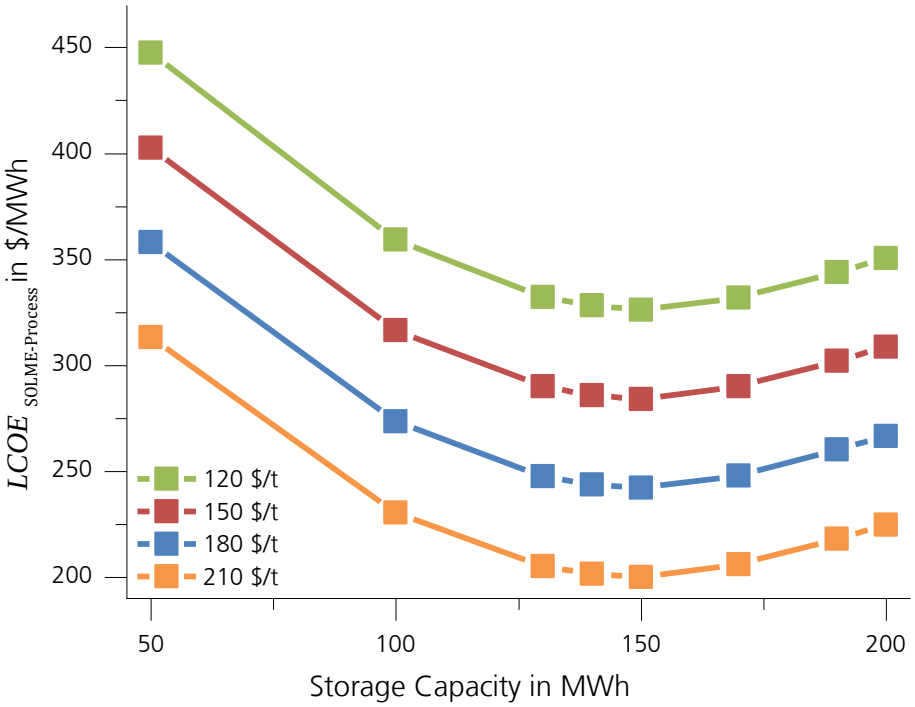

Figure 7-3: LCOE of SOLME Process in dependence of storage capacity with different values for LCOM

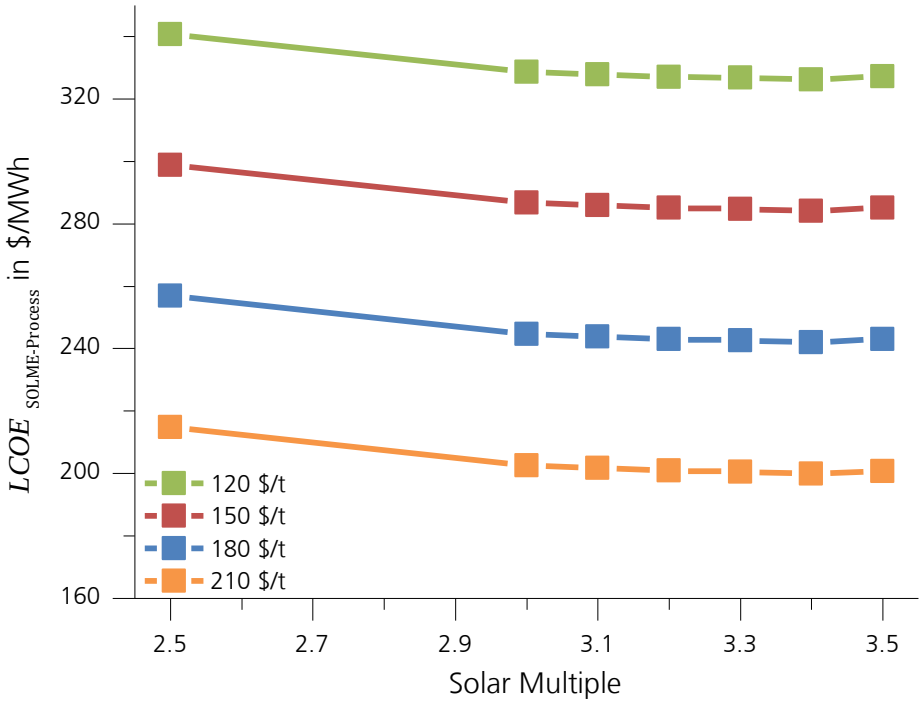

Figure 7-4: LCOE of SOLME Process in dependence of solar multiple with different values for LCOM

The results show parallel curves for the different assumptions of cost of methanol in all three graphs. This indicates that the optimum number of tubes, storage capacity and solar multiple are independent of cost of methanol within the considered range. Therefore, it can be assumed that the procedure gives valid results regarding the optimization of the storage system for the process.

In Figure 7-5 the levelized cost of electricity of the SOLME process is shown in dependence of the number of tubes in the process for an air return ratio of 0.6 and 0.9. The values shown in the figure are determined for the corresponding optimum values for storage size and solar multiple and an assumed revenue from methanol disposition of 150 $/t. For values of air return ratio it can be seen that initially the $LCOE$ is reduced with increasing number of tubes until a minimum is reached at 6 tubes per mole of natural gas per second. Above this value, the $LCOE$ increases with increasing number of tubes. For all investigated values for the number of tubes, the $LCOE$ corresponding to an air return ratio of 0.9 is lower than that for an air return ratio of 0.6.

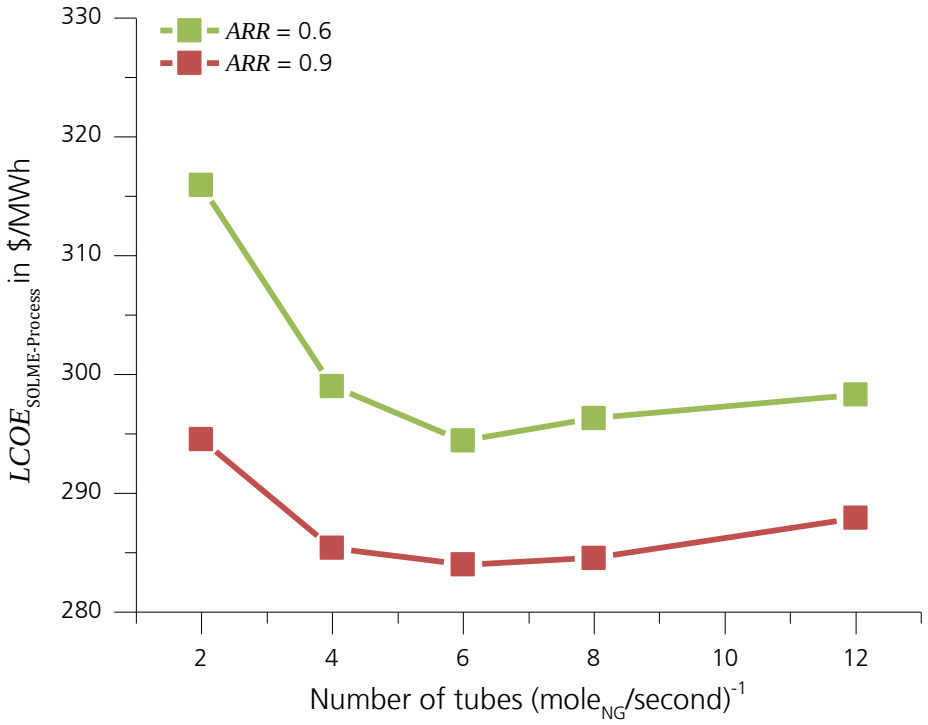

Figure 7-5: LCOE of the SOLME process for Air return ratio of 0.6 and 0.9 , optimum values for storage size and solar multiple, methanol revenue of 150 $/t is assumed.

The initial decrease in the LCOE with increasing number of tubes is caused by an increase in production of methanol and electricity. This in turn is caused by an increase in receiver efficiency by better cooling of the air in the process and corresponding reduction of air return temperature. This effect is stronger for the lower air return ratio, because receiver efficiency is more sensitive to changes in return air temperature. The increase in LCOE above the optimum number of tubes is caused by the increasing cost for the AHR, while the production is only insignificantly increased.

In Figure 7-6 and Figure 7-7 contour plots of the $LCOE_{\text{SOLME-Process}}$ in dependence of the storage size and the solar multiple are shown for air return ratios of 0.6 and 0.9 respectively. In both figures, it can be seen that $LCOE_{\text{SOLME-Process}}$ is decreased for increasing solar multiple and storage size, until an optimum is found for both, above which it starts to decrease. The optimum storage size for a given solar multiple increases with solar multiple up to a value of 3.4, above which it starts to decrease. This is caused by the fact that for a low solar multiple, only small amounts of energy exceed the capacity of the process and have to be stored. Above the optimum of the solar multiple, the operating hours of the

process cannot be significantly increased, while the efficiency of the storage decreases because excess energy that cannot be used in the process has to be disposed of as waste-heat.

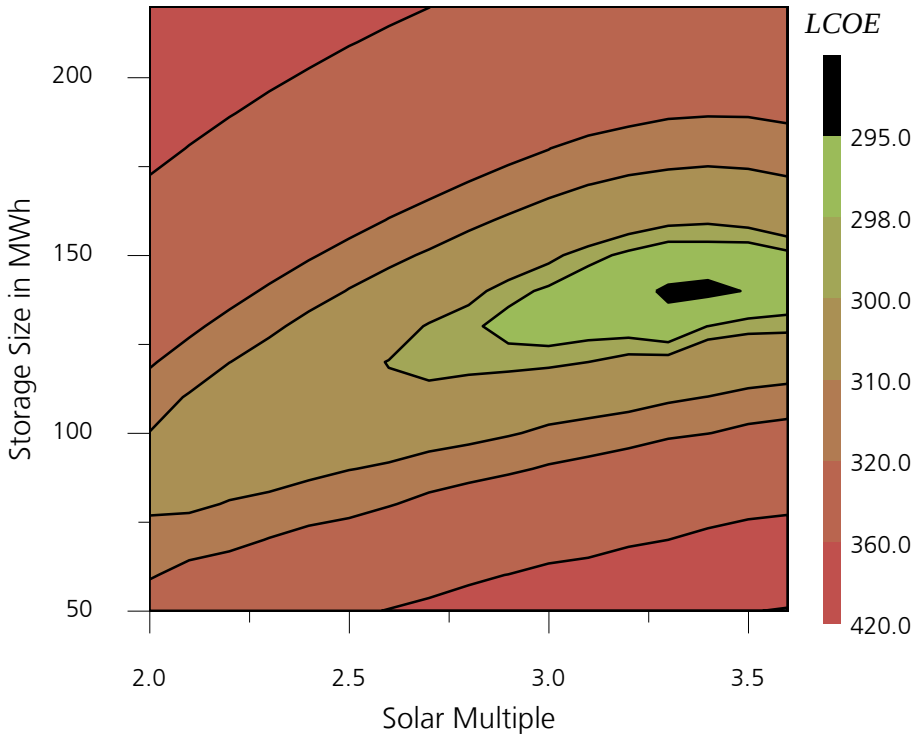

Figure 7-6: The LCOE of the SOLME process with ARR = 0.6 in dependence of storage size and solar multiple. LCOM of 150 $/t is assumed

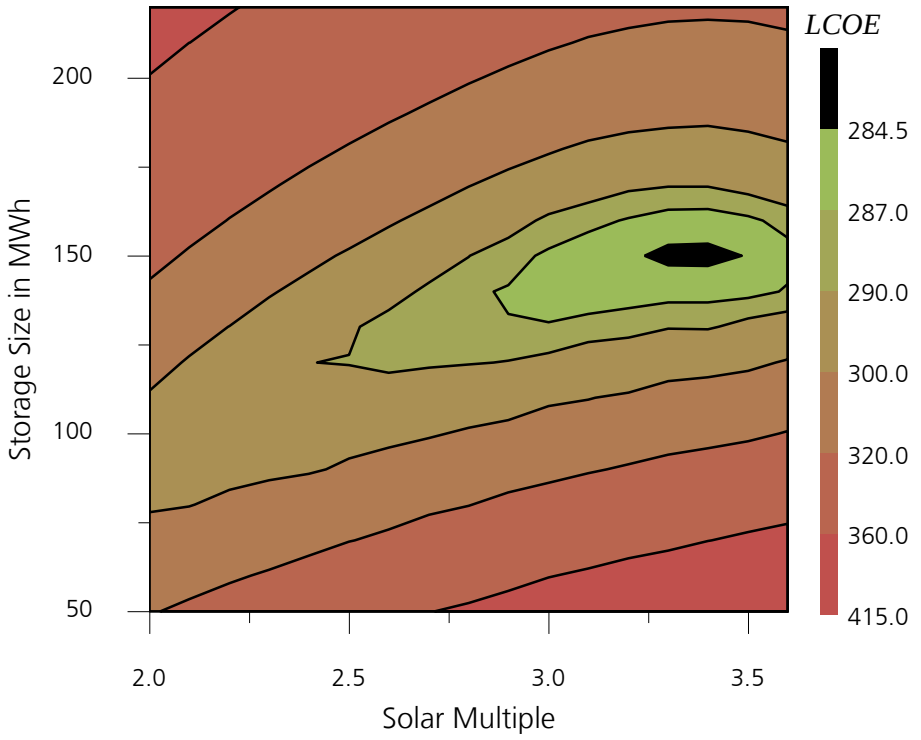

Figure 7-7: The LCOE of the SOLME process with ARR = 0.9 in dependence of storage size and solar multiple. LCOM of 150 $/t is assumed

The Figures Figure 7-6 and Figure 7-7 show that for both air return ratios a solar multiple of 3.4 is optimum. For an air return ratio of 0.6 an optimum storage size of 140 MWh was determined and 150 MWh for an air return ratio of 0.9. A summary of the key results of the economic optimization is given in Table 7-4. These two configurations are further evaluated in the following sub-section.

Table 7-4: Key results of economic optimization for air return ratio of 0.6 and 0.9

	$ARR = 0.6$	$ARR = 0.9$
Solar multiple SM	3.4	3.4
Storage size $Q_{\text{Store,Max}}$ in MWh	140	150
Operating time in h/a	7270	7400
Storage efficiency η_{Storage}	96.5 %	96.4 %
Process Efficiency $h_{\text{SOLME System}}$	3.71 %	4.46 %
Methanol output m_{MeOH} in t/a	$20.9 \cdot 10^3$	$22.3 \cdot 10^3$
Electricity output of SOLME process $E_{\text{El,SOLME,Process}}$ in GWh/a	15.0	15.9
$LCOE_{\text{SOLME,Process}}$ (with $LCOM$ = 150 \$/t) in \$/MWh	294.4	284.0

7.2.2. Relative economic performance

For a meaningful evaluation of the economic performance of the SOLME process, a comparative assessment of the economics is carried out. The economic results of the SOLME system are compared to the reference system. In order to do so, the cost of the reference system, which was presented in sections 6.1 and 6.2, has to be determined. Through this, the $LCOM$ and $LCOE_{\text{Reference}}$ are fixed. Based on this, the $LCOM$, the $LCOE_{\text{SOLME}}$ can be determined. The energy storage to be implemented into the reference solar power plant is assumed to have the same storage capacity as the energy storage in the SOLME process. Furthermore, the external CCGT power plant is taken into account for the SOLME system, in order to provide the same electricity output as the reference system. Some key parameters of the SOLME system as well as the reference system for both cases are given in Table 7-5.

Table 7-5: Results of relative economic evaluation for air return ratio of 0.6 and 0.9, with process parameters in accordance with Table 7-4.

	ARR = 0.6	ARR = 0.9
$E_{\text{EL,SPT,net}}$ in GWh/a	29.5	31.0
$E_{\text{EL,Ref-MeOH,demand}}$ in GWh/a	3.8	4.1
$E_{\text{EL,SOLME-Process,net}}$ in GWh/a	15.0	15.9
$E_{\text{EL,CCGT}}$ in GWh/a	10.8	11.0
$E_{\text{EL,Total}}$ in GWh/a	25.7	27.0
$E_{\text{NG,Ref.}}$ in GWh/a	155.4	166.5
$E_{\text{NG,SOLME Process}}$ in GWh/a	130.9	140.3
$E_{\text{NG, CCGT}}$ in GWh/a	18.0	18.4
$E_{\text{NG,SOLME System}}$ in GWh/a	148.8	158.7
$\Delta E_{\text{NG,Total}}$ in GWh/a	6.5	7.8
$C_{\text{SPT, An}}$ in 10^6\$/a	4.74	4.89
$C_{\text{Ref MeOH, An}}$ in 10^6\$/a	3.68	3.89
$C_{\text{SOLME Process Only, An}}$ in 10^6\$/a	7.53	7.88
$C_{\text{CCGT, An}}$ in 10^6\$/a	0.47	0.49
$LCOM$ in \$/t	176.2	173.9
$LCOE_{\text{Reference}}$ in \$/MWh	184.2	181.4
$LCOE_{\text{SOLME-Process Only}}$ in \$/MWh	257.8	250.4
$LCOE_{\text{SOLME- System}}$ in \$/MWh	168.3	165.9
$\Delta LCOE_{\text{Process Only}}$ in \$/MWh	-73.6	-69.0
$\Delta LCOE_{\text{System}}$ in \$/MWh	15.9	15.5

From the results, it can be seen that the cost of methanol as well as the electricity cost of the reference plant and the SOLME plant and system are reduced when the air return ratio is increased. The difference in the cost of electricity from the reference plant $LCOE_{\text{Reference}}$ and that from SOLME process $LCOE_{\text{SOLME-Process}}$, $\Delta LCOE_{\text{Process}}$ is increased when the air return ratio is increased. This implies that the economic benefit from an increase of air return ratio is more significant for the SOLME process than for the reference solar power plant. This behavior was to be expected, as the return air temperature is significantly higher in the SOLME process than in the reference solar power plant. The difference between the

$LCOE_{\text{Reference}}$ and the cost of electricity from the SOLME system $LCOE_{\text{SOLME-System}}$, $\Delta LCOE_{\text{System}}$ is decreased when the air return ratio is increased. This is in contrast to the expected behavior, because it was shown previously that the efficiency of SOLME benefits more from an increase in air return ratio. However, as can be seen in the values for electricity production by the SOLME process $E_{\text{EL,SOLME-Process,net}}$ and the electricity production by the external CCGT $E_{\text{EL,CCGT}}$ the share of the electricity production in the CCGT of the total electricity production is decreased. With an LCOE of around 50 $/MWh, the electricity from the CCGT is cheap compared to the electricity from the SOLME process or the reference solar power tower. This shows that the value of $\Delta LCOE_{\text{System}}$ should not be the only parameter considered in evaluation. The change in economic performance between two configurations can best be evaluated by observation of $LCOM$ and $LCOE_{\text{SOLME-System}}$. However, in order to assess whether the SOLME system is economically competitive with conventional solar power plants, the value of $\Delta LCOE_{\text{System}}$ is important. As mentioned in section 7.1, when the value is positive, as in both presented cases, an economic benefit exists.

A noticeable effect to be observed in the results is the reduction of $LCOM$ when the air return ratio is increased. As discussed section 7.1, the $LCOM$ is determined by the cost of the reference methanol plant. The production rate of the plant is previously determined by the performance of the SOLME plant. When the air return ratio increases, the methanol output is increased (cf. Table 7-4). Therefore the size of the reference methanol plant is increased. As is mostly the case for upscaling of processes, the specific cost for the product decreases for larger production facilities. This illustrates a deficiency of the evaluation scheme. On the one hand it is meaningful to compare methanol production plants of the same size, while on the other hand methanol production facilities are significantly larger in reality: The Methanol Institute [89] states that average production capacity of a methanol plants is around one million tons per year. It can be assumed that production cost is significantly lower in those facilities. This effect is investigated in the subsequent sub-section 7.2.3.

The overall results show that when only taking into account the SOLME process in comparison with the reference system, the levelized cost of electricity is significantly higher

than for the reference system. However, when taking into account the external CCGT for production of the identical amount of electricity, the levelized cost of electricity is 8.6 % lower for the SOLME system than for the reference system. At the same time, a significant reduction of total natural gas consumption ($\Delta E_{\mathrm{NG,Total}}$) is achieved.

In Table 7-5 the total annual cost C of the different plants was shown. In order to allow for a comprehensive discussion of the data, more detailed breakdown of the cost data is given in Table 7-6. In the table it can be seen that the annuity cost for all process plants increases when the air return ratio is increased from 0.6 to 0.9. This is caused by the fact that the energy provided by the receiver is increased by the higher efficiency. Correspondingly, the throughput of the entire process is increased, causing an increase in plant size and cost. A more detailed list of the component costs is given in the appendix in Table A - 7. The resulting capacity specific capital cost of the reference methanol plant are around 550 $/(t/a). This is below the value given by a report recently published on small scale methanol production facilities [90], which mention 700 to 1000 $/(t/a) for a plant with similar capacity. Even though the resulting value is low, any errors in estimating capital cost will apply to the SOLME plant to the same extent, hence the comparison between the two systems will still be valid. But it also shows that the absolute value of the $LCOM$ and the $LCOE$'s are not reliable.

Table 7-6: Annuity and annual natural gas cost of SOLME - and reference system for Air return ratio of 0.6 and 0.9

	ARR = 0.6	ARR = 0.9
$C_{\mathrm{Annuity,SOLME,\ Process\ Only}}$ in 10^6 $/a	4.82	5.02
$C_{\mathrm{Annuity,CCGT}}$ in 10^6 $/a	0.24	0.25
$C_{\mathrm{Annuity,SPT}}$ in 10^6 $/a	4.18	4.32
$C_{\mathrm{Annuity,MeOH,Ref}}$ in 10^6 $/a	1.02	1.07
$C_{\mathrm{NG,SOLME}}$ in 10^6 $/a	1.57	1.68
$C_{\mathrm{NG,CCGT}}$ in 10^6 $/a	0.22	0.22
$C_{\mathrm{NG,MeOH\ Ref}}$ in 10^6 $/a	1.86	2.00
ΔC_{NG} in 10^6 $/a	0.07	0.10

The results suggest that the cost benefit of the SOLME system compared to the reference system is only partly caused by the reduction in natural gas consumption. In addition to the reduction in natural gas consumption, the investment cost of the SOLME system is lower than for the reference system. This effect is mainly driven by the fact that all the electricity is produced in water steam cycles in the reference system, while it is to a large extent produced in a CCGT in the SOLME system. As the specific investment costs are lower for a CCGT than for a water steam cycle, this has a positive effect on economic performance.

7.2.3. Parameter variation

Similar to the thermodynamic results, assumptions are made regarding the values of some of the parameters. The sensitivity of the results on deviations of the assumptions from the reality is investigated in the following. In accordance with the parameter variation that was carried out in section 6.5, the efficiency of the CCGT in the SOLME system as well as the efficiency of the power block in the reference solar power plant are varied. The effect on the results of the economic investigation is assessed. Furthermore, the cost of CO_2 emissions in the calculation of annual cost of the plants and a larger methanol plant, as it is state of the art, in the reference system are considered.

In Figure 7-8 the results of varying the power block efficiency of the reference solar power plant and the efficiency of the CCGT are shown for an air return ratio of 0.9. The $LCOE$ of the SOLME system, as well as the reference system is shown in dependence of the efficiency of the power block in the reference solar power tower. For the $LCOE$ of SOLME, the results are shown for an efficiency of the CCGT of 60 % and 55 %. The $LCOE$ of the reference system is independent of the CCGT efficiency. The results for an air return ratio of 0.6, that show the same principal behavior are given in Appendix G.5.

The results show that the $LCOE$ is decreased for both systems when the efficiency of the power block of the reference solar power plant is increased. For the reference system this insight is trivial, as the electricity production is increased at constant costs. For the $LCOE$ of the SOLME system, it is not as trivial: By definition of the evaluation scheme, the electricity output of both systems has to be identical. In order for the SOLME system to achieve this, the electricity generation of the CCGT has to be increased, when the efficiency of the

power block of the reference solar power plant is increased. The electricity produced by the CCGT is cheap, therefore the systems overall $LCOE$ is decreased. However, the relative reduction of the performance of the SOLME system is revealed by the decrease of the SOLME efficiency $h_{\text{SOLME, System}}$ that can be observed on the right hand axis.

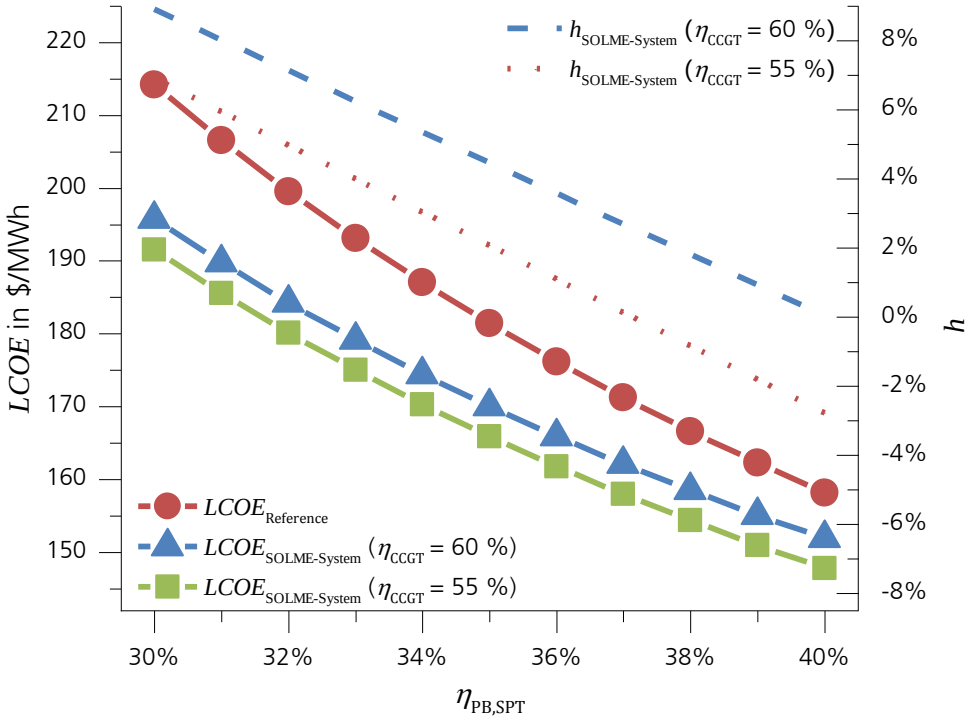

Figure 7-8: Results of the variation of the efficiency of the power block in the reference solar power plant and the efficiency of the CCGT in the SOLME system for air return ratio of 0.9. Reference value of $\eta_{\text{PB,SPT}}$ is 0.35.

In the figure above, it can be seen that for a combination of increased power block efficiency in the reference system and decreased CCGT efficiency in the SOLME system, the overall efficiency of the SOLME system will drop below zero. This implies that the SOLME system has a higher natural gas consumption than the reference system for those configurations. Despite this negative result, for any configuration displayed in the results above, $LCOE_{\text{SOLME-System}}$ is below $LCOE_{\text{Reference}}$. This shows that the economic benefit of the SOLME system is not only caused by a reduction in natural gas consumption, but in addition by lower investment costs. This indicates that an economic benefit of the SOLME system is not limited to configurations that achieve an $h_{\text{SOLME, System}}$ above zero.

In Figure 7-9 results are presented for a variation of assumed cost for CO_2 emissions. The costs are taken into account in the economic model by adding the attributed cost to the overall annual cost. The difference in the CO_2 emissions between the SOLME system and the reference system is determined through the difference of natural gas consumption, as this is the original source of the carbon that is later emitted as CO_2. In the figure, results are shown for the two different values of air return ratio 0.6 and 0.9, as well as for two different scenarios regarding the boundary conditions: Firstly, the reference or optimistic scenario with $\eta_{\text{CCGT}} = 60\ \%$ and $\eta_{\text{PB,SPT}} = 35\ \%$. Secondly the more pessimistic scenario, with $\eta_{\text{CCGT}} = 55\ \%$ and $\eta_{\text{PB,SPT}} = 40\ \%$. The results are presented as the difference in $LCOE$ between the reference system and the SOLME system $\Delta LCOE$ as defined in Eq. (7.5). $\Delta LCOE$ is an indicator on the economic benefit achieved by the SOLME system. The higher its value, the greater the benefit. For values below zero, the SOLME system does not achieve an economic benefit, but a loss.

$$\Delta LCOE = \ LCOE_{\text{Reference}} - LCOE_{\text{SOLME,System}} \tag{7.5}$$

The results show that for the reference scenario $\Delta LCOE$ is increased with increasing cost for CO_2 emissions, while the contrary is the case in the pessimistic scenario. In both cases for the higher air return ratio of 0.9 the development is more positive, i.e. the first effect is stronger, while the second is less drastic. However, the air return ratio causes only a marginal difference in this respect. The decreasing of $\Delta LCOE$ is caused by the fact that the

efficiency of the SOLME system is negative for this set of parameters (as shown in and Figure 7-8).

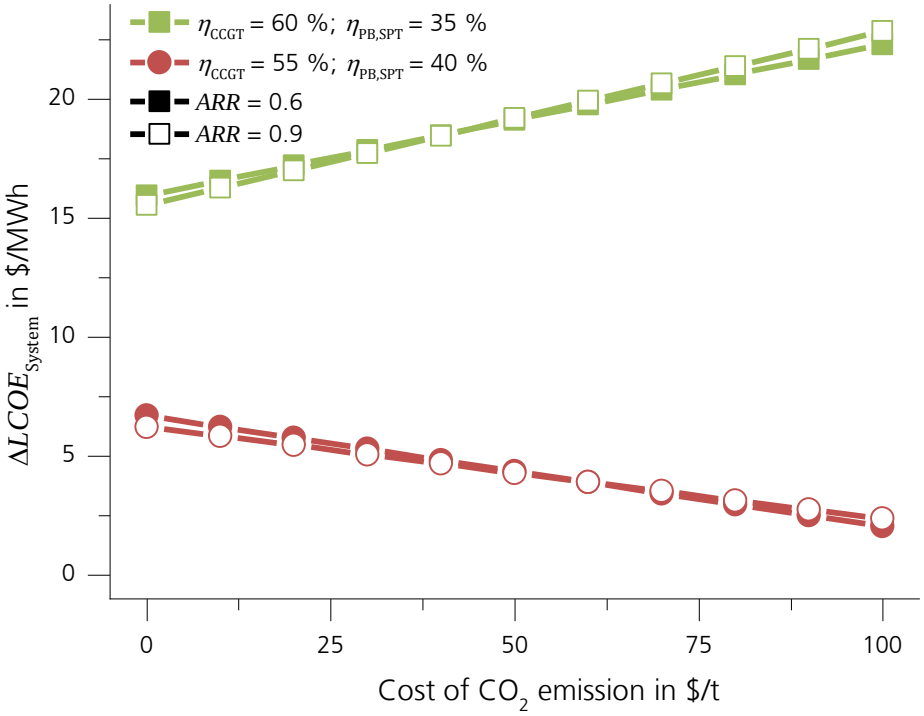

Figure 7-9: Influence of the cost for CO_2 emissions on $\Delta LCOE_{System}$

The influence of the natural gas price on the economic results is presented in Figure 7-10. It can be seen from the results that the economic benefit of the SOLME system $\Delta LCOE$ is increased with increasing natural gas price. The historical data for the natural gas price at Henry Hub between 1997 and 2015 shows that the price fluctuated between values below 3 $ per million BTU (approx.. 10 $/MWh) and above 12 $ per million BTU (approx.. 40 $/MWh) [91]. Therefore, the price range considered in the variation can be considered realistic.

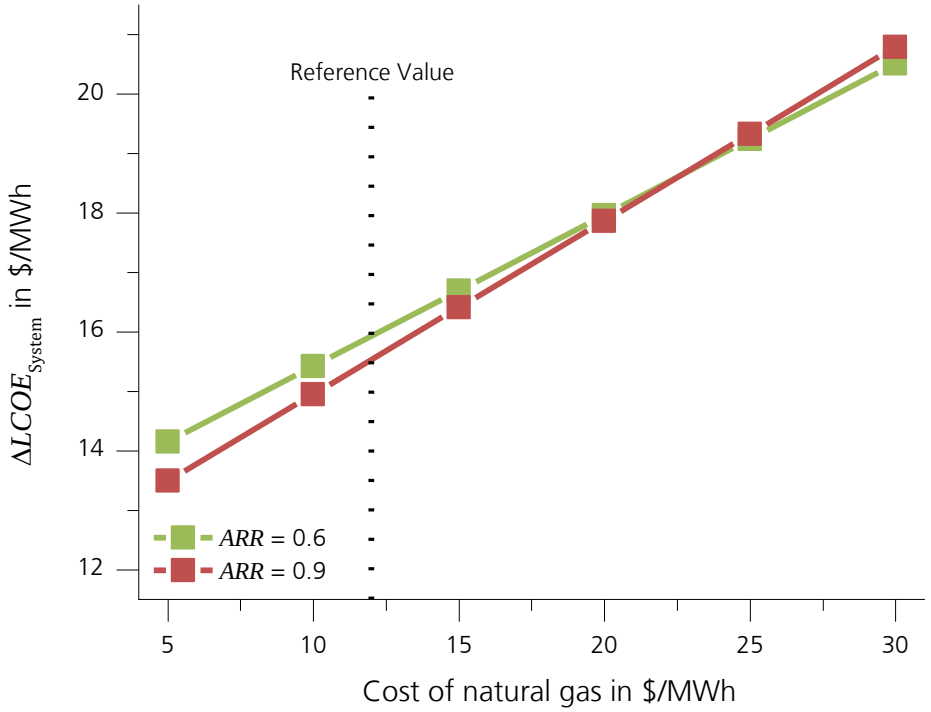

Figure 7-10: Influence of natural gas price on $\Delta LCOE_{,System}$

The final aspect to be investigated in this sub-section is the influence of the size of the methanol plant on the economic results. As already discussed shortly in the previous sub-section, the methanol plant considered in this work is significantly smaller than the state of the art. According to Aasberg-Petersen et al. [21], methanol plants with a production capacity close to 2 million metric tons per year (5000 tons per day) are state of the art. Due to lack of more appropriate data, the plant cost for large plants are estimated by scaling the determined cost of the methanol plant with an exponential factor of 0.6, which is identical to the procedure presented in Eq. (7.5) for the cost of the power block. The resulting investment cost of the plant in dependence of the methanol output and the corresponding specific cost per capacity (t/a) are given in Figure 7-11. The results are prepared with utilization of the data from the case with air return ratio of 0.6. In the figure it can be seen that a significant decrease in specific investment cost for the plant can be expected for an increased plant capacity. For a capacity of around 20 thousand tons of methanol per year, as is the case in this work, a specific plant cost above 500 $/(t/a) is determined. For a plant capacity of a million tons per year, the plant cost is reduced to 120 $/(t/a).

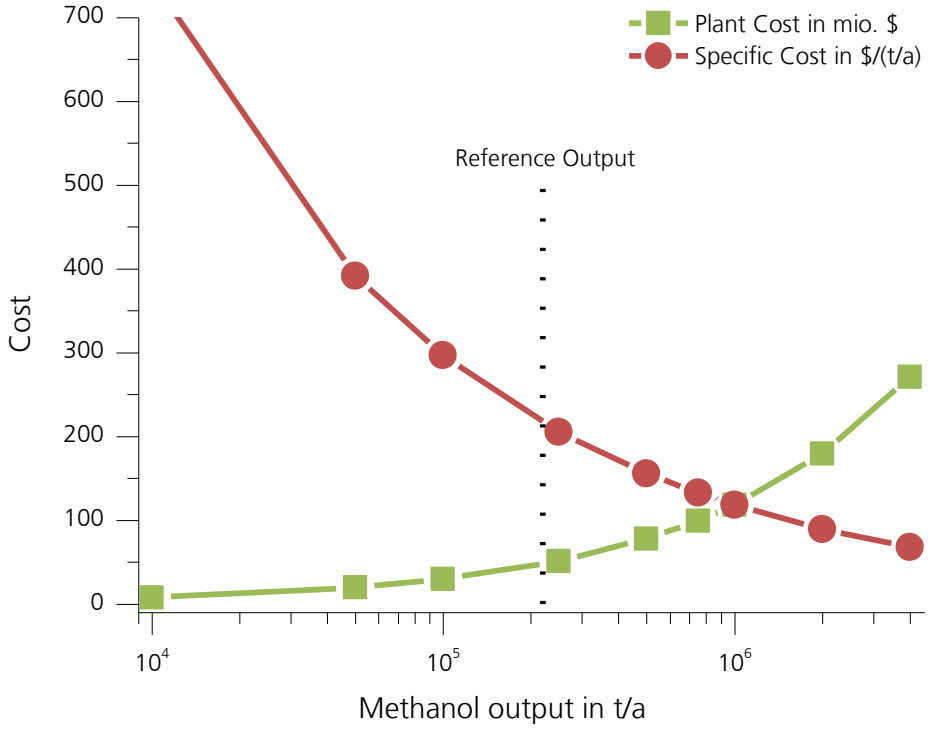

Figure 7-11: Estimated development of absolute and specific investment cost of a methanol plant with plant size

In Figure 7-12 the influence of the variation of reference methanol plant capacity on the economic result is depicted. For clarity of the figure, this is only shown for an air return ratio of 0.6. As could be expected the $LCOE_{\text{Reference}}$ is not influenced by a variation of methanol plant capacity. The $LCOM$ is significantly decreased from a value around 180 \$/t for a plant with a capacity of 20 thousand tons per year to 135 \$/t for a plant with a capacity of one million tons per year. In contrast to that, the $LCOE_{\text{SOLME, System}}$ is increased from 170 \$/MWh to 201 \$/MWh. It can be seen that the $LCOE_{\text{SOLME, System}}$ crosses the line of $LCOE_{\text{Reference}}$ for a plant capacity of 80,000 tons per year. Above this capacity of the reference methanol plant, no economic benefit can be expected from the SOLME process. This is caused by the significant reduction of cost for methanol from a larger plant.

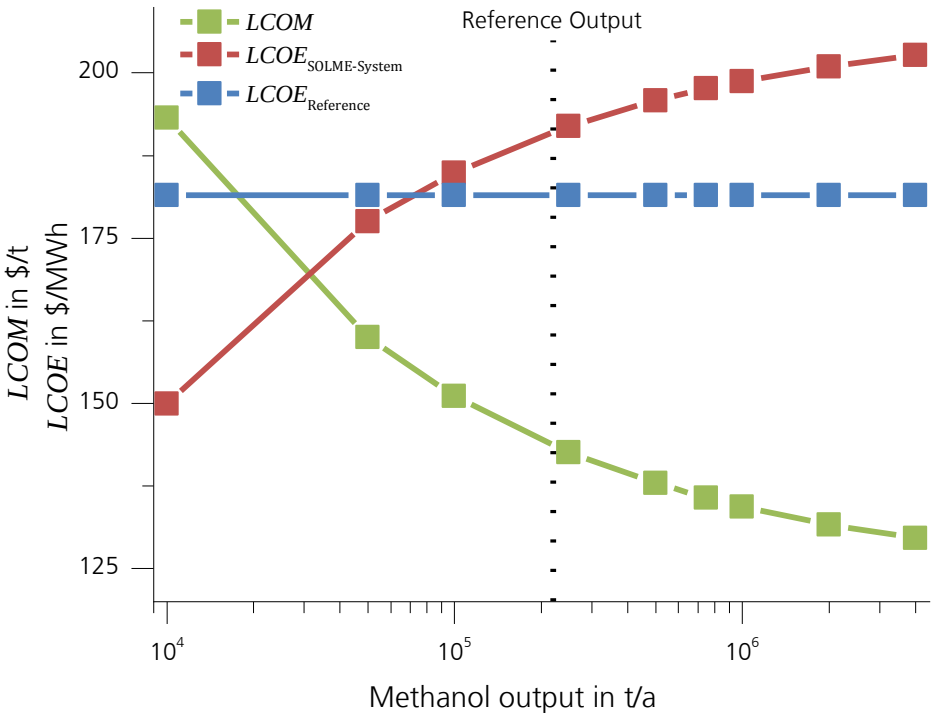

Figure 7-12: Influence of methanol plant size on results of economic analysis.

Despite the above presented results, it should not be assumed that SOLME does not provide an economic benefit in comparison to a common state of the art methanol production facility. Firstly, the consideration that methanol production is commonly carried out in large facilities can just as well be applied to the SOLME plant. For instance, it is possible to build several solar power systems that perform the reforming with subsequent collection of the produced syngas in one large methanol synthesis plant. This will most

probably improve the economic performance of the SOLME process as well. Secondly, as already mentioned, the proposed process will most likely be advantageous in some niche applications for small natural gas wells at a remote location with high solar resource. Therefore, competitiveness with large scale state of the art methanol synthesis plants is not the objective of the process scenario.

7.2.4. Economic performance of SOLME process only

The remuneration of an CCGT in the SOLME system with the feed-in-tariff of a solar power plant is most likely not feasible in reality. A more adequate way of remuneration of the SOLME process would be a reward for reduction of carbon dioxide emissions compared to the state of the art. The idea of this reward is somewhat different to the cost of CO_2 emissions that where discussed for the two systems in sub-section 7.2.3 and will be introduced in the following paragraph. It should be noted that currently conventional solar power plants are substantially subsidized. This can be well observed at the example of the solar power tower plant *Crescent Dunes* that commenced operation in 2015. This power plant has received subsidies of two kinds. As reported by Parkinson [92] it was supported with subsidized loans and furthermore it has a contract for delivering electricity at a price of 135 $/MWh, which is well above the regular price of electricity for industrial consumers below 80 $/MWh (as reported for Nevada by [93]). This is also applicable to the reference solar power plant of this work, which achieves an $LCOE_{\text{Reference}}$ of 181 $/MWh (with ARR =0.9): For an assumed market price of electricity of 80 $/MWh, the total remuneration of the reference solar power tower is 2.7 million $ per year. The reduction of carbon dioxide emissions compared to a CCGT power plant are approximately 12 thousand tons per year. This yields a subsidy of 250 $/t for the reduction of carbon dioxide emissions for the reference solar power plant. This funding cannot be applied to the SOLME process, because it only produces electricity to a smaller extent and would therefore receive a smaller remuneration. For products like methanol these types of subsidized feed-in-tariffs are not common. However, it serves a similar purpose, the reduction of CO_2 emissions. Therefore, a suitable subsidy for all processes that make use of renewable energies can be an appropriately scaled reward for the reduction of CO_2 emissions compared to a reference value.

The influence of such a reward on the economic performance of the SOLME process (i.e. without the external CCGT) is investigated in the following. The reduction of CO_2 emissions of the SOLME process in comparison with fossil based technology is determined: The fossil based technology are the conventional methanol synthesis plant and a CCGT for electricity production. The same is done for the reference solar power plant. The reward for the reduction of CO_2 emissions and the resulting $LCOE$'s are determined. This is carried out considering the reference natural gas price of 12 \$/MWh and an increased natural gas price of 30 \$/MWh. An air return ratio of 0.9 is assumed. The results are shown in Figure 7-13. In the results it can be seen that all $LCOE$'s are reduced with increased reward. It can also be seen that the $LCOE_{\text{SOLME-Process}}$ decreases stronger with the increasing reward. This is caused by the fact that it achieves a higher reduction of CO_2 emissions than the reference solar power plant. Furthermore, the increase in natural gas price causes a decrease in the $LCOE_{\text{SOLME-Process}}$, but does not influence the $LCOE_{\text{Reference}}$. There is also a line added to the diagram that marks the value of 80 \$/MWh which is assumed as a competitive price. It can be seen that SOLME achieves competitiveness at 150 \$/t_{CO2} and 205 \$/t_{CO2} with the higher and lower natural gas prices respectively, while the reference solar power plant achieves competitiveness at a reward above 225 \$/t_{CO2}. This indicates that SOLME can be more economic than conventional solar power tower plants, when high rewards for the reduction of CO_2 emissions are applied. However, for rewards below 100 \$/t_{CO2} this is not the case. In general the values for the rewards for CO_2 emission reduction above which SOLME can become competitive are very high compared to the expected cost of CO_2 certificates in the future. According to Schlesinger et al. [94] their prices are not expected to exceed 100 \$/t_{CO2} (76 €/t_{CO2}).

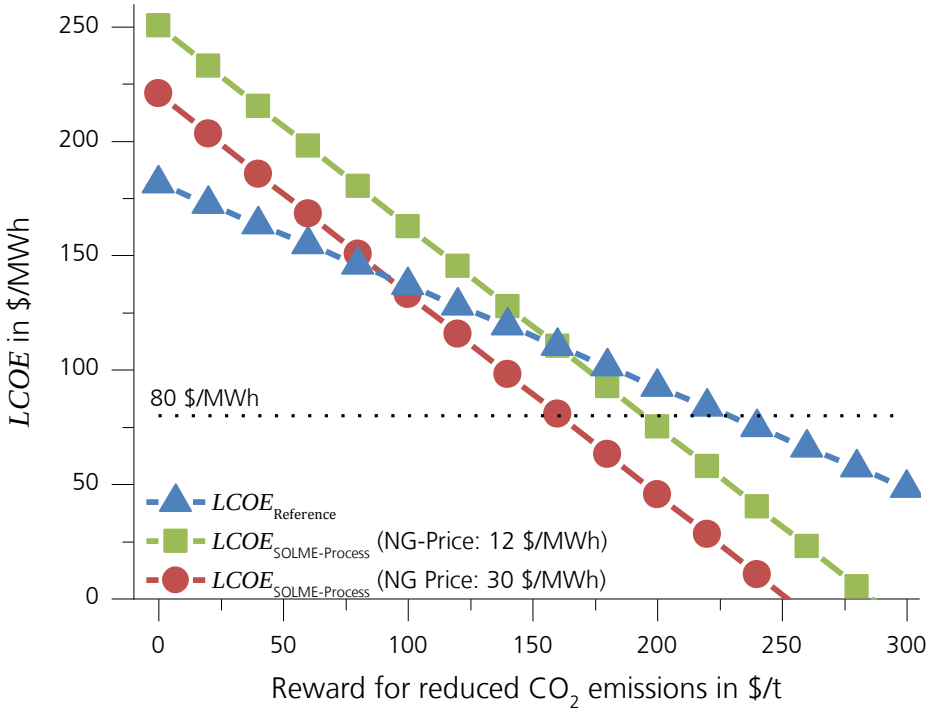

Figure 7-13: *LCOE* of the reference solar power plant and SOLME (process only!) in dependence of Reward for reduced CO_2 emissions for different natural gas price assumptions.

It is expected that the cost of CSP components are reduced in the future. The influence of these potential reductions on the economic performance of SOLME is assessed by reducing the investment cost of the heliostat field, the solar receiver and the storage system to 70 % of the original cost. This is also applied to the reference solar power plant. The price reduction to 70% is an assumption for the year 2020 based on the data given by Trieb [95]. The results for the $LOCE$ are shown in Figure 7-14. In general the same behavior can be observed as in Figure 7-13. However, the absolute values of the $LCOE$'s are lower than in the previous case. It can be seen that the $LCOE_{\text{SOLME, Process}}$ is lower than the $LCOE_{\text{Reference}}$ for smaller rewards than in the previous case. Furthermore, $LCOE_{\text{SOLME, Process}}$ achieves values below 80 \$/MWh for rewards between 75 \$/t_{CO2} and 120 \$/t_{CO2}, depending on the natural gas price. $LCOE_{\text{Reference}}$ only achieves this value for a reward above 130 \$/t_{CO2}.

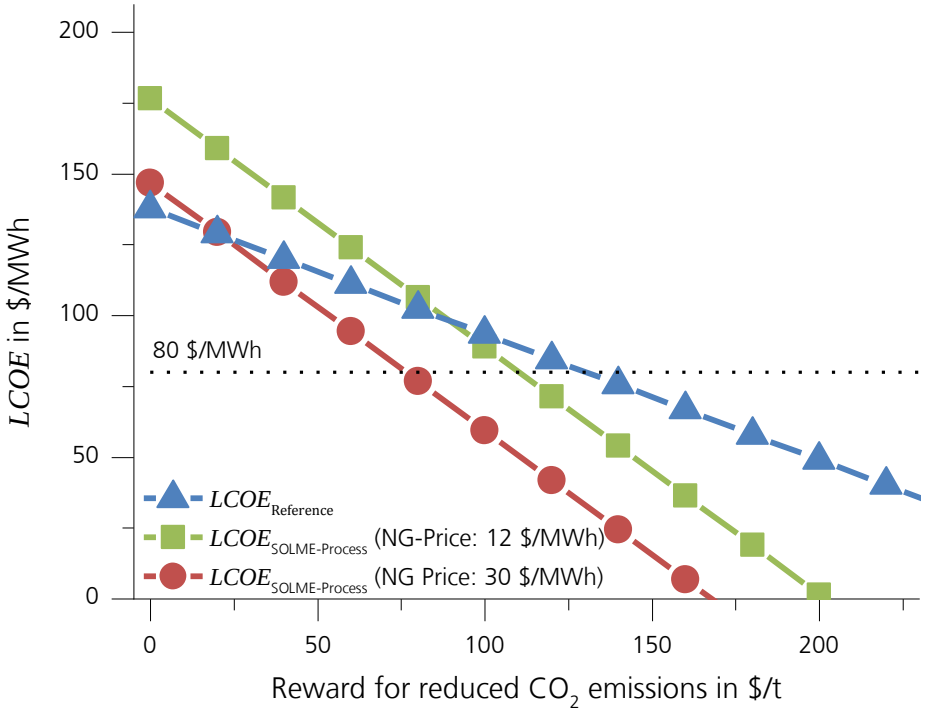

Figure 7-14: LCOE of the reference solar power plant and SOLME (process only!) in dependence of Reward for reduced CO2 emissions for different natural gas price assumptions. Reduced component cost for CSP-Components

The results of this investigation show that economic competitiveness of SOLME is possible when overall competitiveness of CSP is improved. However, at the same time it shows that unreasonably high rewards for CO_2 emission reduction are necessary in order for CSP to be cost competitive. This problem will be alleviated by reduction of the cost for CSP-specific components. The results furthermore showed that SOLME will more likely be cost competitive if the natural gas price is high. This is especially true because it will not only cause a reduction in the $LCOE_{SOLME}$ but may also increase the cost of conventionally produced electricity.

7.3. Summary of economic investigation

The economic optimization of the SOLME process has shown that a high solar multiple and large energy storage that allow for operational time in excess of 7000 h per year lead to an optimum for the SOLME process.

The investigation of the relative economic performance of the SOLME system has shown that a significant economic benefit is possible. A reduction of the LCOE of more than 15 $/MWh compared to the reference system was shown for both values of the air return ratio (0.6 and 0.9). At the same time the natural gas consumption is significantly lower in the SOLME system.

The parameter variations have shown that, similar to the results of the thermodynamic investigations, changing the assumed efficiency of the power block in the reference solar power tower and the efficiency of the CCGT have a significant influence on the results. If the efficiency of the solar power block in the reference solar power plant is higher and the efficiency of the CCGT is lower than assumed, this causes a reduction of the determined benefit.

It was also shown that an increase of the natural gas price will enhance the advantage of SOLME, if an actual reduction of natural gas consumption is achieved. The competitiveness with the large state of the art methanol production plants with production capacity in excess of 1 million tons of methanol per year is questionable for the SOLME process. This indicates that the SOLME process is mainly an interesting application for relatively small gas fields. Also bigger plant sizes for the SOLME process are possible. Though it should be noted that upscaling is limited by the heliostat field and a methanol output in the range of conventional state of the art methanol plants is not likely for the SOLME process.

It was assessed whether the SOLME process can be competitive even if the external CCGT is not taken into account. It was shown that this is only possible for very high rewards for the reduction of CO_2 emissions. However if the CSP-related component costs are reduced, and/or the natural gas price rises, the SOLME process will be cost competitive with conventional CSP technology at rewards for CO_2 emission reduction as low as 25 $/t.

8. Conclusions

The overall goal of this work was to assess the efficiency and cost of utilization of solar energy in industrial or chemical processes. As an example of a solarized industrial process, methanol production was investigated. A new process was developed to produce methanol via solar reforming of natural gas. Conventional evaluation criteria, such as energetic efficiency, are not applicable to such a process because those processes are not motivated by energetic considerations but by the need of a certain product. An evaluation criterion was developed that evaluates the efficiency of renewable energy utilization in such processes. In essence this criterion enables to assess if the renewable energy utilization in the process in focus is more efficient than utilization of the same form of energy for electricity production. This evaluation is carried out by comparing the fossil fuel consumption of the investigated process to that of the reference process. Based on the evaluation criterion it was shown that processes operating below 1000 °C can be efficiently driven by concentrated solar energy at state of the art concentration ratios. If higher concentration ratios are applied this will also be possible for processes operating at higher temperatures. Additionally, these solarized industrial processes allow for a more flexible utilization of solar energy. Conventional solar power plants are limited to operation within the range of power transmission lines to consumers. This is not the case if a commodity such as methanol is produced. As is state of the art, methanol can be transported via ship from remote locations to the location of demand. Furthermore, the temporal deviation between supply and demand is not a problem in the production. Most conceivable chemical products like methanol can, in contrast to other methods of energy storage, be stored for very long time intervals with large quantities. Therefore, they can be used for seasonal energy storage.

In a more rigorous approach, the solarized methanol production process (SOLME process) was modelled and simulations were carried out to evaluate its energetic and economic performance. An open volumetric receiver was considered to convert the solar radiation into heat that is provided to the reforming reactor. In order to make use of waste heat streams, the process also produces electricity. Several process parameters were varied with

the aim of maximizing the previously defined evaluation criterion. The results show that the SOLME process has the potential to make more efficient use of the solar energy than for the case in electricity production from concentrated solar power. A CCGT power plant is considered to convert natural gas into electricity so that the combination of SOLME process and the CCGT produce the same amount of electricity as the reference solar power tower. The results of this combination show a significant reduction in natural gas consumption compared to a system of conventional solar power tower and methanol synthesis with the same output of electricity and methanol. The predicted value of the evaluation criteria $h_{\mathrm{SOLME\ System}}$ is in the range of 4.3 % and 5.4 %, corresponding to natural gas savings with respect to the conventional solar power tower and methanol synthesis plant of 43 and 54 kWh per MWh of solar energy input to the process.

In the subsequent economic optimization, some components were sized. These components were the thermal energy storage and the air heated reformer. This allowed for a prediction of the process efficiency in an economically optimum configuration. The optimization results indicate that a large heat storage allowing for more than 7000 operating hours per year is optimum. With the optimum configurations, the value of the evaluation criteria $h_{\mathrm{SOLME\ System}}$ will be between 3.7 % and 4.5 %. Furthermore the comparison of economics of the SOLME system and the reference system showed that the levelized cost of electricity of the SOLME system is approximately 15 $/MWh lower than for the reference system, while the cost for methanol is set identical for both. For one part this economic benefit is caused by the reduction in natural gas consumption, to another part by the different way of electricity production. In the reference system, all electricity is produced in a water steam cycle, raising high capital costs. In the SOLME system, a large fraction of the electricity is produced in a gas turbine enabling significantly lower capital costs.

In this work both the reference system and the SOLME system were each evaluated as one system. This means that all electricity produced by the SOLME system, as well from the SOLME process as the external CCGT was assumed to be dispositioned at the same price. This price was compared to the price of electricity from the reference solar power tower. These high electricity prices well in excess of 100 $/MWh are only possible due to feed-in-tariffs supported by subsidies or the will of utility services to reduce their CO_2 emissions.

Assuming the current practice of feed-in-tariffs it is not possible to apply these subsidies to electricity produced in a CCGT. Therefore, in reality the methanol from the SOLME process would have to be subsidized in order to allow for competitiveness of the SOLME process. This would also be applicable to other solarized industrial process that produces other products than electricity and can possibly be done by rewarding the reduction of CO_2 emissions compared to a reference technology. When significant rewards for the reduction of CO_2 emissions are applied, the SOLME process itself can be economically competitive, without taking the CCGT into the balance. High natural gas prices further improve the competitiveness of the SOLME process.

In summary, both the thermodynamic as well as the economic results are very promising for SOLME. They show that competitiveness with conventional solar energy utilization is very likely and even advantages are possible. In addition to these promising results, the process allows for a more flexible utilization of solar energy, even at remote locations without substantial electricity consumers. In general the results indicate that very efficient application of concentrated solar power in chemical processes is possible by using state of the art process units.

The focus of future research in this topic should be a validation of the results in an experimental campaign. Simultaneously, some effort should be put into development of concepts for efficient air-heated reformers at reasonable costs. Furthermore, the development of solar receiver especially designed for application with solar reforming or other similar process should be established. This is mainly the case, because these processes make use of heat at temperatures well in excess of those commonly required in water steam cycles for electricity production. In addition to that, a further focus of future development should be put on small-scale application, for instance on islands or remote locations with methane rich gas resources and poor infrastructure. Those methane-rich gas resources may be small natural gas wells or biogas sources. Such scenario will be interesting for supply of a solar fuel and will also allow for conversion of stranded-methane resources into an easily transportable form for its disposition on the world market.

Bibliography

1. IPCC, *Summary for Policymakers*, in: T.F. Stocker, D. Qin, G.-K. Plattner, M. Tignor, S.K. Allen, J. Boschung, A. Nauels, Y. Xia, V. Bex, P.M. Midgley (Eds.) Climate Change 2013: The Physical Science Basis. Contribution of Working Group I to the Fifth Assessment Report of the Intergovernmental Panel on Climate Change, Cambridge University Press, Cambridge, United Kingdom and New York, NY, USA, 2013, ISBN: ISBN 978-1-107-66182-0, pp. 1–30.
2. Höök, M., Tang, X., *Depletion of fossil fuels and anthropogenic climate change—A review*, Energy Policy, 52 (2013), 797-809, http://dx.doi.org/10.1016/j.enpol.2012.10.046
3. IPCC, *Summary for Policymakers*, in: M. Parry, O. Canziani, J. Palutikof, P. van der Linden, C. Hanson (Eds.) Climate Change 2007: Impacts, Adaptation and Vulnerability: Contribution of Working Group II to the Fourth Assessment Report of the Intergovernmental Panel on Climate Change, Cambridge University Press, Cambridge, UK, 2007, ISBN: 0521880106, pp. 7-22.
4. *Key World Energy Statistics*, International Energy Agency (IEA), 2014, URL: www.iea.org/publications/freepublications/publication/KeyWorld2014.pdf, Date Accessed: 5 May 2015
5. *Erneuerbare Energien auf einen Blick*, Bundesministerium für Wirtschaft und Energie, URL: http://www.bmwi.de/DE/Themen/Energie/Erneuerbare-Energien/erneuerbare-energien-auf-einen-blick.html, Accessed: 01.07.2016
6. Ermanoski, I., Siegel, N.P., Stechel, E.B., *A New Reactor Concept for Efficient Solar-Thermochemical Fuel Production*, Journal of Solar Energy Engineering, 135 (2013), 031002-031002, 10.1115/1.4023356
7. Rostrup-Nielsen, J.R., Sehested, J., Nørskov, J.K., *Hydrogen and synthesis gas by steam- and CO2 reforming*, in: Advances in Catalysis, Academic Press, 2002, ISBN: 0360-0564, pp. 65-139.
8. Bartholomew, C.H., Farrauto, R.J., *Fundamentals of industrial catalytic processes*, 2nd ed., Wiley, Hoboken, New Jersey, USA, 2006, ISBN: 9780471457138.
9. Agrafiotis, C., von Storch, H., Roeb, M., Sattler, C., *Solar thermal reforming of methane feedstocks for hydrogen and syngas production—A review*, Renewable and Sustainable Energy Reviews, 29 (2014), 656-682, http://dx.doi.org/10.1016/j.rser.2013.08.050
10. Sugarmen, C., Rotstein, A., Fisher, U., Sinai, J., *Modification of gas turbines and operation with solar produced syngas*, Journal of Solar Energy Engineering, 126 (2004), 867-871, doi:10.1115/1.1758725
11. McNaughton, R., *Improving Efficiency of Power Generation from Solar Thermal Natural Gas Reforming*, at SolarPACES, Berlin, Germany, 15.-18. September 2009.
12. Sheu, E.J., Mitsos, A., *Optimization of a hybrid solar-fossil fuel plant: Solar steam reforming of methane in a combined cycle*, Energy, 51 (2013), 193-202, http://dx.doi.org/10.1016/j.energy.2013.01.027
13. Solbiopolysy, *Biofuel polygeneration system integrating MSW landfill and solar energy*, URL: solbiopolysy-lro.ung.si/, Accessed: 01/08/2014

14. Rostrup-Nielsen, J.R., *Catalytic Steam Reforming*, in: John R. Anderson (Ed.) Catalysis: Science and Technology, Springer-Verlag, Berlin, Germany, 1984, ISBN: 9780387126654.
15. Fraenkel, D., Levitan, R., Levy, M., *A solar Thermochemical Pipe Based on the CO2-CH4 (1:1) System*, International Journal of Hydrogen Energy, 11 (1986), 267–277, DOI: 10.1016/0360-3199(86)90187-4
16. Levitan, R., Levy, M., Rosin, H., Rubin, R., *Closed-loop operation of a solar chemical heat pipe at the Weizmann Institute solar furnace*, Solar Energy Materials, 24 (1991), 464-477, http://dx.doi.org/10.1016/0165-1633(91)90083-W
17. Apt, J., Newcomer, A., Lave, L.B., Douglas, S., Dunn, L.M., *An Engineering-Economic Analysis of Syngas Storage*, DOE/NETL-2008/1331, Natonal Energy Technology Laboratory (NETL), 2008,
18. Bertau, M., Offermanns, H., Plass, L., Schmidt, F., Wernicke, H.-J., *Methanol: The basic chemical and energy feedstock of the future - Asingers Vision Today*, Springer-Verlag Berlin, Heidelberg, 2014, ISBN: 978-3-642-39709-7.
19. Olah, G.A., Goeppert, A., Prakash, G.S., *Beyond oil and gas: the methanol economy*, 1. ed., Wiley-VCH, Weinheim, Germany, 2006, ISBN: 9783527312757.
20. Yang, C.-J., Jackson, R.B., *China's growing methanol economy and its implications for energy and the environment*, Energy Policy, 41 (2012), 878-884, http://dx.doi.org/10.1016/j.enpol.2011.11.037
21. Aasberg-Petersen, K., Stub Nielsen, C., Dybkjær, I., Et Perregaard, J., *Large scale methanol production from natural gas*, Haldor Topsoe, (2008), 22
22. Liu, K., Song, C., Subramani, V., *Hydrogen and Syngas Production and Purification Technologies*, Wiley, Hoboken, New Jersey, USA, 2010, ISBN: 0471719757.
23. Aasberg-Petersen, K., Dybkjær, I., Ovesen, C., Schjødt, N., Sehested, J., Thomsen, S., *Natural gas to synthesis gas – catalysts and catalytic processes*, Journal of Natural Gas Science and Engineering, 3 (2011), 423-459, http://dx.doi.org/10.1016/j.jngse.2011.03.004
24. van den Bussche, K., Froment, G., *A steady-state kinetic model for methanol synthesis and the water gas shift reaction on a commercial Cu/ZnO/Al 2 O 3 catalyst*, Journal of Catalysis, 161 (1996), 1-10, http://dx.doi.org/10.1006/jcat.1996.0156
25. Huber, G.W., Iborra, S., Corma, A., *Synthesis of transportation fuels from biomass: chemistry, catalysts, and engineering*, Chemical Reviews, 106 (2006), 4044-4098, DOI:10.1021/cr068360d
26. Stieglitz, R., Heinzel, V., *Thermische Solarenergie Elektronische Ressource Grundlagen, Technologie, Anwendungen*, in: SpringerLink : Bücher, Springer, Berlin, Heidelberg, 2012
27. Pitz-Paal, R., Buck, R., Heller, P., Hirsch, T., Steinmann, W.-D., *Solar Thermal Power Production*, in: Transition to Renewable Energy Systems, Wiley-VCH Verlag GmbH & Co. KGaA, 2013, ISBN: 9783527673872, pp. 307-338.
28. Kodama, T., *High-temperature solar chemistry for converting solar heat to chemical fuels*, Progress in Energy and Combustion Science, 29 (2003), 567-597, DOI:10.1016/S0360-1285(03)00059-5
29. Steinfeld, A., Schubnell, M., *Optimum aperture size and operating temperature of a solar cavity-receiver*, Solar Energy, 50 (1993), 19-25, DOI: 10.1016/0038-092x(93)90004-8

30. *Concentrating Solar Power*, International Renewable Energy Agency (IRENA) and Energy Technology Systems Analysis Programme of the International Energy Agency (IEA-ETSAP), 2013, URL: https://www.irena.org/DocumentDownloads/Publications/IRENA-ETSAP%20Tech%20Brief%20E10%20Concentrating%20Solar%20Power.pdf,
31. Sheu, E.J., Mokheimer, E.M.A., Ghoniem, A.F., *A review of solar methane reforming systems*, International Journal of Hydrogen Energy, 40 (2015), 12929-12955, http://dx.doi.org/10.1016/j.ijhydene.2015.08.005
32. Langnickel, U., Böhmer, M., *Test results and operating experience with the ASTERIX-facility (in German: Testergebnisse und Betriebserfahrungen mit der ASTERIX-Anlage)*, in: M. Becker, M. Böhmer, K. H. Funken (Eds.) Solar test facility Alermía - Reports if the final presentation in the project SOTA (in German: Solares Testzentrum Almería - Berichte der Abschlusspräsentation des Projektes SOTA), C.F. Müller, Karlsruhe, 1993, ISBN: 3788074817, pp. vii, 390.
33. Kolb, G.J., *An evaluation of possible next-generation high-temperature molten-salt power towers*, SAND2011-9320, Sandia Natuional Laboratories, Alburquerque, New Mexico, USA, 2011,
34. McNaughton, R., *Solar Steam Reforming Using a Closed Cycle Gaseous Heat Transfer Loop*, at SolarPACES 2012, Marrakech, Morocco, 11.-14. September 2012.
35. Uhlig, R., Flesch, R., Gobereit, B., Giuliano, S., Liedke, P., *Strategies Enhancing Efficiency of Cavity Receivers*, Energy Procedia, 49 (2014), 538-550, DOI: 10.1016/j.egypro.2014.03.058
36. Buck, R., Muir, J.F., Hogan, R.E., Skocypec, R.D., *Carbon dioxide reforming of methane in a solar volumetric receiver/reactor: the CAESAR project*, Solar Energy Materials, 24 (1991), 449 - 463, DOI:10.1016/0165-1633(91)90082-V
37. Abele, M., Wörner, A., Brose, G., Buck, R., Tamme, R., *Test Results of a Receiver Reactor for Solar Methane Reforming and Aspects of further application of this Technology*, in Proceedings of the Solar Thermal Concentrating Technologies: 8th International Symposium, 1996, Köln, Germany, October 6-11.
38. *SOLREF - Solar Steam Reforming of Methane rich Gas for Synthesis Gas Production - 75 Month Periodic Activity Report*, Deutsches Zentrum für Luft- und Raumfahrt (DLR), Cologne, Germany, 2010,
39. Tamme, R., Buck, R., Epstein, M., Fisher, U., Sugarmen, C., *Solar Upgrading of Fuels for Generation of Electricity*, Journal of Solar Energy Engineering, 123 (2001), 160-163, DOI:10.1115/1.1353177
40. Rubin, R., Karni, J., *Carbon Dioxide Reforming of Methane in Directly Irradiated Solar Reactor With Porcupine Absorber*, Journal of Solar Energy Engineering, 133 (2011), DOI:10.1115/1.4003678
41. Anikeev, V.I., Kirillov, V.A., *Basic design principles and some methods of investigation of catalytic reactors-receivers of solar radiation*, Solar Energy Materials, 24 (1991), 633-646, http://dx.doi.org/10.1016/0165-1633(91)90097-5
42. Alexopoulos, S., Hoffschmidt, B., *Solar tower power plant in Germany and future perspectives of the development of the technology in Greece and Cyprus*, Renewable Energy, 35 (2010), 1352-1356, DOI: 10.1016/j.renene.2009.11.003
43. von Storch, H., Roeb, M., Stadler, H., Sattler, C., Hoffschmidt, B., *Efficiency potential of indirectly heated solar reforming with different types of solar air receivers*, Applied

Thermal Engineering, 92 (2016), 202-209, http://dx.doi.org/10.1016/j.applthermaleng.2015.09.065
44. Tiddens, A., Röger, M., Stadler, H., Hoffschmidt, B., *A tracer gas leak rate measurement method for circular air circuits*, Flow Measurement and Instrumentation, 47 (2016), 45-53, http://dx.doi.org/10.1016/j.flowmeasinst.2015.12.001
45. Zunft, S., Hänel, M., Krüger, M., Dreißigacker, V., Göhring, F., Wahl, E., *Jülich Solar Power Tower—Experimental Evaluation of the Storage Subsystem and Performance Calculation*, Journal of Solar Energy Engineering, 133 (2011), 031019-031019, DOI: 10.1115/1.4004358
46. Wesenberg, M.H., *Gas Heated Steam Reformer Modelling*, Department of Chemical Engineering, orwegian University of Science and Technology, 2006, Doctoral Thesis
47. Pattison, R.C., Baldea, M., *A thermal - flywheel approach to distributed temperature control in microchannel reactors*, AIChE journal, 59 (2013), 2051-2061, DOI: 10.1002/aic.13991
48. Luyben, W.L., *Design and control of a methanol reactor/column process*, Industrial & Engineering Chemistry Research, 49 (2010), 6150-6163, DOI: 10.1021/ie100323d
49. Dolezal, R., *Kombinierte Gas-und Dampfkraftwerke*, Berlin, Heidelberg, New York, Barcelona, Hongkong, London, Mailand, Paris, Singapur, Tokio: Springer, (2001)
50. Zhao, Y., Hong, H., Jin, H., *Evaluation criteria for enhanced solar–coal hybrid power plant performance*, Applied Thermal Engineering, 73 (2014), 577-587, http://dx.doi.org/10.1016/j.applthermaleng.2014.08.003
51. Bai, Z., Liu, Q., Lei, J., Li, H., Jin, H., *A polygeneration system for the methanol production and the power generation with the solar–biomass thermal gasification*, Energy Conversion and Management, (2015), DOI: 10.1016/j.enconman.2015.02.031
52. Sternberg, A., Bardow, A., *Power-to-What? - Environmental assessment of energy storage systems*, Energy & Environmental Science, 8 (2015), 389-400, DOI: 10.1039/c4ee03051f
53. Schwarzbözl, P., Pitz-Paal, R., Schmitz, M., *Visual HFLCAL-A software tool for layout and optimisation of heliostat fields*, in Proceedings of the SolarPACES 2009, 2009, Berlin, Germany, 15.-18. September 2009.
54. Peng, D.-Y., Robinson, D.B., *A new two-constant equation of state*, Industrial & engineering chemistry fundamentals, 15 (1976), 59-64, DOI: 10.1021/i160057a011
55. Schwarzbözl, P., *The User's Guide to HFLCAL*, A Software Program for Heliostat Field Layout Calculation. Software Release Visual HFLCAL VH12. Köln, (2009)
56. Winter, C.-J., Sizmann, R.L., Vant-Hull, L.L., *Solar power plants: fundamentals, technology, systems, economics*, Springer Verlag, Berlin, Heidelberg, 1991, ISBN: 978-3-642-64759-8.
57. Avila-Marin, A.L., *Volumetric receivers in solar thermal power plants with central receiver system technology: a review*, Solar Energy, 85 (2011), 891-910, DOI:10.1016/j.solener.2011.02.002
58. Pitz-Paal, R., *Development of a slective volumetric receiver for solar power towers: Parameter studies and exergetic evaluation (in german), DLR Research Report*, German Aerospace Center, Cologne, Germany, 1993,

59. Ahlbrink, N., *Model based evaluation and optimization of the open receiver technology ,in German (Modellgestüzte Bewertung und Optimierung der offenen Luftreceivertechnologie)*, RWTH - Aachen, 2013, Dissertation
60. Personal Communication: Ahlbrink, N. (DLR), Temperature dependence of thermal conductivity SiC honeycomb structure to Henrik von Storch
61. Nonino, C., Del Giudice, S., Comini, G., *Laminar forced convection in three-dimensional duct flows*, Numerical Heat Transfer, Part A Applications, 13 (1988), 451-466
62. von Storch, H., Stadler, H., Roeb, M., Hoffschmidt, B., *Efficiency potential of indirectly heated solar reforming with open volumetric solar receiver* Applied Thermal Engineering, (2015), DOI: 10.1016/j.applthermaleng.2015.05.026
63. Xu, J., Froment, G.F., *Methane steam reforming, methanation and water - gas shift: I. Intrinsic kinetics*, AIChE journal, 35 (1989), 88-96, DOI:10.1002/aic.690350109
64. *VDI - Heat Atlas (in german)*, Verein Deutscher Ingenieure (Ed.), 10. ed., Springer Verlag, Berlin, 2006, ISBN: 9783540255048.
65. Petukov, B.S., Roizen, L.I., High Temperature, 2 (1964), 65-68
66. Gnielinski, V., *A new method for calcuation of the heat transfer in the transient regime between laminar and turbulent flow in tubes (in german)*, Forschung im Ingenieurwesen, 61 (1995), 240-248, DOI:10.1007/BF02607964
67. *VDI - Heat Atlas*, Verein Deutscher Ingenieure (Ed.), 2. ed., Springer Verlag, Heidelberg, 2010, ISBN: 9783540778769.
68. Baehr, H.D., Stephan, K., *Mass - and Heat Transfer (in German: Wärme-und Stoffübertragung)*, 6. ed., Springer-Verlage, Berlin, Heidelberg, 2008, ISBN: 978-3-540-87688-5.
69. Peters, P.E., Schiffino, R.S., Harriott, P., *Heat transfer in packed-tube reactors*, Industrial & Engineering Chemistry Research, 27 (1988), 226-233, DOI:10.1021/ie00074a003
70. *R-67-7H*, Haldor Topsøe AS, URL: http://www.topsoe.com/business_areas/ammonia/processes/~/media/PDF%20files/Steam_reforming/Topsoe_steam_reforming_cat_r%2067%207h.ashx, Accessed:
71. Pedernera, M.N., Piña, J., Borio, D.O., Bucalá, V., *Use of a heterogeneous two-dimensional model to improve the primary steam reformer performance*, Chemical Engineering Journal, 94 (2003), 29-40, http://dx.doi.org/10.1016/S1385-8947(03)00004-4
72. Achenbach, E., *Heat and flow characteristics of packed beds*, Experimental Thermal and Fluid Science, 10 (1995), 17-27, http://dx.doi.org/10.1016/0894-1777(94)00077-L
73. Hicks, R., *Pressure drop in packed beds of spheres*, Industrial & engineering chemistry fundamentals, 9 (1970), 500-502, DOI: 10.1021/i160035a032
74. von Storch, H., Stadler, H., Roeb, M., Hoffschmidt, B., *Efficiency potential of indirectly heated solar reforming with open volumetric solar receiver*, Applied Thermal Engineering, 87 (2015), 297-304, http://dx.doi.org/10.1016/j.applthermaleng.2015.05.026
75. Rout, K.R., Jakobsen, H.A., *A numerical study of fixed bed reactor modelling for steam methane reforming process*, The Canadian Journal of Chemical Engineering, 93 (2015), 1222-1238, 10.1002/cjce.22202

76. Finn, A., O'Brien, J., *Processing of Carbon Dioxide Rich Gas*, at GPA Annual Conference, Madrid, 17th - 19th September 2014.
77. Wang, M.Q., Huang, H.S., *A full fuel-cycle analysis of energy and emissions impacts of transportation fuels produced from natural gas*, ANL/ESD--40, 2000, URL: http://www.osti.gov/energycitations/servlets/purl/750803-oStj0b/native/, Date Accessed: 28. Jan. 2013
78. Ferriere, A., Romero, M., Tellez, F., Zarza, E., Steinfeld, A., Langnickel, U., Shpilrain, E., Popel, O., Epstein, M., Karni, J., *Road Map Deliverable (WP 3 Deliverable No7)*, R. Pitz-Paal, J. Dersch, B. Milow (Eds.), European Concentrated Solar Thermal Road Mapping (ECOSTAR), SES-CT-2003-502578, 2005, URL: http://www.promes.cnrs.fr/uploads/pdfs/ecostar/ECOSTAR.Roadmap.pdf, Date Accessed: 01 October 2015
79. Sun, Y., Edwards, J., *Solar-to-Fuel Energy Conversion Analysis of Solarised Mixed Reforming of Methane*, Energy Procedia, 69 (2015), 1828-1837, http://dx.doi.org/10.1016/j.egypro.2015.03.159
80. Maulbetsch, J.S., DiFilippo, M.N., *Cost and value of water use at combined cycle power plants*, California Energy Commission (Ed.) PIER Energy-Related Environmental Research, 2006,
81. *Projected Costs of Generating Electricity 2010*, International Energy Agency, Nuclear Energy Agency, Organisation for Economic Co-operation and Development, Washington, Palo Alto, 2010, ISBN: 9789264084308.
82. *Methanex posts regional contract methanol prices for North America, Europe and Asia*, Methanex Corporation, URL: https://www.methanex.com/our-business/pricing, Accessed: 11. May 2015
83. *CEPCI - Economic Indicators, Jan. 2008*, Chemical Engineering, URL: http://www.engr.uconn.edu/~ewanders/Design/Chemical%20Engineering%20Cost%20Indices%20Jan%202008.pdf, Accessed: 07. May 2015
84. *CEPCI - Economic Indicators, Jan. 2015*, Chemical Engineering, URL: http://www.isr.umd.edu/~adomaiti/chbe446/literature/ChECostIndexJan2015.pdf, Accessed: 29. April 2015
85. *Historical Exchange Rates*, Oanda, URL: http://www.oanda.com/lang/de/currency/historical-rates/, Accessed: 07. May 2015
86. Hernández-Moro, J., Martínez-Duart, J.M., *CSP electricity cost evolution and grid parities based on the IEA roadmaps*, Energy Policy, 41 (2012), 184-192, http://dx.doi.org/10.1016/j.enpol.2011.10.032
87. Ulrich, G.D., Vasudevan, P.T., *Chemical engineering process design and economics : a practical guide*, 2nd ed., Process Pub., Durham, N.H., 2004, ISBN: 0970876823.
88. Vogel, W., Kalb, H., *Large-Scale Solar Thermal Power: Technologies, Costs and Development*, Wiley, 2010, ISBN: 9783527630004.
89. *The Methanol Industry*, Methanol Institute, URL: http://www.methanol.org/Methanol-Basics/The-Methanol-Industry.aspx, Accessed: 10. Sept. 2015
90. *Natural Gas Utilization via Small-Scale Methanol Technologies*, Ben Franklin Technology Partners' Shale Gas Innovation & Commercialization Center (Ed.) ADI Analytics LLC, April 2015, URL:

http://www.sgicc.org/uploads/8/4/3/1/8431164/bftp_methanol_white_paper_vf.pdf, Date Accessed: 11. September 2015
91. *Henry Hub Natural Gas Spot Price*, 2015, U.S. Energy Information Administration, URL: http://www.eia.gov/dnav/ng/hist/rngwhhdm.htm, Accessed: 11. September 2015
92. Parkinson, G., *World's biggest solar tower + storage plant to begin generation this month*, 14 May 2015, RE new economy, URL: http://reneweconomy.com.au/2015/worlds-biggest-solar-tower-storage-plant-to-begin-generation-this-month-22860, Accessed: 14 September 2015
93. *Electric Power Monthly - Table 5.6.A. Average Price of Electricity to Ultimate Customers by End-Use Sector*, 26 August 2015, U.S. Energy Information and Administration (eia), URL: http://www.eia.gov/electricity/monthly/epm_table_grapher.cfm?t=epmt_5_6_a, Accessed: 14 September 2015
94. Schlesinger, M., Hofer, P., Kemmler, A., Kirchner, A., Koziel, S., Ley, A., Piegas, A., Seefeldt, F., Straßburg, S., Weinert, K., Lindenberger, D., Knaut, A., Malischek, R., Nick, S., Panke, T., Paulus, S., Tode, C., Wagner, J., Lutz, C., Lehr, U., Philip, U., *Entwicklung der Energiemärkte - Energiereferenzprognose - Kurzfassung zum Endbericht*, Bundesministerium für Wirtschaft und Technologie, Berlin/Köln/Osnabrück, 2014, URL: http://www.bmwi.de/BMWi/Redaktion/PDF/Publikationen/entwicklung-der-energiemaerkte-energiereferenzprognose-kurzfassung,property=pdf,bereich=bmwi2012,sprache=de,rwb=true.pdf, Date Accessed: 12. August 2015
95. Trieb, F., *Global potential of concentrating solar power*, in Proceedings of the SolarPACES 2009, Berlin, Germany, 15.-18. September 2009.

Appendix

Appendix A Estimation of efficiency of solarization

For the estimation of the efficiency, it is assumed that the solar power plant in the reference system is a solar power tower and the fuel is gaseous and therefore converted into electricity in a combined cycle gas turbine power plant.

The Energy to the process in dependence of the solar energy supply is given by:

$$E_{\mathrm{SIP}} = E_{\mathrm{Solar}} \cdot \eta_{\mathrm{Concentration}} \cdot \eta_{\mathrm{Receiver}}(T_{\mathrm{Process}})$$

The Energy to the industrial process in the reference system is identical to the energy to the process and due to the neglecting of losses by heat provision with fuel, it equals the fuel energy demand:

$$E_{\mathrm{Reference}} = E_{\mathrm{SIP}} = E_{\mathrm{Fuel,Reference}}$$

The electricity production from solar energy is given by:

$$E_{\mathrm{El,SPT}} = E_{\mathrm{Solar}} \cdot \eta_{\mathrm{Concentration}} \cdot \eta_{\mathrm{Receiver}}(T_{\mathrm{WSC}}) \cdot \eta_{\mathrm{Carnot,WSC}}$$

With $\eta_{Receiver}$ as given in Eq.(2.14) and $\varepsilon = 1$, η_{Carnot} for a process at Temperature i is given in the following.

$$\eta_{\mathrm{Carnot,i}} = 1 - \frac{T_{\mathrm{Ambient}}}{T_{\mathrm{i}}}$$

The electricity production from CCGT has to be equal to the production from the solar power tower:

$$E_{\mathrm{El,CCGT}} = E_{\mathrm{El,SPT}}$$

Hence,

$$E_{\mathrm{Fuel,CCGT}} = \frac{E_{\mathrm{El,SPT}}}{\eta_{\mathrm{Carnot,CCGT}}}$$

When applying these findings to Eq.(4.3), the efficiency of solarization will yield

$$h_{\text{Solarization}} = \frac{E_{\text{Fuel,Reference}} - E_{\text{Fuel,CCGT}}}{E_{\text{Solar}}},$$

after some simple transformations it can be depicted as

$$h_{\text{Solarization}} = \eta_{\text{Rec}}(T_{\text{SIP}}) - \eta_{\text{Rec}}(T_{\text{WSC}}) \cdot \frac{\eta_{\text{Carnot}}(T_{\text{WSC}})}{\eta_{\text{Carnot}}(T_{\text{CCGT}})}$$

The fixed parameters used for calculation of the values in in Figure 4-2 are given in Table A - 1. With the values given in the Table, the equation can be further simplified:

$$h_{\text{Solarization}} = 0.1874 + \frac{\sigma}{I_{\text{AP}}} \cdot (4.72 \cdot 10^{11} - T_{\text{SIP}}^4)$$

Table A - 1: Temperatures used in the exemplary calculation of f_P

T_{WSC}	873 K
T_{CCGT}	1573 K
$T_{ambient}$	298 K
DNI	1000

Appendix B Data for Field Layout

Appendix B.1. HFLCAL Input Data

Table A - 2: Data for heliostat field layout in HFLCAL

Heliostat reflective Area	121.34 m²
Heliostat reflectivity	90 %
Beam error	3.3 mrad
ideal focal length	
Field layout type	slip planes
AMIN	19.00 m
AR	13.44 m
BR	0.0172 m
USTART	64 m
FPACK	1
Height of receiver	120 m
Tower height and diameter	140 m / 10 m
Receiver tilt angle (from horizontal)	25.33 °
Aperture shape	rectangular (square)

Appendix B.2. Correction factor for heliostat field efficiency for variation of flux density.

The field efficiency is determined for different flux densities and the deviation from the reference flux of 700 kW is determined. A third order polynomial is fitted to predict the deviation.

Table A - 3: Results of flux density variation in heliostat field layout

Flux onto Aperture	Aperture Area	Side length of square	η_{Field}	Deviation from reference	Deviation calcluated by polynomial	Relative deviation in efficiency prediction
	m²	m	%			
400	125.0	11.18	70.4	0.0146	0.0145	9.94E-05
450	111.1	10.54	70.29	0.0130	0.0130	4.69E-06
500	100.0	10.00	70.16	0.0111	0.0111	9.14E-06
550	90.9	9.53	70	0.0088	0.0088	-4.63E-05
600	83.3	9.13	69.82	0.0062	0.0062	-3.55E-05
650	76.9	8.77	69.61	0.0032	0.0033	-1.18E-04
700	71.4	8.45	69.39	0	0.0000	-2.47E-05
750	66.7	8.16	69.14	-0.0036	-0.0035	-5.85E-05
800	62.5	7.91	68.9	-0.0071	-0.0074	3.42E-04
850	58.8	7.67	68.59	-0.0115	-0.0115	1.94E-07
900	55.6	7.45	68.3	-0.0157	-0.0159	2.06E-04
950	52.6	7.25	67.97	-0.0205	-0.0205	6.73E-05
1000	50.0	7.07	67.63	-0.0254	-0.0254	5.56E-06
1050	47.6	6.90	67.28	-0.0304	-0.0304	4.37E-06
1100	45.5	6.74	66.92	-0.0356	-0.0356	4.73E-05
1150	43.5	6.59	66.53	-0.0412	-0.0410	-1.83E-04
1200	41.7	6.45	66.15	-0.0467	-0.0466	-1.05E-04
1250	40.0	6.32	65.77	-0.0522	-0.0523	1.18E-04
1300	38.5	6.20	65.37	-0.0579	-0.0581	1.65E-04

Appendix C OVR model

Appendix C.1. Correlations for model

Effective thermal conductivity of absorber structure:

$$\lambda_{eff,Abs}(T_{W,i}) = \frac{4.914 \cdot T_{W,i} + 2.926}{T_{W,i} + 208.7}$$

Nusselt correlation for wall-air heat transfer coefficient in absorber structure:

$$Nu(x) = 2{,}3 \cdot \frac{\frac{x}{d_h Re \cdot Pr}}{0{,}066 - 0{,}0071 \cdot Pr^{-0{,}75} + \frac{x}{d_h Re \cdot Pr}} + (0{,}799 \cdot Pr^{-0{,}0279} - 0.201)$$

$$\gamma = 0.0479 \cdot log_{10} Pr - 0.439$$

Appendix D Optimum Flux density

For determination of the optimum flux density to be used in the simulations in dependence of the hot air temperature, it is interpolated between the values given in Table A - 4.

Table A - 4: Data for selection of flux density for simulations

T_{HA}	Cavity	No Cavity
600	650	500
700	750	600
800	900	700
900	1000	850
1000	1150	900

Appendix E Reforming Kinetics

$$r_1 = \frac{k_1}{p_{\mathrm{H_2}}^{2,5}} \frac{\left(p_{\mathrm{CH_4}} p_{\mathrm{H_2O}} - \frac{p_{\mathrm{H_2}}^3 p_{\mathrm{CO}}}{K_1}\right)}{DEN^2}$$

$$r_2 = \frac{k_2}{p_{\mathrm{H_2}}} \frac{\left(p_{\mathrm{CO}} p_{\mathrm{H_2O}} - \frac{p_{\mathrm{H_2}} p_{\mathrm{CO_2}}}{K_2}\right)}{DEN^2}$$

$$r_3 = \frac{k_3}{p_{H_2}^{3,5}} \frac{\left(p_{\mathrm{CH_4}} p_{\mathrm{H_2O}}^2 - \frac{p_{\mathrm{H_2}}^4 p_{\mathrm{CO_2}}}{K_3}\right)}{DEN^2}$$

with the rate coefficients k_j with j = 1…3:

$$k_\mathrm{j} = A_{\mathrm{j,rate}} \exp\left(-\frac{E_j}{RT}\right),$$

With the the values for $A_{\mathrm{j,rate}}$ and E_j given in the table below.

	Reaction 1	Reaction 2	Reaction 3
$A_{\mathrm{j,rate}}$	$4.225 \cdot 10^{15}$	$1.955 \cdot 10^{6}$	$1.02 \cdot 10^{15}$
E_j [kJ/mol]	240.1	67.13	243.9

and for DEN with the adsorption koefficients K_j with j = CO, H_2, CH_4 or H_2O.

$$DEN = 1 + K_{\mathrm{CO}} p_{\mathrm{CO}} + K_{\mathrm{H_2}} p_{\mathrm{H_2}} + K_{\mathrm{CH_4}} p_{\mathrm{CH_4}} + \frac{K_{H_2O} p_{\mathrm{H_2O}}}{p_{\mathrm{H_2}}}$$

$$K_\mathrm{j} = A_{\mathrm{j,Ads}} \exp\left(-\frac{\Delta H_\mathrm{J}}{RT}\right),$$

With the values for $A_{\mathrm{j,Ads}}$ and ΔH_j given in the table below.

	CO	H_2	CH_4	H_2O
$A_{\mathrm{j,rate}}$	$8.23 \cdot 10^{-5}$	$6.12 \cdot 10^{-9}$	$6.65 \cdot 10^{15}$	$1.77 \cdot 10^{5}$
E_j [kJ/mol]	-70.65	-82.90	-38.28	88.68

K_i with i = 1…3 are the equilibrium constants for each of the equation, determined by setting the value of the Gibbs free enthalpy to zero.

Appendix F Correlations for AHR Model

Appendix F.1. Correlations for annulus

Nusselt correlation for fully developed turbulent flow from Ref. [64], chapter Gb:

$$Nu_{Tube} = \frac{\left(\frac{\xi}{8}\right) RePr}{1 + 12{,}7\sqrt{\frac{\xi}{8}}\left(Pr^{\frac{2}{3}} - 1\right)} \left\{1 + \left(\frac{d_h}{l}\right)^{\frac{2}{3}}\right\}$$

With

$$\xi = (1{,}8\, log_{10}\, Re - 1{,}5)^{-2}$$

Correction factor for concentric annulus:

$$\frac{Nu_{\text{Annulus}}}{Nu_{\text{Tube}}} = \frac{0{,}86\left(\frac{r_{\text{An,in}}}{r_{\text{An,o}}}\right)^{0{,}84} + \left[1 - 0{,}14\left(\frac{r_{\text{An,in}}}{r_{\text{An,o}}}\right)^{0{,}6}\right]}{1 + \left(\frac{r_{\text{An,in}}}{r_{\text{An,o}}}\right)}$$

Nusselt correlation for laminar flow from ref. [67]

$$Nu = (Nu_1^3 + Nu_2^3)^{\frac{1}{3}}$$
$$Nu_1 = 3.66 + 1.2a^{0.8}$$
$$Nu_2 = f_g \sqrt[3]{Re\, Pr \frac{d_{\text{h}}}{l}}$$
$$f_{g,i} = 1.65[1 + 0.14a^{-0.5}]$$
$$a = \left(\frac{di}{do}\right)$$

Pressure drop in the annulus, from Ref. [64] chapter L1:

$$\Delta p = \zeta \cdot \frac{l_{reactor}}{d_h} \cdot \rho_{Air} \cdot \frac{u_{Air}^2}{2}$$

with ζ for turbulent conditions

$$\zeta = \frac{0.3164}{\sqrt[4]{Re_{\mathrm{An}}}}$$

and for laminar conditions

$$\zeta = \frac{64}{Re}$$

Appendix F.2. Correlations for reactor tube

Nusselt correlation for wall heat transfer coefficient of packed beds from Ref. [69]:

$$Nu_{\mathrm{W}} = 4.9 \cdot \left(\frac{d_{\mathrm{Particle}}}{d_{\mathrm{Tube,in}}}\right)^{0.26} \cdot Re_{\mathrm{Particle}}^{0,45} \cdot Pr^{\frac{1}{3}}$$

Pressure drop correlation from Ref. [73]:

$$\frac{dp}{dz} = -\frac{6.8(1-\psi)^{1.2}}{\psi^3} Re_{\mathrm{Particle}}^{-0.2} \cdot \frac{\rho u^2}{d_{Particle}}$$

Appendix F.3. Calculation of thermal conductivity of packed bed

The thermal conductivity of the packed bed is determined in relation to the thermal conductivity of the fluid with the factor k_{bed}, which is determined with the Zehner/Bauer/Schlünder model.

$$k_{bed} = \frac{\lambda_{bed}}{\lambda_f}$$

with

$$k_{bed} = (1-\sqrt{1-\psi}\,\psi[(\psi - 1 + k_G^{-1})^{-1} + k_{rad}] + \sqrt{1-\psi}\big[\varphi k_p + (1-\varphi)k_c\big]$$

with

$$k_c = \frac{2}{N}\left\{\frac{B\big(k_p + k_{rad} - 1\big)}{N^2 k_g k_p}\ln\left(\frac{k_p + k_{rad}}{B\big[k_G + (1-k_G)\big(k_p + k_{rad}\big)\big]}\right) + \frac{B+1}{2B}\left[\frac{k_{rad}}{k_g} - B\left(1 + \frac{1-k_G}{k_g}k_{rad}\right)\right] - \frac{B-1}{Nk_G}\right\}$$

$$N = \frac{1}{k_G}(1 + \ (k_{rad} - Bk_G)/k_p) \ - B\ (\frac{1}{k_G} - 1)\ (1 + \frac{k_{rad}}{k_p})$$

$$B = C_f \left[\frac{(1-\psi)}{\psi}\right]^{\frac{10}{9}}$$

$$C_f = 2.5\left[1 + \left(\frac{d_i}{d_a}\right)^2\right]$$

$$k_{rad} = \frac{\lambda_{rad}}{\lambda} = \frac{4\sigma}{\left(\frac{2}{\varepsilon_W}\right) - 1} T^3 \frac{d}{\lambda_f}$$

$$k_G = \left[1 + \left(\frac{l}{d}\right)\right]^{-1}$$

With l as the average free path lengths of the molecules, calculated according to VDI-heat atlas [64], Mg11 (german version).

Appendix G Data for economic investigation

Appendix G.1. CEPCI indices

Year	Index
1958	100
1999	390.6
2000	394.1
2001	394.3
2002	395.6
2003	402
2004	444.2
2005	468.2
2006	499.6
2007	525.4
2008	575.4
2009	521.9
2010	550.8
2011	585.7
2012	584.6
2013	567.3
2014 (Sept)	580.1

Appendix G.2. Cost for common process components

All data in Table A - 5 is based on information by Ulrich and Vasudevan [87]. The second column gives information on where in the book the information is retrieved from. The polynomial always has the form $y = A_0 + A_1 \cdot x + A_2 \cdot x^2 + A_3 \cdot x^3 + A_4 \cdot x^4$.

Table A - 5: Polynomials for determinaiton of process unit cost

Component Type	Specific source	A_0	A_1	A_2	A_3	A_4	x	y	Further factors
Compressor (turbo, excl. drive)	Fig. 5.30	12e3	735	-4.5E-2	5,6E-6	-2.5E-10	Fluid Power (kW)	C_p	F_BM= 2.5 for Carbon Steel
Generator/ electric motor	Fig 5.45	191	53	-7e-3	9.8E-7	4.5E-11	Shaft Power (kW)	C_p	F_BM= 1.5
Heat Exchanger (Shell & Tube)	Fig. 5.36	2.6E3	106	-0.16	2E-4	-9.0E-8	Area (m²)	C_p	F_p, F_BM, next rows F_M= 1.0 for carbon steel = 3.0 for nickel based alloys
Heat exchanger (shell & tube) (pressure factor)	Fig. 5.37	0.95	7.2E-3	-8E-5	4.7E-7	-9.1E-10	Pressure (bar)	F_p	-
Heat Exchanger (shell & tube) (bare module)	Fig. 5.38	1.9	1.3	2.4E-3	-8.6E-5	9.9E-8	$F_\mathrm{p} \cdot F_\mathrm{M}$	F_BM	
CCGT	Fig 5.8	1.2E6	1.8E6	-1.3E4	1.0E2	-2.9e-1	Capacity ($MW_{Electric}$)	C_BM	-
Process vessel, vertical, 1 m diameter	Fig 5.44	2.4E3	2.1E3	1.1E-1	5E-1	-7.8E-3	Height (m)	C_p	F_p, if pressure > 4 bar F_M= 1 for carbon steel

Process vessel, vertical, 3 m diameter	Fig 5.44	11E3	5.3E3	-1.1E2	3.1	2.9E-2	Height (m)	C_{p}	F_{p}, if pressure > 4 bar F_{M}= 1 for carbon steel
Process vessel (pressure factor)	Fig. 5.45	1.0	6E-2	-2.5E-4	8.5E-7	-9.3E-10	Pressure (bar)	F_{p}	-
Process vessel (bare module	Fig 5.46	2.5	1.7	0	0	0	$F_{\mathrm{p}} \cdot F_{\mathrm{M}}$	F_{BM}	-
Pump (centrifugal) (incl. motor drive)	Fig. 5.49	2.6E3	5E2	-4.9	2.3E-2	-3.8E-5	Shaft power (kW)	C_{p}	F_{M}= 1.0 for cast steel, F_{p} F_{BM}
Pump (centrifugal) (pressure factor)	Fig. 5.50	0.71	4e-2	-2.7E-4	9.1E-7	1.1E-9	Suction pressure (bar)	F_{p}	-
Pump (centrifugal) (bare module)	Fig 5.51	1.8	1.6	-7.2E-3	7.9E-4	-2.6E-5	$F_{\mathrm{p}} \cdot F_{\mathrm{M}}$	F_{BM}	-
Reformer furnace	Fig 5.27	79E3	81	-7E-4	7.6E-9	-3.3E-14	Heating Duty (kW)	C_{p}	F_{BM}= 2.7 for stainless steel F_{p}=1.05 for p_{Ref} ≈50 bar

The diameter and height of the separator that removes the condensed water from the syngas (*separator-Reforming*) and the separator (*separator methanol*) and flash (*flash methanol*) in the methanol synthesis part of the SOLME and the reference methanol synthesis process are determined with the procedure recommended for this purpose by Ulrich and Vasudevan [77] (p.287 ff.). The resulting values are given in Table A - 6. The is determined for a diameter of 1 m and then scaled to the actual diameter with the same procedure shown for the power block in eq. (7.5), with an exponential factor of 0.864, as that was the factor determined between a diameter of 1 m and 3 m.

Table A - 6: Diemnsions of process vessel in SOLME - and reference methanol plant

Component	Diameter im m	Height in m
Separator reforming, SOLME	0.82	4.10
Separator methanol, SOLME	0.05	0.14
Flash methanol, SOLME	0.47	2.33
Separator reforming, reference methanol plant	0.77	3.86
Separator methanol, reference methanol plant	0.04	0.13
Flash methanol, reference methanol plant	0.43	2.15

Appendix G.3. Determination of cost of distillation column

The procedure presented below is retrieved from [48].

The heat transfer area A_{HX} of the condenser and the reboiler are determined with the effective heat transfer coefficients U and the cost (bare module in \$ of 2010) with the correlation given below.

- Reboiler: U = 8.52 kW/m²
- Condenser: U = 4.26 kW/m²

$$C_{\mathrm{BM,Condenser/Reboiler}} = 7296 \cdot A_{\mathrm{HX}}^{0.65}$$

The height of the column H_{Col} is fixed at 13.92 meters, as it is defined by the number of stages, which is independent of volume flow. The diameter D_{Col} is determined as a function of the molar feed flow rate:

$$D_{\mathrm{Col}} = 0.0046 \cdot F_{\mathrm{Feed}} \left(\frac{kmol}{h}\right) + 0.6948$$

The resulting bare module cost of the column is a function of the diameter and the heigt:

$$C_{\mathrm{BM,Col}}(\$_{2010}) = 17640 \cdot D_{\mathrm{Col}}^{1.066} \cdot H_{\mathrm{Col}}^{0.802}$$

Appendix G.4. Plant cost data for SOLME system and reference system

All costs in the table below are given in million $ and refer to the annual cost. For component costs it is the annuity of the investment, considering an interest rate of 8 %.

Table A - 7: Cost data

	$ARR = 0.6$	$ARR = 0.9$
Total annual cost		
SOLME system	8.01	8.36
Reference system	8.42	8.78

	$ARR = 0.6$	$ARR = 0.9$
Annuity of investment		
SOLME system	5.07	5.27
SOLME plant	4.82	5.02
Heliostat field	0.82	0.82
Receiver & tower	0.94	0.97
Storage system	1.32	1.41
Power block (WSC)	0.51	0.53
Air heated reformer	0.20	0.21
Methanol reactor	0.11	0.11
Compressors & pumps	0.41	0.45
Distillation column	0.07	0.07
CCGT (internal)	0.39	0.41
Other	0.06	0.05
CCGT (external)	0.24	0.25
Reference system	5.20	5.40
Solar power plant	4.18	4.32
Heliostat field	0.82	0.82
Receiver & tower	0.94	0.97
Storage system	1.32	1.41
Power block	1.10	1.12
Methanol plant	1.02	1.07
Reforming reactor	0.26	0.27
Methanol reactor	0.11	0.11
Compressors	0.30	0.31
Power Block	0.25	0.26
Distillation Column	0.06	0.07
Other	0.05	0.06

	$ARR = 0.6$	$ARR = 0.9$
Operation & maintenance		
SOLME system	0.81	0.84
SOLME plant	0.79	0.82
CCGT	0.01	0.01
Reference System	1.00	1.03
Solar power tower	0.94	0.97
Methanol plant	0.06	0.06
Natural Gas		
SOLME System	1.79	1.90
SOLME Plant	1.57	1.68
CCGT	0.22	0.22
Reference (methanol plant only)	1.86	2.0
Cost for electricity in Reference methanol plant (only internal)	0.38	0.41
Water Supply (Reforming)		
SOLME	0.35	0.35
Reference	0.35	0.35

Appendix G.5. Result of parameter Variation for $ARR = 0.6$

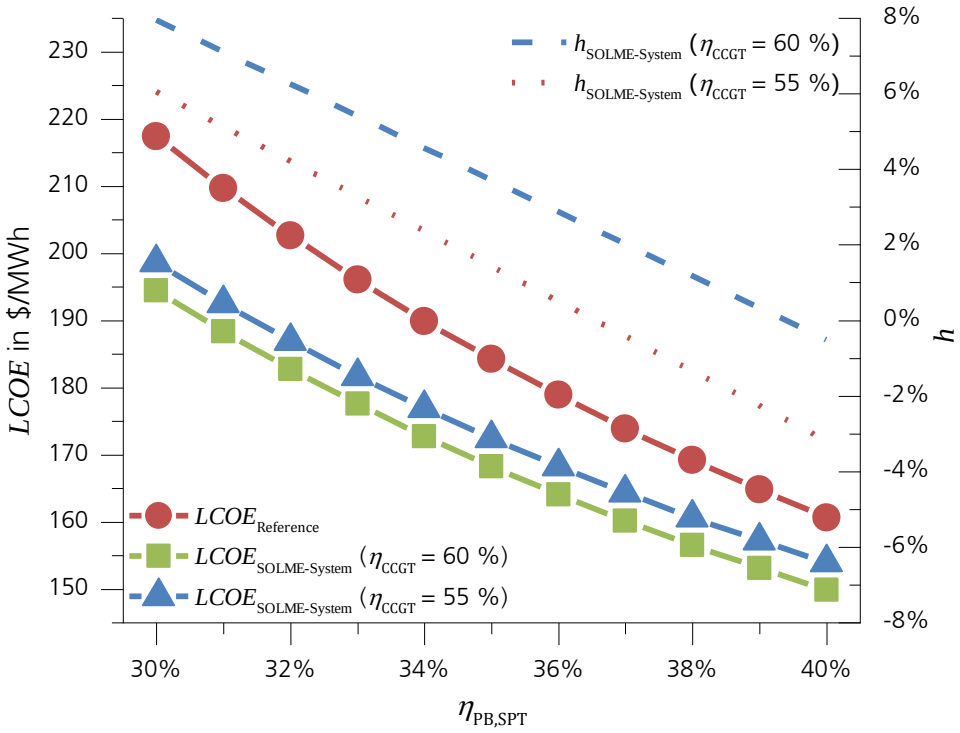

Figure A - 1: Results of the variation of the efficiency of the power block in the reference solar power plant and the efficiency of the CCGT in the SOLME system for air return ratio of 0.6. Reference value of $\eta_{PB,SPT}$ is 0.35